Univerzita Karlova

3. lékařská fakulta

Disertační práce

Praha, 2022 **MUDr. Zbyněk Straňák**

Univerzita Karlova

3. lékařská fakulta

Disertační práce

Implantace nanovlákenného nosiče pro buňky retinálního pigmentového epitelu do subretinálního prostoru na zvířecím modelu

Subretinal implantation of a carrier for retinal pigment epithelium in minipigs

Školitel: prof. MUDr. Pavel Kuchynka, CSc.

Školitel konzultant: doc. MUDr. Pavel Studený, Ph.D., MHA

Prohlášení:

Prohlašuji, že jsem závěrečnou práci zpracoval samostatně a že jsem řádně uvedl a citoval všechny použité prameny a literaturu. Současně prohlašuji, že práce nebyla využita k získání jiného nebo stejného titulu.

Souhlasím s trvalým uložením elektronické verze mé práce v databázi systému meziuniverzitního projektu Theses.cz za účelem soustavné kontroly podobnosti kvalifikačních prací.

V Praze, 30.1.2022

ZBYNĚK STRAŇÁK

Podpis:

Identifikační záznam:

Pro tvorbu identifikačního záznamu se řiďte normami ČSN ISO 690 a ČSN ISO 690-2.

STRAŇÁK, Zbyněk. Implantace nanovlákenného nosiče pro buňky retinálního pigmentového epitelu do subretinálního prostoru na zvířecím modelu (Subretinal implantation of a carrier for retinal pigment epithelium in minipigs). Praha, 2022. Počet stran, počet příloh. Disertační práce. Univerzita Karlova, 3. lékařská fakulta, Oftalmologická klinika. Vedoucí závěrečné: Školitel: prof. MUDr. Pavel Kuchynka, CSc. Školitel konzultant: doc. MUDr. Pavel Studený, Ph.D., MHA

Klíčová slova: retinální pigmentový epitel (RPE), subretinální implantace, nanovlákenný nosič, miniprase, věkem podmíněná makulární degenerace (VPMD)

Keywords: retinal pigmented epithelium (RPE), subretinal implantation, nanofibrous membrane, minipigs, age-related macular degeneration (AMD)

Obsah

Seznam zkratek.....6
Abstrakt.....7
Abstract.....9
1. Úvod.....11
2. Přehled současných poznatků
    2.1. Anatomie, histologie, fyziologie a patofyziologie RPE.....11
    2.2. Vyšetřovací metody RPE.....12
    2.3. Základní klinické jednotky spojené s dysfunkcí RPE.....13
    2.4. Současné možnosti terapie VPMD.....13
    2.5. Operační techniky zadního segmentu oka.....15
    2.6. Slibné přístupy v léčby sítnicových onemocnění.....16
    2.7. Buněčná terapie.....21
3. Hypotézy a cíle práce.....24
4. Popis použitých experimentálních metod, včetně statistických.....24
    4.1. Etická komise a podpora.....24
    4.2. Zvířecí model a operační zázemí.....24
    4.3. Operační technika.....25
5. Materiál
    5.1. Nosiče RPE.....26
    5.2. Přehled původu užívaných buněk RPE.....27
6. Výsledky.....28
7. Diskuse.....29
8. Závěr a zhodnocení cílů a hypotéz práce.....34
9. Seznam použité literatury
10. Přílohy

Seznam zkratek:

CNS	centrální nervový systém
CNV	choroideální neovaskulární membrána
hRPE	lidské primární buňky retinálního pigmentového epitelu
hiPSC	lidské indukované pluripotentní buňky
iPSC	indukované pluripotentní buňky
OCT	optická koherenční tomografie
LCA2	Leberova kongenitální amauróza typu 2
LP	léčivý přípravek
PDT	fotodynamická terapie
PPV	pars plana vitrektomie
RBCs	retinální bipolární buňky
RGCs	retinální gangliové buňky
RPE	retinální pigmentový epitel
ÚŽFG AV	Ústav živočišné fyziologie a genetiky Akademie věd
VEGF	vaskulární endoteliální růstový faktor
VPMD	věkem podmíněná makulární degenerace
ZSM	zadní sklivcová membrána

Abstrakt

Věkem podmíněná makulární degenerace (VPMD) je hlavní příčinou praktické slepoty ve vyspělých zemích. VPMD je jedním z mnoha onemocnění sítnice, které vzniká na základě absence a/nebo dysfunkce retinálního pigmentového epitelu (RPE). Existují dva hlavní typy VPMD (vlhká a suchá), které se liší v etiopatogenezi a oftalmologickém nálezu. Dosavadní terapie je možná pouze u vlhké formy VPMD, kdy dochází k tvorbě neovaskularizací prostupujících z choroidey a následného sáknutí či krvácení v subretinálním prostoru s deteriorací světločivných a ostatních neuronálních buněk sítnice. Neovaskularizaci lze částečně předejít opakovanými intra-vitreálními aplikacemi anti-VEGF preparátů. Bez léčby je výsledkem disciformní jizva na sítnici a ireverzibilní porucha zraku. Aktuálním trendem v léčbě VPMD je snaha o zavedení inovativních chirurgických postupů, které mají potenciál pro zlepšení závažné oftalmologické morbidity zvláště u non-respondentů farmakologické terapie.

Cílem práce bylo zhodnocení úspěšnosti a optimalizace operačního postupu, který umožňuje kontrolovaně a bezpečně transplantovat buňky RPE.

Úspěšnost transplantace buněk RPE ve formě epitelu, který plní okamžitě po transplantaci funkci selektivní bariéry, je závislá na výběru nosiče. Optimální buněčný nosič umožňuje zpevnit transplantovaný buněčný plát a lepší manipulaci s vulnerabilními buňkami RPE.

V předoperačním období jsou na zvoleném nosiči kultivovány buňky určené k transplantaci a takto hotový produkt je implantován do subretinálního prostoru (v našem případě na prasečím modelu). Charakteristikám nosiče (složení, tloušťka, rozměry a tvar) bylo nutné přizpůsobit implantační nástroje pro chirurgický výkon. Optimalizaci charakteristik nosiče ve vztahu k úspěšné implantaci byla věnována první fáze projektu. V pooperačním období byla úspěšnost chirurgického výkonu hodnocena vyšetřením sítnice pomocí fundus-kamery, optické koherenční tomografie (OCT) a histopatologicky.

Výsledkem našeho projektu je nano-nosič oválného tvaru (5.2mm x 2.1mm), který byl implantován u 18 živých zvířat (celkem 29 očí) s celkovou úspěšností 93.1%. Ve čtyřech případech (13.7%) se vyskytlo perioperační odchlípení sítnice (ve 2 případech se podařila sítnice opět úspěšně přiložit, u dalších 2 případů bylo odchlípení spojeno s masivním

perioperačním subretinálním krvácením a operace byla ukončena). Ve čtyřech případech došlo v pooperačním období k zakalení optických medií a následné vyšetření vyšetření nebylo možné (histologické vyšetření však prokázalo zdravou a přiloženou sítnici bez známek zánětu nebo jiného poškození a tyto oči byly tedy zařazeny do skupiny úspěšných operací).

Závěr. Popsanou operační technikou jsme schopni dosáhnout, přes vysokou míru technické obtížnosti zákroku, velmi vysokého procenta úspěšnosti. Operační technika je tedy s ohledem na charakter výkonu relativně bezpečná a reprodukovatelná.

Abstract

Age-related macular degeneration (AMD) is the leading cause of practical blindness in developed countries. AMD is one of many retinal diseases that arise from the absence and/or dysfunction of the retinal pigment epithelium (RPE). There are two main types of VPMD (wet and dry), which differ in etiopathogenesis and ophthalmological findings. To date, therapy is only possible for the wet form of AMD, where neovascularization permeating from the choroid and subsequent oozing or bleeding in the subretinal space with deterioration of rod and cone cells and other neuronal cells occurs. Neovascularization can be partially prevented by repeated intra-vitreal applications of anti-VEGF agents. Without treatment, the result is a disciform retinal scar and irreversible visual impairment. A current trend in the treatment of AMD is the attempt to introduce innovative surgical procedures that have the potential to improve severe ophthalmic morbidity, particularly in non-responders to pharmacological therapy.

The aim of this study was to evaluate the success rate and optimize a surgical procedure that allows for controlled and safe transplantation of RPE cells.

The success of transplantation of RPE cells in the form of an epithelium that acts as a selective barrier immediately after transplantation is dependent on the choice of the carrier. The optimal cell carrier allows for a firmer transplanted cell sheet and better handling of vulnerable RPE cells.

In the preoperative period, the cells to be transplanted are cultured on the chosen carrier and the finished product is implanted into the subretinal space (in our case, in a porcine model). The characteristics of the carrier (composition, thickness, dimensions and shape) had to be adapted to the implantation tools for the surgical procedure. The optimization of the carrier characteristics in relation to successful implantation was the focus of the first phase of the project. In the postoperative period, the success of the surgical procedure was evaluated by fundus-camera examination, optical coherence tomography (OCT) and histopathology.

As a result of our project, an oval-shaped nano-carrier (5.2mm x 2.1mm) was implanted in 18 live animals (29 eyes in total) with an overall success rate of 93.1%. Four cases (13.7%) had

perioperative retinal detachment (in 2 cases the retina was successfully reattached, in the other 2 cases the detachment was associated with massive perioperative subretinal hemorrhage and the surgery was terminated). In 4 cases, the optical media became cloudy in the postoperative period and follow-up examination was not possible (however, histological examination showed a healthy and reattached retina without signs of inflammation or other damage and these eyes were therefore included in the group of successful operations).

Conclusion. With the described surgical technique we are able to achieve, despite the high degree of technical difficulty of the procedure, a very high success rate. Thus, the surgical technique is relatively safe and reproducible with respect to the nature of the procedure.

1. Úvod

Předkládaná disertační práce je souborem 5 publikací zaměřených na implantaci nosiče pro buňky retinálního pigmentového epitelu do subretinálního prostoru u miniprasat. První studie popisuje prvotní implantát kruhového tvaru a jeho základní vlastnosti. Druhý článek je článkem přehledovým, zabývající se inovativními postupy v léčbě sítnicových onemocnění. Tématem třetí publikace je porovnání komerčně dostupných nosičů pro buňky RPE s naším nanovlákenným nosičem. Čtvrtá publikace již popisuje první výsledky implantace nosiče s primárními lidskými buňkami RPE a konečně poslední, pátá, studie popisuje náš operační postup a jeho úspešnost napříč všemi použitými buňkami s novým nosičem, což je primární cíl mého postgraduálního studia.

2. Přehled současných poznatků

2.1 Anatomie, histologie, fyziologie a patofyziologie RPE

Oční koule je složena ze tří vrstev. Tunica fibrosa je zevní vrstva složená z rohovky a skléry. Tato vrstva tvoří vlastní stěnu oka, v případě rohovky se také podílí na refrakčních vlastnostech optického aparátu oka. Střední vrstva, tunika vasculosa, se skládá z cévnatky, řasnatého tělesa a duhovky. Jedná se o vysoce vaskularizovanou vrstvu s mnohými funkcemi zajišťující mimo jiné výživu (cévnatka), regulaci tlaku oka (řasnaté těleso) nebo třeba regulaci množství světla dopadajícího na sítnici (duhovka). Tunica nervosa, vnitřní vrstva oka je tvořena samotnou sítnicí a retinálním (ev. duhovkovým) pigmentovým epitelem. Sítnice obsahuje specializované nervové buňky sloužící k detekci světla (tyčinky a čípky) a dále ohromné množství buněk zajišťujících modulaci výsledného signálu a přenosu do centrálního nervového systému (CNS), stejně jako množství buněk podpůrných. Retinální pigmentový epitel se nachází pod sítnicí spočívající na své bazální membráně (Bruchova membrána) OBR1. Jedná se o epitel tvořený cylindrickými buňkami hexagonálního průřezu. Bazální část lpí pevně při Bruchově membráně, postranní membrány buněk obsahují četná buněčná spojení typu zonulae occludentes et adherentes. Morfologický nález tedy ukazuje výraznou apikobazální

orientaci s pokročilou funkcí oddělovat neuroretinu od cévnatky. Rozdíl v elektrickém potenciálu nad a pod RPE lze měřit jako transepiteliální resistenci (TER). Hodnotu TER lze považovat za indikátor kvality RPE.

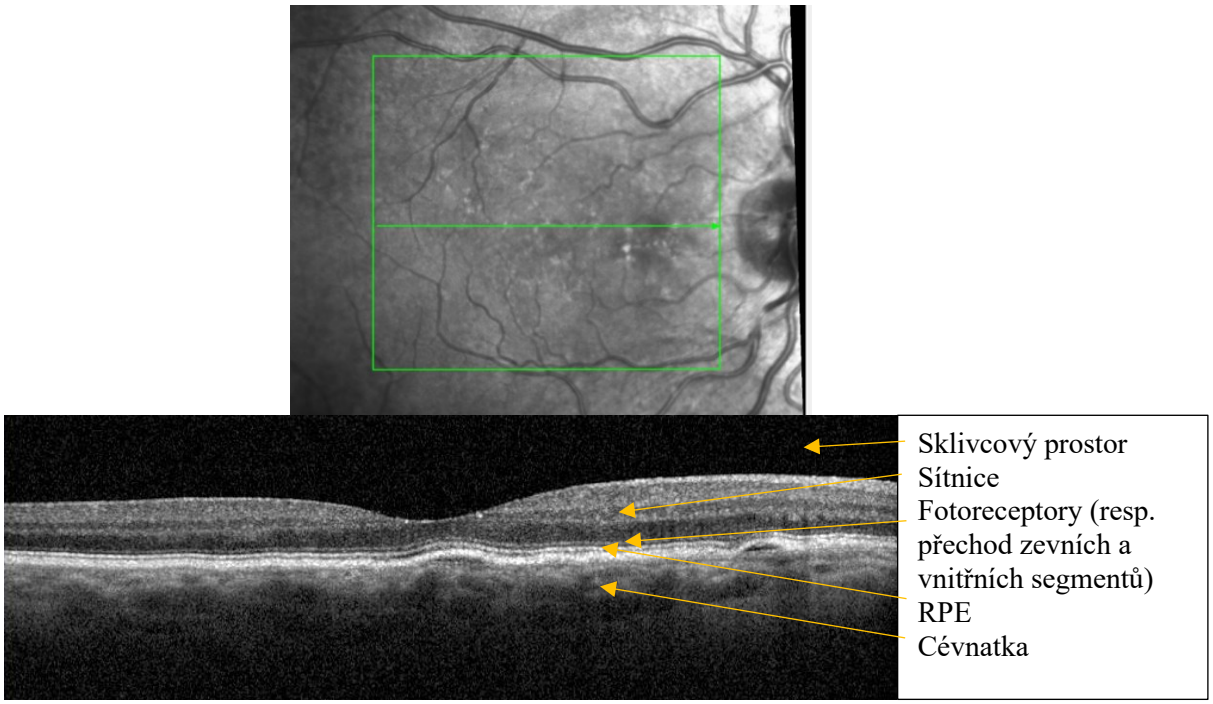

OBR 1: náhledový snímek z OCT vyšetření. Nahoře foto zadního pólu, dole sken OCT s popisem nejdůležitějších částí zadního segmentu oka

2.2 Vyšetřovací metody RPE

Sítnice je pro svoji unikátní polohu a dobrou vyšetřitelnost velmi oblíbeným cílem inovativních postupů jako například genové terapie, optogenetiky, buněčné terapie nebo bioniky. V dnešní době máme možnost sítnici, a potažmo tedy RPE, snadno vyšetřit včetně vedení fotodokumentace s aplikací nejrůznějších filtrů akcentujících požadovanou tkáň či patologii.

2.2.1 Barevné foto

Funduskamera (sítnicová kamera) je digitální fotoaparát uzpůsobený k zachycení sítnice. Dříve vyžadovalo pořízení snímku úzké výseče sítnice arteficiální mydriázu, dnes existují i přenosné širokoúhlé kamery umožňující snímkování bez mydriázy. OBR 2

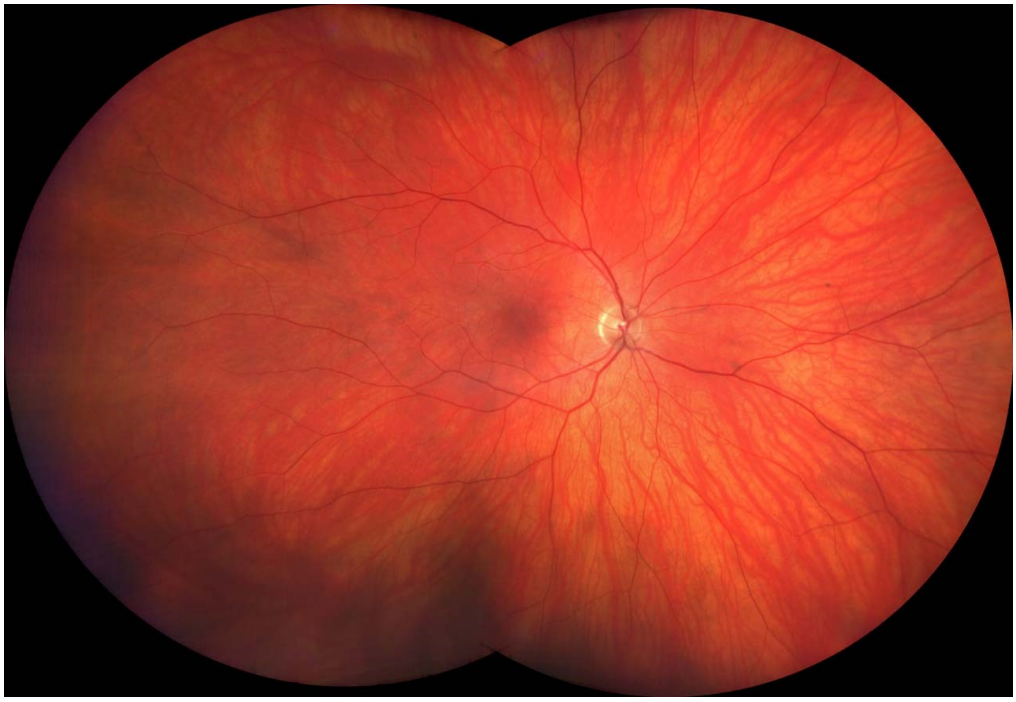

OBR 2: složený snímek očního pozadí z kamery Zeiss Clarus 700 (zdroj: https://www.zeiss.com/meditec/int/product-portfolio/retinal-cameras/zeiss-clarus-700.html)

2.2.2 Autofluorescence fundu

Jedná se o modifikaci barevného fota sítnice zachycující fluorescenci emitovanou endogenními intracelulárními fluorofory, která odráží stav, a do jisté míry i funkci, RPE.

2.2.3 Angiografie

Jedná se o vyšetření s použitím kontrastní látky ozřejmující průtok retinálním a choroidálním řečištěm a detekujícím poruchy ve vnitřní či zevní hematookulární bariéře.

2.2.4 OCT

Naprostý zlom v diagnostice sítnicových onemocnění přineslo vyšetření OCT. Snímek z OCT nám přináší prakticky „in vivo histologický snímek" centrální části sítnice bez nutnosti s okem jakkoliv manipulovat. Jedná se o vyšetření bezkontaktní, rychlé a pro pacienta i personál jednoduché. OBR 1. Dalším posunem pak je nadstavba OCT v podobě OCT angiografie, kdy přístroj umožňuje zobrazení cévního řečiště sítnice a tím umožňuje odhalení některých patologií, jako např. vlhké formy VPMD, OBR 3.

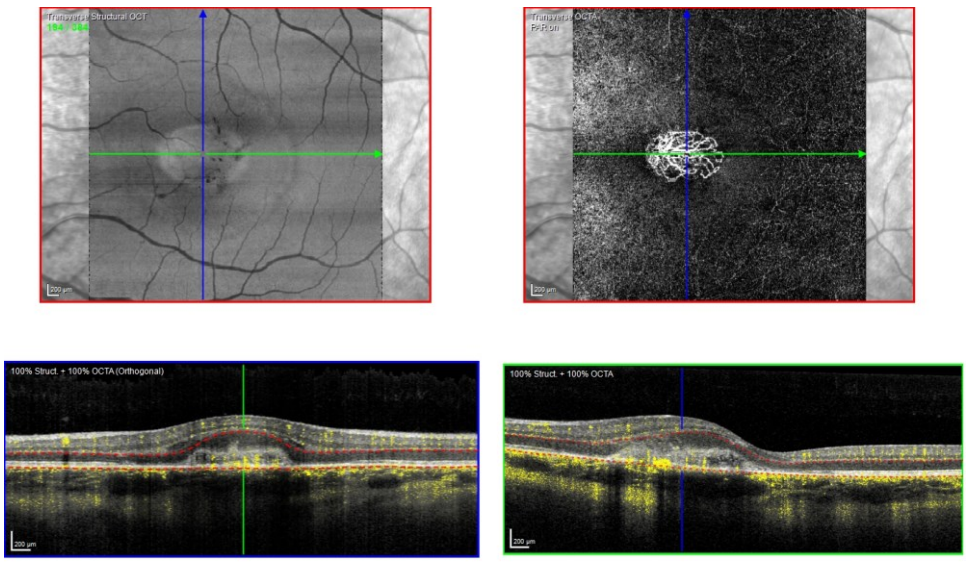

OBR 3: Angio-OCT. Na snímku nahoře vpravo je patrna klasická CNV, dole jsou umístěny odpovídající skeny sítnice ve vertikálním a horizontálním řezu.

2.3 Základní klinické jednotky spojené s dysfunkcí RPE

Věkem podmíněná makulární degenerace (VPMD), Stargardtova choroba nebo například retinitis pigmentosa. Ač odlišné klinické jednotky, ve všech těchto případech nacházíme poškození retinálního pigmentového epitelu (RPE)[1)], které následně vede k ireverzibilní ztrátě nervových buněk sítnice a zhoršení zrakových funkcí.

VPMD je sama o sobě nejčastější příčinou praktické slepoty ve vyspělých zemích [2)]. VPMD je charakterizována změnami v místě nejostřejšího vidění (makula). Z počátku dochází ke kumulaci odpadních produktů metabolismu fotoreceptorů/ buněk RPE. To vede k tvorbě drůz

subretinálně a ev. atrofizaci v případě suché formy VPMD nebo ke zvýšené produkci VEGF a následné tvorbě nových, patologických, cév (CNV) mezi RPE a sítnicí s tendencí k extravazaci tekutin a ev. krvácení či tvorbě fibrovaskulárních komplexů s navazujícím poškozením sítnice a progresí do praktické slepoty. Hlavním rizikovým faktorem pro rozvoj VPMD je, tak jak název napovídá, věk. VPMD se vzhledem k demografickým datům v celé Evropě, stává závažným socioekonomickým problémem [3)].

2.4 Současné možnosti terapie VPMD

Přes historicky vyšší množství různých léčebných přístupů v léčbě VPMD dnes prakticky využíváme pouze omezené množství léčebných modalit. K léčbě suché formy VPMD t.č. bohužel nemáme k dispozici žádnou léčebnou modalitu. Naštěstí, přestože suchá forma VPMD tvoří přibližně 90 % případů, je zodpovědná pouze za 10 % pacientů s praktickou slepotou. Progresi tohoto typu onemocnění lze zpomalit pomocí doplňků stravy s obsahem luteinu [4)]. Vlhká forma VPMD tvoří pouze asi 10 % pacientů s VPMD. Bohužel se jedná o formu agresivní, která může v průběhu měsíců vést k výraznému zhoršení zrakových funkcí a je zodpovědná za přibližně 90 % pacientů s praktickou slepotou v rámci VPMD. Na léčbu vlhké formy VPMD se nyní zaměřujeme především. Historicky se zkoušely různé formy chirurgických zákroků (např. extrakce CNV) nebo laserové ošetření CNV lokalizovaných mimo makulární oblast. Jednalo se však o zákroky destruktivní s vysokým podílem nežádoucích účinků. Prvním milníkem bylo zavedení fotodynamické terapie (PDT), kdy se do žíly pacienta injektovala fotosenzitivní látka, která v místě extravazace (narušené hematookulární bariéry) reagovala s laserovým paprskem a způsobila termické poškození dané cévy a její následnou konstrikci. PDT byla první léčebná modalita s nadějí na stabilizaci vizu [5)]. Revolucí pak byl příchod preparátů blokujících VEGF. Prvním registrovaným preparátem pro oční využití byl LP Macugan a následně LP Lucentis. Právě LP Lucentis znamenal obrat v prognóze „praktické slepoty“ k „šanci na zlepšení“ a pacienti poprvé začali získávat písmena na optotypech po zahájení léčby [6)]. Všechny nyní dostupné anti-VEGF preparáty jsou dostupné ve formě

intravitreálních léčiv (aplikovaných injekčně do sklivce) a je nutné aplikaci opakovat v závislosti na aktivitě onemocnění (ideálně se udává přibližně 7 aplikací za rok).

2.5 Operační techniky zadního segmentu oka

Základním operačním výkonem v léčbě onemocnění sítnice je pars plana vitrektomie (PPV). Jedná se o metodu podobnou laparoskopii, kdy do oka vstoupíme většinou třemi malými otvory (25 gauge, cca 0.5 mm). Jeden otvor slouží pro infuzi (stabilizace tlaku během operace) a další dva jsou pracovní. Jeden pro světlo a druhý pro pracovní nástroj. Dovnitř oka hledíme pomocí mikroskopu a systému čoček skrz rohovku a vlastní čočku po navození arteficiální mydriázy. OBR 4

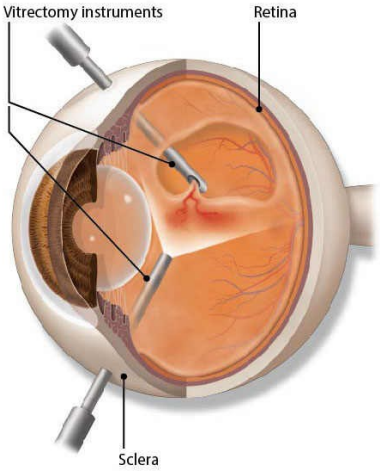

OBR 4: schéma pars plana vitrektomie, obr. https://www.aao.org/eye-health/diseases/vitreomacular-traction-treatment

V průběhu tohoto zákroku odsajeme sklivec (samotná vitrektomie) a následně můžeme postupovat dále dle dané patologie od použití laseru, přes mechanické sloupnutí membrán na sítnici (peelinig) po provedení odchlípení sítnice od RPE a vložení arteficiálního implantátu. S nástupem PPV byly ostatní chirurgické metody pro léčbu sítnicových onemocnění potlačeny na minimum.

2.6 Slibné přístupy v léčbě sítnicových onemocnění

Retinální protézy

Jedná se o zařízení, která jsou schopna přeměnit světelný signál přicházející do oblasti oka na elektrický stimul přes zařízení umístěné na sítnici. Typickým cílem stimulace nejsou fotoreceptory, které většinou vlivem onemocnění chybí, ale některé výše uložené buňky, jako jsou retinální bipolární buňky (RBCs) a retinální gangliové buňky (RGCs). Částečně je tak narušeno zpracování signálu samotnou sítnicí, kdy je přenos signálu z fotoreceptoru na bipolární buňku a následně gangliovou modifikován velkým množstvím dalších faktorů jako např. amakrinními či horizontálními buňkami (tzn. processing). Retinální protézy se většinou dělí podle umístění na epiretinální, subretinální a suprachoroideální. Epiretinální protézy (OBR 5 A) jsou výhodné z hlediska snazšího operačního přístupu a snadné aktivace gangliových buněk. Naopak nevýhodou je zcela nekontrolovatelné zpracování obrazu sítnicí, kdy jsou kromě samotných gangliových buněk aktivovány často i okolo ležící axony, a signál tak nevypadá jako světelný bod [7)]. Opačným příkladem jsou subretinální protézy (OBR 5 B). Zde se musíme připravit na náročnou operační techniku, nicméně aktivovány jsou zbývající fotoreceptory, ev. RBCs, a signál tedy neobchází zpracování v sítnici [8)]. Suprachoroideální implantáty jsou používány méně, především pro operační náročnost a větší vzdálenost elektrod od sítnice (OBR 5 C).

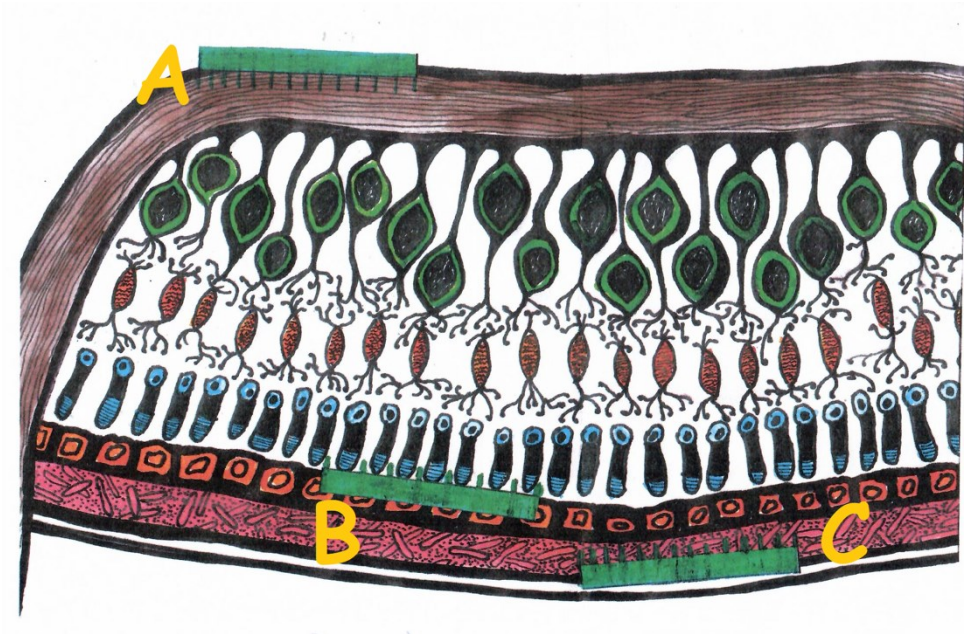

OBR 5: možnosti umístění retinálních protéz ve vztahu k sítnici

Dnes jsou nejčastěji prezentovány implantáty Argus II (Second Sight, Sylmar, USA), Alpha AMS (Retina Implant AG, Reutlingen, Německo) a Photovoltaic Retinal Implant (PRIMA) Bionic Vision System (Pixium vision, Paříž, Francie).

Nejrozšířenějším implantátem je Argus II, který již byl implantován více než 200 pacientům. Jedná se o epiretinální implantát s elektrodami umístěnými v šesti řadách po deseti. Jde o kameru připevněnou na speciálních brýlích generující signál, který je modulován v externím zařízení. Následně je radiofrekvenčně přes cívku přenesen do subkonjuktiválně uloženého příjímače, který se dále přenáší transsklerálně k samotnému implantátu stimulujícímu sítnici [9)]. Nejlepší dokumentovaná zraková ostrost byla pouze 20/1260, nicméně implantát výrazně zlepšil orientaci pacienta v prostoru či například v hledání předmětů na stole [10)]. Mezi nejčastější nežádoucí události patří eroze či dehiscence spojivky, domnělá endoftalmitida nebo hypotonie oka. Byly také hlášeny případy vnímaného nesouladu fixního obrazu z kamery s pohybem očí mimo přímý směr.

Genová terapie

Možnost stanovení diagnózy na úrovni genu a klinické testování nových cílených terapií umožnily vznik geneticky zaměřené klinické péče v oftalmologii. Terapie založené na znalosti genetické příčiny onemocnění představují zcela nový přístup. Oko je vzhledem ke snadné dostupnosti, malým rozměrům, imunologickému privilegiu, kompartmentalizaci a možnosti kontralaterální kontroly ideálním cílovým orgánem pro klinické hodnocení. Genová terapie je léčebný postup, při němž je do genomu buněk vnesen genetický materiál, který nahrazuje nebo ovlivňuje expresi proteinu účastnícího se patogeneze konkrétního onemocnění[11)]. K vývoji a využití genové terapie je třeba určit gen odpovědný za vznik onemocnění a znát jeho funkce. Pokud je příčinou onemocnění nedostatek produktu mutovaného genu, stačí začlenit normální sekvenci genu do genomu příslušných buněk nebo vnesením terapeutického genu zmírnit projevy onemocnění. Pokud však patologicky působí pozměněný produkt mutovaného genu charakteru aberantního proteinu, je nutné mutovaný gen buď zablokovat, nebo ho opravit OBR 6. Zároveň léčba nesmí mít negativní dopady na životně důležité funkce organismu. [12, 13)]

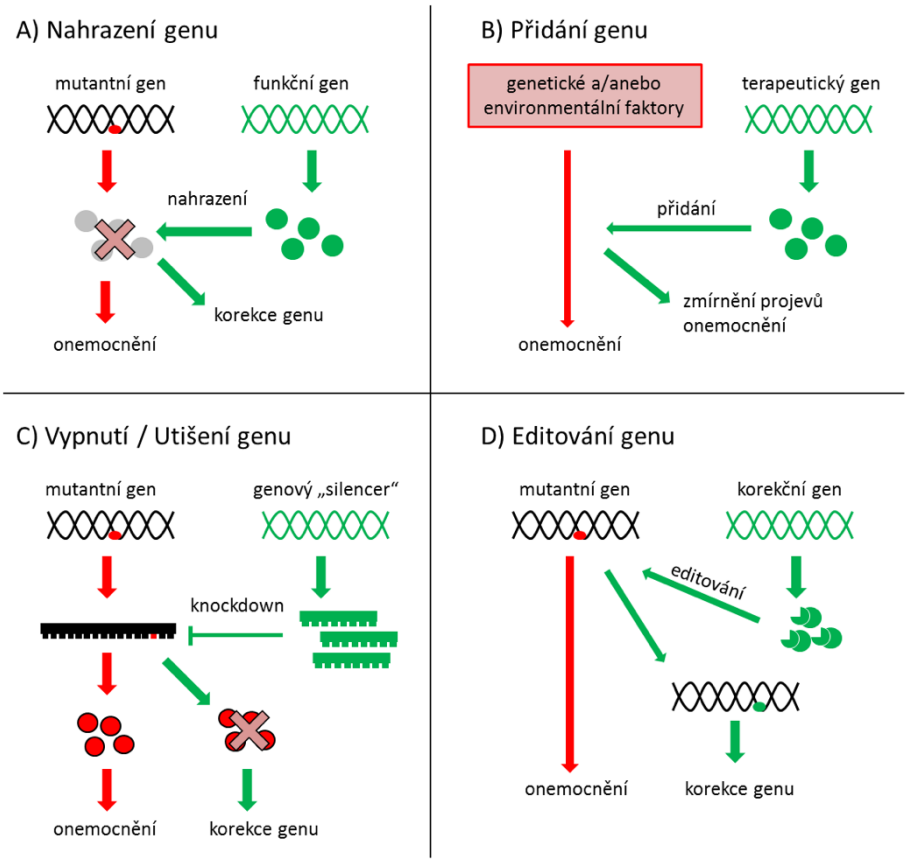

OBR 6: základní možnosti genové terapie

Genovou terapii lze provádět buď in *vivo, kdy* jsou cílové buňky po celou dobu léčby součástí organismu, nebo in vitro, k*dy jsou* cílové buňky z těla organismu odebrány a po provedení léčby vráceny na původní místo[14]. Podmínkou úspěchu je aplikovat léčbu v tzv. terapeutickém okénku, kdy ještě nedošlo k nevratnému poškození tkáně.

Genetická informace se přenáší do cílových buněk pomocí nosičů zvaných vektory. Ideální vektor by měl pronikat do velkého počtu cílových buněk a exprese vneseného genu by měla probíhat po dostatečně dlouhou dobu, aby bylo dosaženo požadovaného terapeutického účinku. Vektor navíc nesmí být pro cílové buňky toxický či vyvolávat u příjemce nežádoucí účinky, jakými jsou virové infekce či autoimunitní reakce[15].

Při léčbě onemocnění sítnice se k aplikaci vektorů nejčastěji využívají intravitreální a subretinální injekce. Aplikace do sklivce je sice pro sítnici méně invazivní, ale přenos DNA

probíhá zejména ve vnitřních vrstvách sítnice, tedy v Müllerových a gangliových buňkách. Bariéru průniku vektorů a léčiv do větší hloubky sítnice tvoří vnitřní limitující membrána a další sítnicové vrstvy. Pro aplikaci virových vektorů do vrstvy fotoreceptorů a vrstvy buněk RPE je vhodnější subretinální aplikace, kdy je vektor injikován do puchýřku mezi uvedenými vrstvami, a je tak s nimi v těsném kontaktu[16)].

Mezi prvními byla pro genovou terapii navržena Leberova kongenitální amauróza 2 (LCA2), a to hlavně díky časné manifestaci onemocnění, relativně dlouho zachované struktuře sítnice a dostupnosti zvířecích modelů [17)]. LCA2 je autozomálně recesivní choroba vznikající na podkladě mutací v genu RPE65[18)].Tento gen je téměř výlučně exprimován v RPE, kde se podílí na recyklaci opsinu a rodopsinu. Nedostatečná funkce nebo absence RPE65 následně vede k degeneraci foto*recept*orů. Gen RPE65 byl od roku 2007 klinicky testován při *z*kouškách s genovou terapií, které vyústily v roce 2017 ve schválení první genové terapie pro klinickou oftalmologickou praxi americkým Úřadem pro kontrolu potravin a léčiv a v roce 2018 Evropskou lékovou agenturou[19)].

Optogenetika

V nejširším slova smyslu je optogenetika definována jako technika, při které je pomocí vektoru do neuronové buňky vnesen gen kódující protein senzitivní na světlo, s jehož pomocí je následně cílová buňka excitována. V očním lékařství se typicky jedná o vložení světločivého proteinu do některé ze subpopulací buněk sítnice [20)], které primárně nemají světločivou funkci OBR 7.

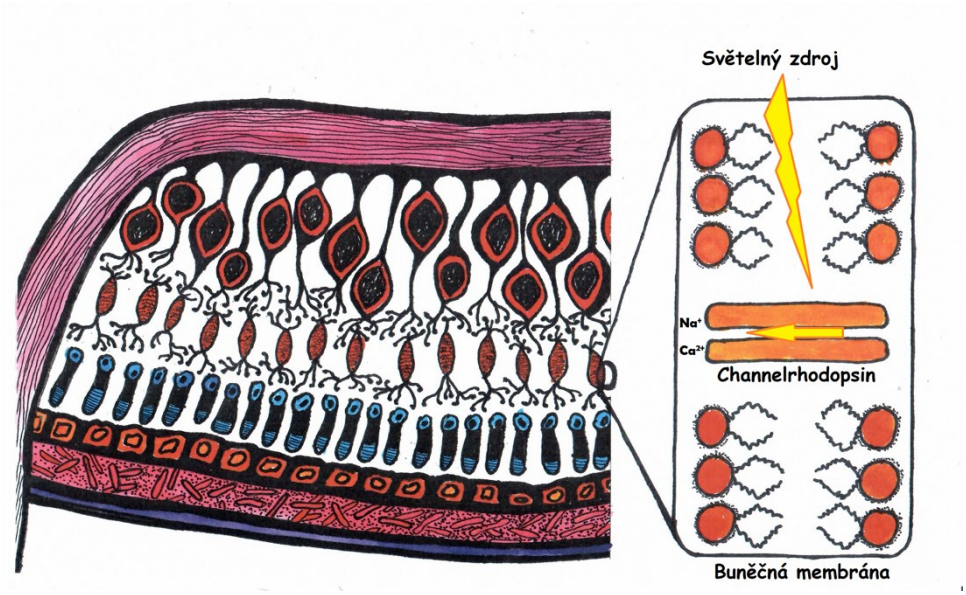

OBR 7: princip optogenetiky

V praxi je nejdříve třeba najít vhodný fotosenzitivní protein, který následně vložíme do vhodného vektoru (nejčastěji adenovirového) a zacílíme na správnou buňku. Posledním krokem je odpovídající „osvícení“ takto ošetřené sítnice.

Jako světločivý protein lze využít například dva typy opsinu: typ 1 (mikrobiální) nebo typ 2 (zvířecí). Nejčastěji se využívá typ 1, který má mnoho poddruhů, ale v zásadě se vždy jedná o iontový kanál, který lze aktivovat světlem (např. channelrhodopsin, halorodopsin, archeorhodopsin)[21)]. Po aktivaci iontového kanálu dochází ke změně v polarizaci buňky a následně k přenosu signálu dále. Typ 2 je fotosenzitivní protein spřažený s G-proteinem. Po aktivaci probíhá intracelulární signální kaskáda chemických přeměn s výsledným otevřením spřaženého kationtového kanálu. Hlavní výhodou typu 1 oproti typu 2 je jednodušší molekula obsahující přímo iontový kanál, nevýhodou pak často vyšší nároky na intenzitu světla nutnou ke změně polarizace buňky.

V lidské sítnici nalézáme více než sto různých druhů neuronálních buněk [22)], které spolu do určité míry interagují, a tím zajišťují komplexní zpracování obrazu ještě před odesláním signálu dále do centrální nervové soustavy prostřednictvím axonů gangliových buněk. Veškeré snahy o nedodržení přirozeného postupu fotoreceptor-bipolární buňka-gangliová buňka proto

povedou k narušení sítnicového zpracování obrazu, a tím ke snížení jeho kvality. Naše snahy proto vždy cílí na co nejzevnější vrstvy sítnice[23)]. Je možné užít poškozené fotoreceptory, které již nemají zevní segmenty (zde je výhodou zachované zpracování signálu sítnicí), nebo při obejití tohoto mechanismu, rovnou bipolární a ev. gangliové buňky.

Posledním krokem je zachycení světla ošetřenou buňkou. Různé kanály jsou citlivé na různé vlnové délky světla. To je třeba mít na zřeteli s ohledem na možnost fototoxicity. Například channelrhodopsin je nejcitlivější v krátkých vlnových délkách a vyžaduje, tak jako většina kanálů typu 1, větší počet zásahů fotony. To spolu s nižším podílem modrého světla, obzvláště za zhoršených světelných podmínek, a nižší propustností těchto vlnových délek optickými prostředími oka vyžaduje pro správné fungování nutnost vyšší intenzity světla v těchto vlnových délkách[24)]. Toho lze dosáhnout pouze pomocí externího světelného zdroje, což může mít nepříznivý vliv v důsledku fototoxicity.

2.7 Buněčná terapie

Jak již bylo řečeno dříve, v dnešní době sice umíme pacienty s VPMD léčit, ale neumíme je vyléčit. Dalším zlomem v léčbě onemocnění sítnice by mohlo být nahrazení defektních buněk buňkami novými. V posledních letech se těmito postupy zabývá mnoho výzkumných pracovišť, jelikož důkazy ověřující koncept (proof-of-concept) jsou obecně přijímány[25, 26, 27)].

Na počátku výzkumu stála snaha o autologní transplantace (např. autologní RPE-choroidální štěp nebo subretinální injektáž suspenze autologních buněk RPE) či snaha o makulární translokace. Přestože někteří autoři popsali částečné zlepšení zrakových funkcí[28)], v klinické praxi tyto zákroky nejsou rozšířeny pro vysoký výskyt nežádoucích komplikací (krvácení, proliferativní vitreoretinopatie, odchlípení sítnice, distorze obrazu u makulární translokace, špatná apikobazální orientace u suspenze buněk)[29,30,31)].

Pokrok v operačních technikách a buněčné biologii nyní nabízí možnost transplantovat i jiné než autologní buňky. Nejčastěji se v literatuře setkáváme s lidskými embryonálními kmenovými buňkami (hESC-RPE, human embryonic stem cells)[32)] a lidskými indukovanými pluripotentními buňkami (iPSC-RPE, human induced stem cells)[33)]. Buňky embryonální získáváme po fertilizacii oocytu odběrem z blastocysty, zatímco indukované pluripotentní

buňky získáváme reprogramováním somatické buňky, typicky fibroblastu[34]. Za tento objev byla v roce 2012 udělena Nobelova cena (Shinya Yamanaka, Sir John B. Gurdon). Výsledným produktem obou metod je pluripotentní buňka, kterou můžeme dále směrovat do vývoje v RPE. Hlavní výhodou při užití iPSC-RPE je to, že se jedná o autologní zdroj, proto pacienta není nutno zatěžovat imunosupresí. Naopak nevýhodou je stáří buňky (zdrojová buňka je stejně stará jako pacient, ze kterého je odebrána), stejná genetická výbava (přetrvávání případných genetických abnormalit) a dosud nejistý teratogenní potenciál (chybí dlouhodobá data)[35]. Užití hESC-RPE je výhodné především pokud je žádoucí transplantovat buňky s odlišným genetickým základem (geneticky podmíněné choroby včetně mitochondriálních), nutná je ovšem imunosuprese. OBR 8

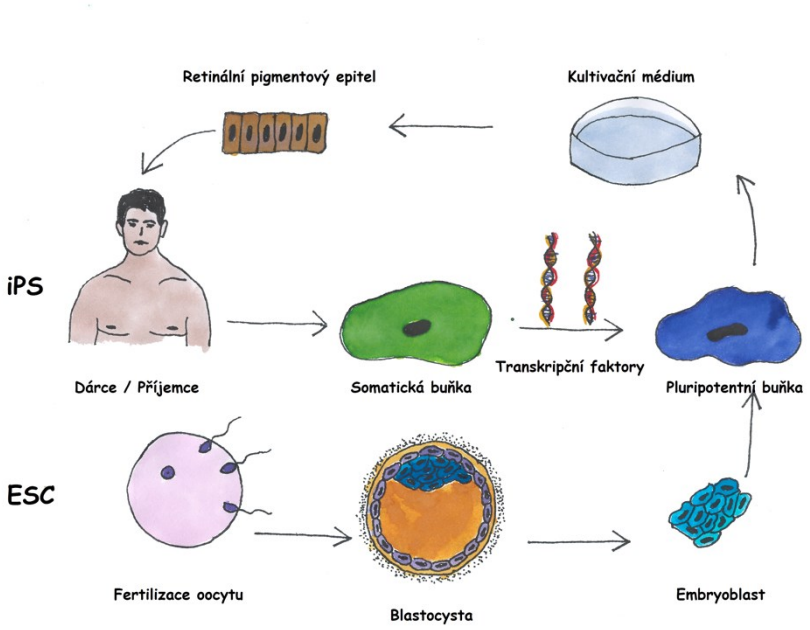

OBR 8: základní rozdíl mezi iPS a ESC

Druhým kritickým okamžikem v buněčné terapii sítnice je operační technika. Dnes jsou ve výzkumu hlavní tři směry: 1. subretinální injekce buněčné suspenze OBR 9A, 2. subretinální implantace buněčného plátu ve formě epitelu OBR 9B, 3. subretinální implantace buněčného plátu na podpůrném nosiči OBR 9C.

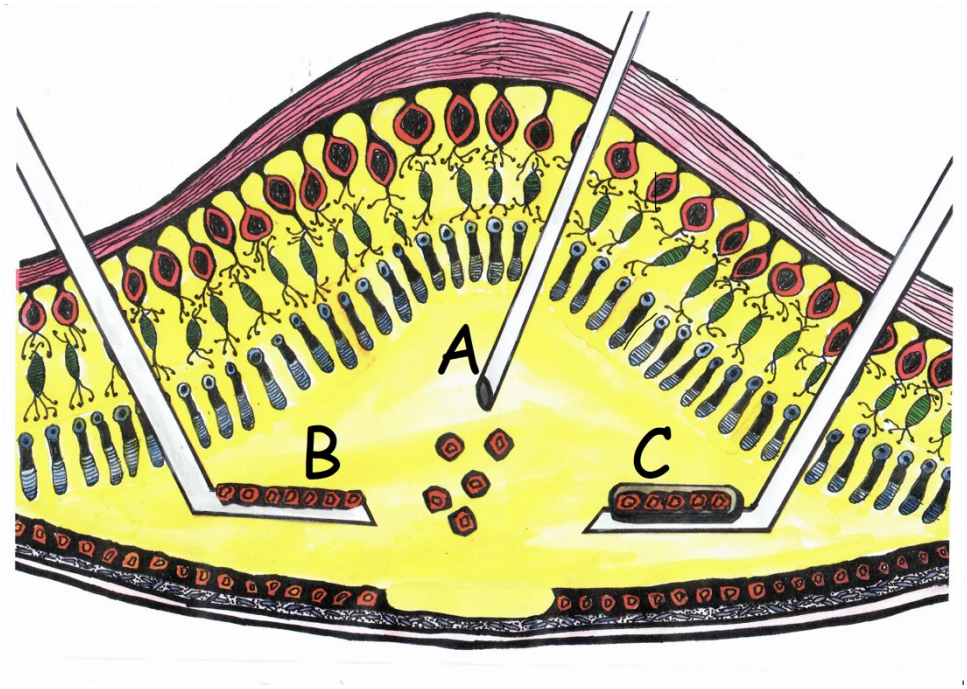

OBR 9: základní chirurgické přístupy při transplantaci RPE

Zatímco injektáž buněčné suspenze je technicky poměrně jednoduchá, nelze zcela odhadnout, zda implantované buňky budou mít správnou apikobazální orientaci a zda budou schopné vytvořit funkční monovrstvu s dostatečnou transepiteliální resistencí (TER, udává odpor měřený mezi apikální a bazální stranou epitelu, hodnota bývá považována za ukazatel integrity epitelu). Na tomto procesu se podílí mj. Bruchova membrána, která bývá u postižených často patologicky změněná[36]. Subretinální implantace buněčného plátu s nebo bez podpůrného nosiče s sebou nese náročnou operační techniku, která je však vyvážena správnou apikobazální orientací a in vitro měřitelným TER, jehož hodnoty nám mohou předem pomoci určit kvalitu implantovaných buněk. Pokud implantujeme bez podpůrného nosiče, buněčný plát se může peroperačně rolovat a buňky odlupovat. Pokud využijeme podpůrný nosič, je manipulace snazší[37], ale je třeba volit nosič dostatečně porézní, aby nebránil v difúzi živin a odpadních látek.

3. Hypotézy a cíle práce

3.1 Hypotézy

3.1.1 Subretinální implantace nanovlákenného nosiče vede k mnohým peroperačním i pooperačním komplikacím.

3.1.2 Sítnice bude na subretinální nosič reagovat zánětlivými změnami

3.2 Cíle práce

3.2.1 Optimalizace tvaru subretinálního nosiče, přizpůsobení implantační kanyly tvaru a vlastnostem nosiče bez ohledu na typ přenášených buněk

3.2.2 Optimalizace chirurgického zákroku s minimalizací nežádoucích událostí

3.2.3 Zhodnocení úspěšnosti operačního zákroku

3.2.4 Zhodnocení reaktivních změn sítnice po implantaci nosiče

4. Popis použitých experimentálních metod

4.1 Etická komise a podpora

Operace byly prováděny v souladu s Guidelines of the Declaration of Helsinki a v souladu s The Association for Research in Vision and Ophthalmology (ARVO) statement for use of animals in ophthalmic and visual research. Pokus byl schválen etickou komisí Ústavu Živočišné fyziologie a genetiky, Akademie věd ČR, Liběchov, ČR, no. 60/2016. Studie byla prováděna za podpory GAČR (Project Number 18-04393S) a TAČR (KAPPA projekt TO01000107).

4.2 Zvířecí model a operační zázemí

Implantace subretinálních nosičů byla prováděna na populaci "Liběchovských" miniprasat stáří 12-36 měsíců obou pohlaví [38)]. Operaci provádíme za hluboké celkové anestezii na očním operačním sále v rámci Ústavu Živočišné fyziologie a genetiky AV v Liběchově za pomoci očního operačního mikroskopu vybaveného pro operace na zadním segmentu Hi-R NEO 900A (Haag-Streit Surgical, Wedel, Germany) s bezkontaktním systémem čoček MERLIN BIOM (Volk, Mentor, OH, USA) a záznamovým zařízením Full HD medical 2-piece camera Sony PMW-

10MD (Sony, Tokyo, Japan), vitrektomu R-Evolution CR (Optikon, Rome, Italy) a laseru dle potřeby: zelený laser a endo sondou Merilas 532α (Meridian, Thun, Switzerland) OBR 10 a 11. V případě použití xenotransplantátu je zvíře imunosuprimované pomocí takrolimu[39]. Po zákroku zvířata pravidelně kontrolujeme. Každý den makroskopicky, zda nedochází k patologickému výtoku z oční štěrbiny, zda se zvíře nesnaží oko dřít o stěny kotce či jinak bolestivě nereaguje a zda obecně celkově prospívá. Jednou za 1-2 týdny (dle protokolu) v celkové anestézii kontrolujeme nález na operačním sále pomocí oftalmoskopu, provádíme fotodokumentaci a snímky OCT dle potřeby. Zvířata ponecháváme do kontrolního vyšetření v 1., 2., 4. nebo 8. týdnu dle protokolu a následně je prase v hluboké anestezii utraceno vykrvácením.

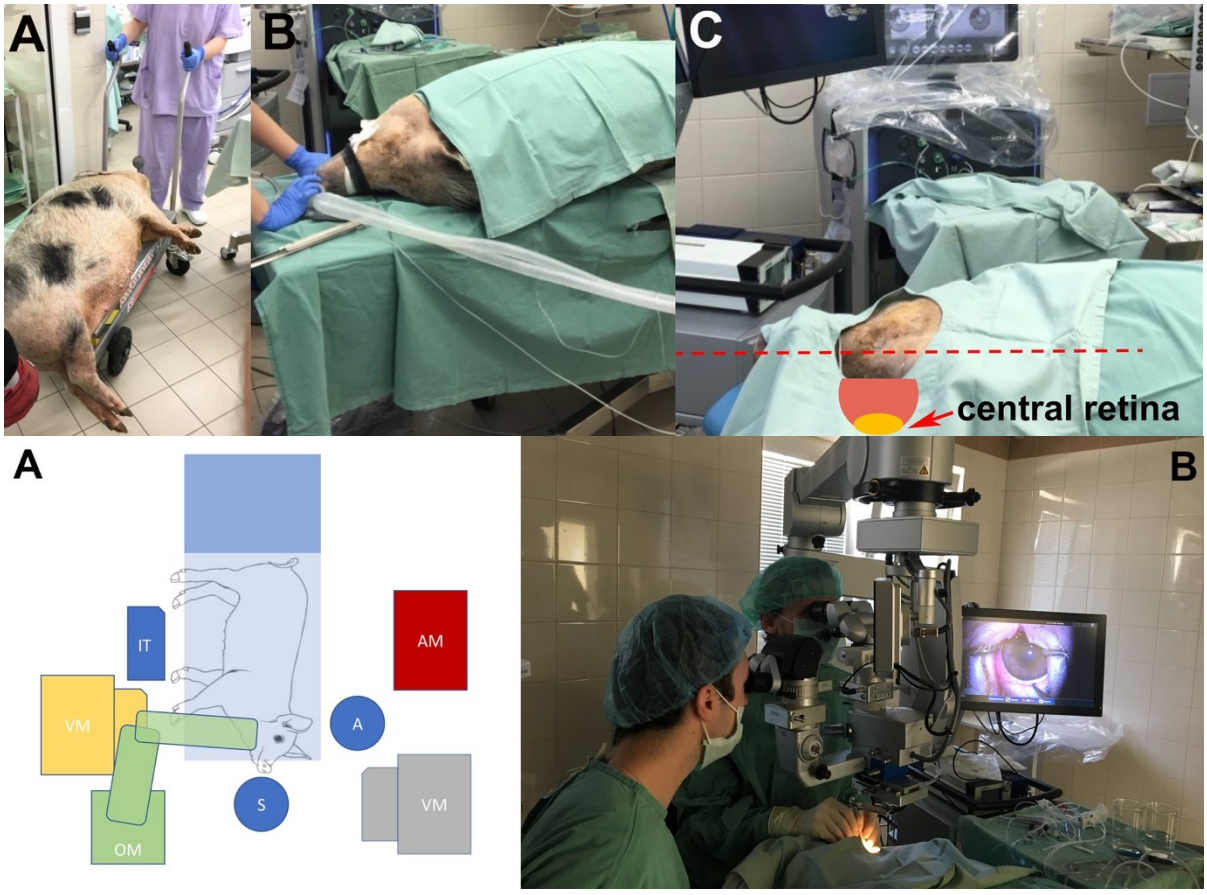

OBR 10: manipulace se zvířetem, rozmístění operačních přístrojů, foto z výkonu

4.3 Operační technika

Samotný operační výkon je detailně popsán v přiložené publikaci včetně seznamu použitých materiálů. Stručně: operační výkon probíhá za aseptických podmínek. Po zavedení 3x23 gauge portů OBR 12 provedeme zcela standartní pars plana vitrektomii s odloučením zadní sklivcové

membrány (ZSM), která se u prasat chová podobně jako u dětských pacientů – je “pastózní” a ZSM se často odlučuje “ve vrstvách”. Proto je obvykle nutné si ZSM vizualizovat pomocí např. diprofosu. Následuje vytvoření subretinálního puchýře pomocí 41 gaugové subretinální kanyly. V místě zamýšlené retinotomie provede endodiatermii a následně retinotomii pomocí retinálních nůžek. V dalším kroku provádíme peritomii a následně za postupné koagulace sklerotomii v rozsahu cca 3 mm. Vitrektomem odstraníme prolabující sklivec a ev. doplníme koagulaci dle potřeby. Nyní lze provést samotnou implantaci nosiče pomocí našeho unikátního injektoru. Následuje náročná fáze operace, kdy je třeba co nejrychleji zašít skléru ve velmi obtížných podmínkách (prasečí oko je zapadlé a rána ve skléře, na poměry oční chirurgie, veliká s protékající tekutinou z infuze). Po sutuře skléry kontrolujeme pozici nosiče, kterou můžeme ev. upravit pomocí retinální pinzety. Na závěr vyměníme vodu za vzduch s odsátím veškeré subretinální tekutiny. Provedeme výměnu za silikonový olej a následně extrahujeme vstupní porty a rány zašijeme.

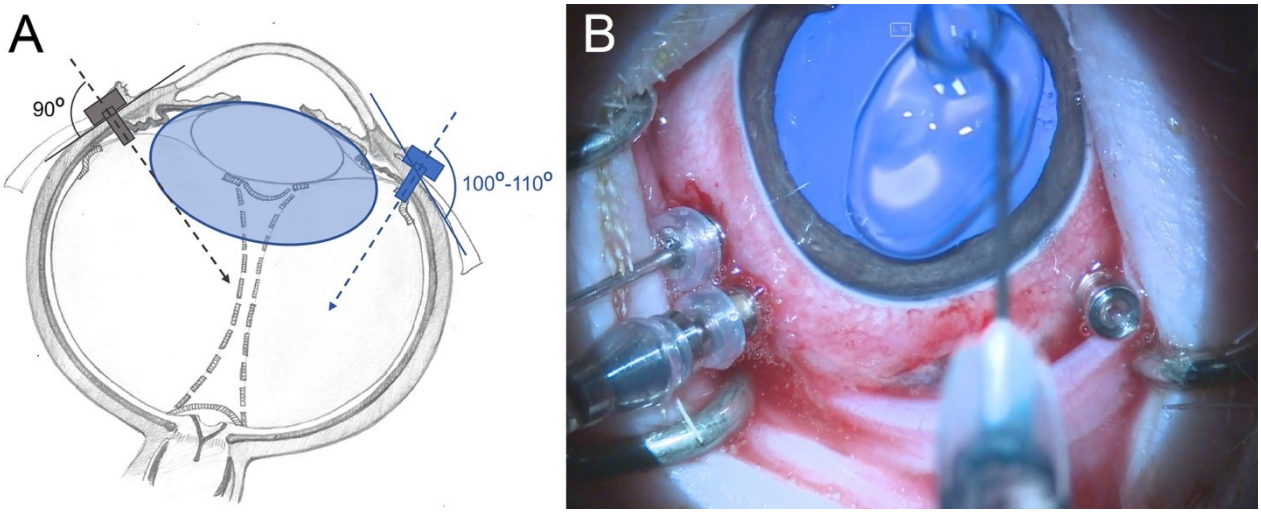

OBR 11: rozmístění 23ga portů

5. Materiál

5. 1 Nosič RPE

Jedná se nanovlákenný nosič připravovaný pomocí elektrospiningu z poly(L-lactide-co-DL-lactide) (LLA/DLLA 90/10, Mw 868 270 g/mol, PDI 2.3). Tloušťka vláken je 380um (standartní odchylka, SD 10 nm). Tato vlákna jsou vpletena do tužší periferní obruče vyříznuté laserem do požadovaného tvaru z poly (ethylen tereftalátové) (PET) folie o tloušťce 36 µm zaručující stabilitu nosiče. OBR 12. Tloušťka celého nosiče je 3.7 µm a odhadovaná porozita je 72%[40, 41].

Tím je zajištěna dobrá propustnost živin s udržením mechanické stability implantovaného produktu.

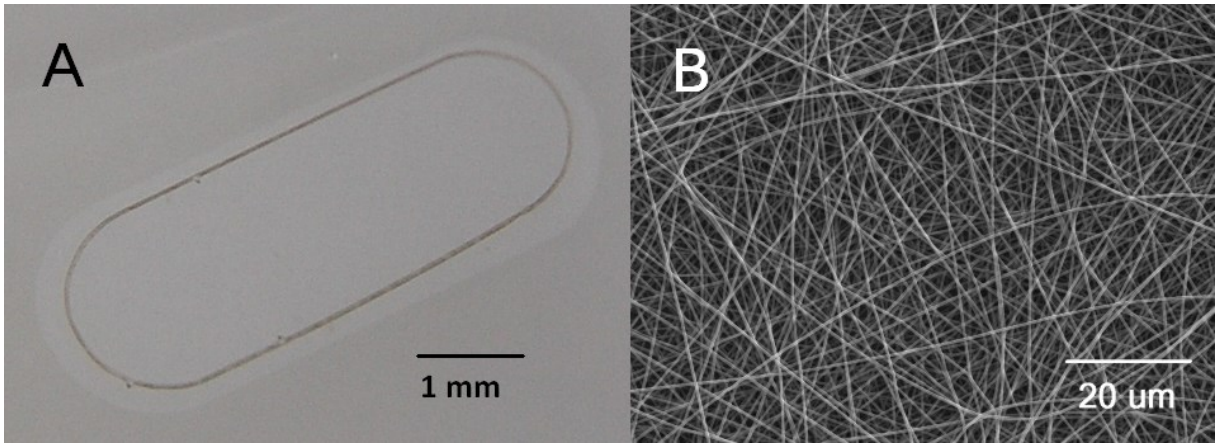

OBR 12: nanovlákenný nosič RPE

Připravený nosič se vkládá do unikátní ručně vyrobené implantační kanyly respektující anatomické vlastnosti prasečího bulbu a umožňující vizuální kontrolu nosiče během implantace OBR 13. Jedná se o průhlednou plastovou kapiláru s nakládacím okénkem v přední části. Do tohoto okénka se vloží implantát a kovovou planžetou je posunut do přechodové zóny. Takto je nástroj vložen do oka (sklivcové dutiny) a ústím přiložen k předem připravené retinotomii. Dalším tlakem na kovovou planžetu dojde k vyklouznutí implantátu do místa určení.

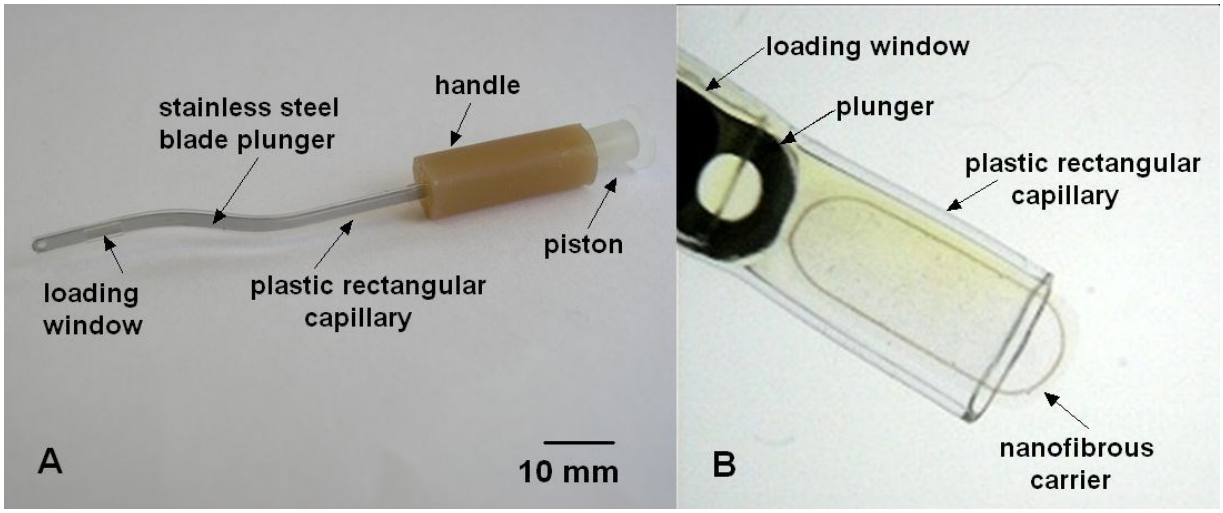

OBR 13: implantační kanyla

5. 2 Přehled původu užívaných buněk RPE

Všechny hodnocené operace probíhaly s nosičem popsaným v kapitole 5.1. Tento nosič byl implantován 1) bez buněk (2 oči), 2) s lidskými primárními RPE buňkami (13 očí), s lidskými iPSc-RPE (14 očí). Rozdíl mezi jednotlivými variantami buněk je v principu popsán v kapitole 2.7.

6. Výsledky

Výsledky subretinální implantace nanovlákeného nosič jsou shrnuty v tabulce 1

Celkem počet zvířat	18
Celkový počet očí	36
Počet operovaných očí	29
Počet úspěšných implantací	27
Počet neúspěšných implantací	2
Průměrná doba operace	57 min
Úspěšnost	93.1%

Za úspěšnou implantaci považujeme takový stav, kdy je na konci operace nosič v subretinálním prostoru, sítnice je přiložena a dokážeme posléze verifikovat pozici implantátu a stav sítnice histologií. Neúspěšný zákrok je definován jako zákrok bez implantace nosiče nebo zákrok s takovými perioperačními komplikacemi, kdy předpokládáme nevyšetřitelnost nebo bolestivost oka v důsledku těchto komplikací. Perioperačně došlo u celkem čtyř očí k odchlípení sítnice. Ve dvou případech se podařilo sítnici opět přiložit a úspěšně implantovat, v dalších dvou případech bylo odchlípení sítnice spojeno s masivním subretinálním krvácením. Operace byla ukončena a zvíře bezprostředně utraceno. Celková úspěšnost operačního zákroku tedy činila 93.1 %.

Ve sledovacím období bylo u všech zvířat provedeno OCT vyšetření spolu s fotodokumentací fundu OBR 14. Ve čtyřech případech nebylo s postupem času možné sítnici vyšetřit pro kalení nitrooční čočky (pravděpodobně důsledek perioperačního dotyku čočky s nástroji), nicméně histologie neukázala v těchto případech žádnou další abnormalitu. V místě retinotomie nebyly stopy po proliferativní reakci a samotný nosič byl dobře patrný přes semitransparentní tkáň sítnice bez známek zánětlivých změn. Na OCT nebyly patrny žádné hyper – nebo hypo-reflektivní zóny, sítnice byla pouze lehce ztluštělá oproti normě. Bruchova membrána se zdála být intaktní. Nosič se zdá být dobře tolerován i v případě, že je osazen arteficiálními buňkami RPE. Po provedení euthanasie byly bulby enukleovány a fixovány ve 4 % paraformaldehydu

po dobu 24 hodin. Přední část oka byla odříznuta a poté bylo možno vizuálně lokalizovat nosič nasálně od papily zrakového nervu. Vzorky byly zmrazeny a dále zpracovány dle předem definovaných protokolů v závislosti na typu experimentu a původu buněk.

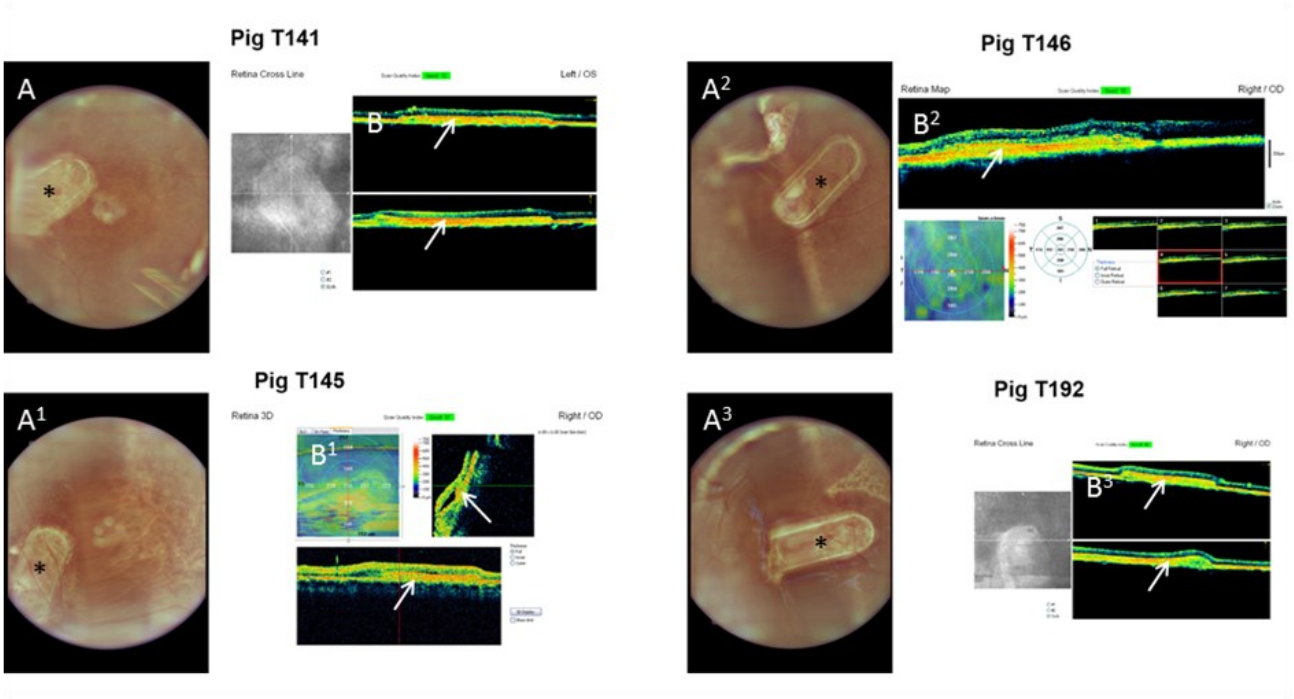

OBR 14: pooperační foto fundu a sken OCT

Na OBR 15 vidíme oblast sítnice po barvení pomocí haematoxylinu-eosinu zahrnující implantát bez buněk RPE. Morfologické změny jsou nevýrazné a zavrhují hypotézu předpokládající změny neuroretiny po implantaci nanovlákenného nosiče do subretináního prostoru na prasečím modelu.

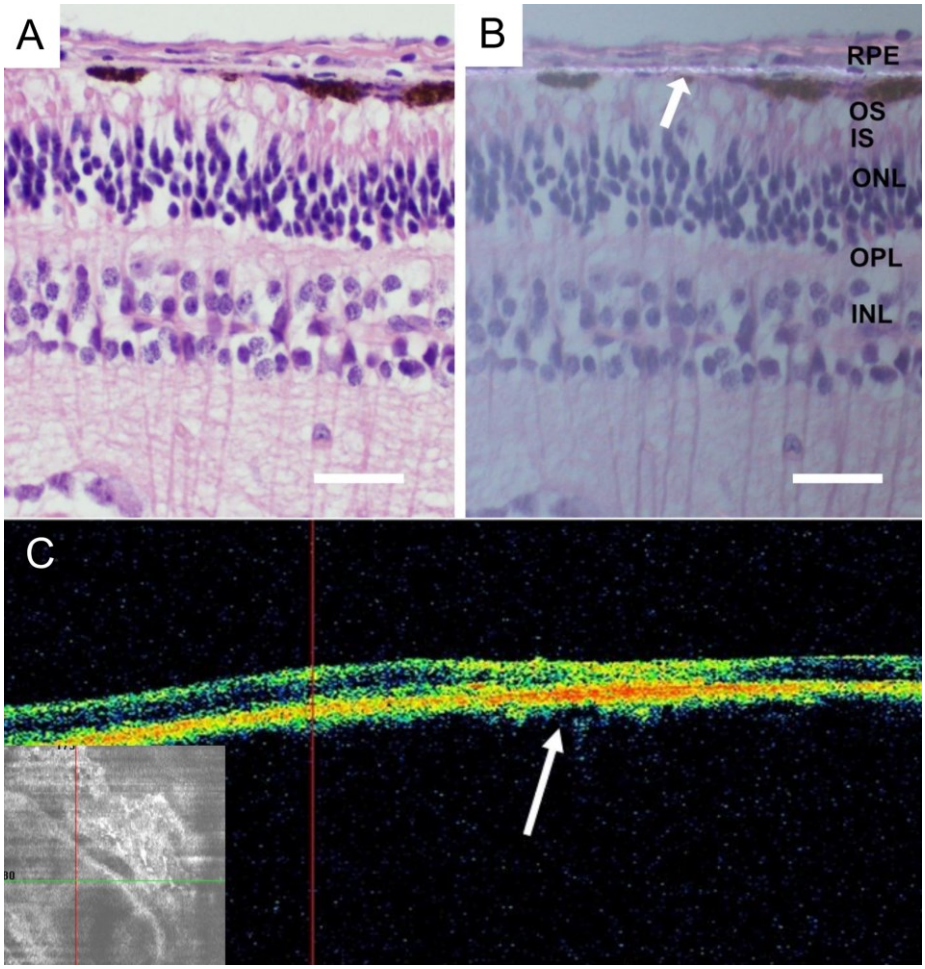

OBR15: histologické vyšetření sítnice po implantaci nosiče bez buněk RPE

7. Diskuse

Transplantace RPE různého původu se považuje za jednu ze slibných léčebných modalit budoucnosti a patří ji vysoká pozornost mnohých výzkumných skupin cílících na léčbu sítnicových degenerativních onemocnění, jako například VPMD[25, 26, 27, 40, 42, 43, 44, 45, 46, 47, 48)].

Základní myšlenkou tohoto přístupu je náhrada postiženého RPE buňkami, které jsou kultivovány in vitro a jejichž vlastnosti a kvalitu můžeme ještě před transplantací ověřit[49-53)].

Implantace těchto buněk nejrůznějšího původu na subretinálním podpůrném nosiči se zdá být nejlogičtější cestou. Dostatečně porézní nosič netvoří bariéru látkové výměny a udržuje správný tvar epitelu, zajišťuje správnou apiko-bazální orientaci a zároveň dodává dostatečnou mechanickou odolnost při samotné manipulaci s buňkami, ať už při přípravě buněk, nebo při samotném zákroku.

V současné době je při experimentech s RPE používaná celá škála experimentálních zvířat za účelem zdokonalit operační techniku a potvrdit účinnost léčby sítnicových onemocnění spojených s dysfunkcí RPE. Nejčastěji se setkáváme s experimenty na králících, prasatech, psech a primátech. Tato zvířata řadíme mezi modely s velkým okem. Do této skupiny patří i "Liběchovská" miniprasata, která primárně sloužila jako model v biomedicínském výzkumu na poli neurodegenerativních onemocnění (např. Parkinsonově nebo Huntingtonově chorobě). Tato miniprasata mají relativně velký mozek s cévním zásobením a imunologickou odezvou, která je podobná mozku člověka. Díky těmto vlastnostem jsou často považována za model první volby. Navíc, na rozdíl od primátů, je jejich chov výrazně méně finančně náročný a udržení stabilních podmínek jednodušší. V roce 2018 Shrader a Greentree publikovali podrobný popis Göttingenských miniprasat užívaných pro oční výzkum [38, 40, 54)]. Tento model je využíván již přes šedesát let vzhledem ke snadnému chovu, rozumné velikosti, dobře zmapovanému genomu a velmi podobné anatomii oku lidskému. Oko miniprasete má podobné rozměry, objem, vlastnosti sklivce, barevné vidění. Na rozdíl od lidského oka nemají miniprasata makulu a foveolu, tedy místo nejostřejšího vidění, nicméně nasálně od terče zrakového nervu se nachází "area centralis", kde je vyšší koncentrace čípků a tvoří tak zónu ostřejšího vidění. Všechny tyto vlastnosti jsou aplikovatelné i na Liběchovský druh, který je křížencem vícero druhů, včetně Göttingenského[38, 55, 56)]. Miniprasata tak postupně v preklinických oftalmologických studiích vytlačují psy a primáty.

Na základě naší rešerše není dosud jednoznačně stanovená, popsaná a obecně přijímaná operační technika popisující krok za krokem vitreoretinální postup implantace u velkých modelových očí, především pak miniprasat. Tento zákrok je vždy náročný z pohledu etického, organizačního, logistického, technického a v neposlední řadě finančního.

V roce 2015 Popelka a kolektiv popsali výsledky subretinální implantace inovativního nanovlákenného nosiče na podpůrném "kroužku" implantovaného do oka "Liběchovského" miniprasete[40)]. Tyto experimenty a chirurgická technika s injektorem vlastní výroby byly dále zlepšovány až do současné podoby v článku autorů Lytvynchuk a Straňák. V současné době máme dobře definovaný a reprodukovatelný nosič buněk i protokol pro předoperační, perioperační i postoperační péči o zvíře.

Duarri a kol. publikovali v roce 2021 výsledky subretinální injektáže suspenze buněk hiPSC-RPE na prasečím modelu s geografickou atrofií. Dle našeho názoru je však pro plnění

fyziologického účelu těchto buněk extrémně důležitá správná orientace buněk, konkrétně jejich správná apiko-bazální orientace, a forma celistvého epitelu (těsná spojení mezi buňkami). V případě injikované suspenze buněk tyto cíle nelze zaručit.

Tím se dostáváme k jednomu z nejdůležitějších aspektů buněčné terapie onemocnění asociovaných s poruchou funkce RPE a sice k náročné operační technice. Právě peroperační a pooperační komplikace definují primární úspěch či neúspěch celého projektu. Rozměry a místo sklerotomie a retinotomie by mělo být zváženo peroperačně. Jejich nevhodné umístění či rozměry mohou vést k odchlípení sítnice, hypotonii, episklerálnímu, choroideálnímu a/nebo sítnicovému krvácení stejně jako např. k vysoké míře víření tekutiny ve sklivcovém prostoru a následnému poškození nosiče. V pooperační péči nás zajímá riziko proliferativní vitreoretinopatie, endoftalmitidy, hypotonie, odchlípení sítnice a riziko progrese katarakty [26, 45, 46, 47].

V roce 2012 Stanzel a kol. publikoval nový operační postup implantace subretinálního nosiče na králících (chinchilla bastard rabbits (hmotnosti 2-2.5 kg)). Autoři měli celkovou úspěšnost transplantace 74.2 % na 23 očích[45]. Pro potřeby tohoto experimentu byla vyvinuta speciální infuzní kanyla s otvory po stranách zajišťující rovnoměrnější plnění sklivcové dutiny tekutinou (prevence přímého vodního proudu do oblasti implantace a nižší riziko tvorby amoce a kolapsu připraveného sítnicového „puchýře“ před implantací). V naší práci jsme tyto rizika i s běžnou infuzní kanylou nezaznamenali. Možné vysvětlení je použití zvířete s větším okem a také provedení jádrové vitrektomie s ušetřením zbylého sklivce v místě infuze, který tak mohl proud tekutiny „brzdit“. Dalším občasným problémem u autorů Stanzel a kol. bylo uvíznutí implantátu v injekční kanyle, což autor vysvětluje možným uvíznutím zbytku sklivce na povrchu sítnice, který se následně dostal do kanyly. Toto bylo částečně redukováno enzym-asistovanou vitrektomií (ještě před samotným zákrokem se injikovala do sklivce látka narušující jeho celistvost). Ve většině případů pak ještě autoři posouvali nosič dále od retinotomie pomocí dalších instrumentů. I v naší studii docházelo občas k zaseknutí nanovlákna mezi posuvnou planžetu a stěnu injektoru a nosič tak mohl být přichycen k injektoru a vytahován zpět směrem do sklivcového prostoru. Tato komplikace se nicméně vždy vyřešila jemným zastrčením implantátu zpět do subretinálního prostoru pomocí světelné sondy. Zbytková vlákna sklivce v místě retinotomie jsme nezaznamenali. V našem souboru byla často využívána možnost nabarvení ZSM pomocí triamcinolonu. Takto vizualizovaná ZSM byla s naprostou jistotou odloučena a sklivec se již dále na zadním pólu oka nenacházel.

V takovém případě je role enzym-asistované vitrektomie diskutabilní. V našem souboru jsme se dále snažili vyhnout manipulaci s nosičem po injektáži (posunutí dále od retinotomie) a injikovali rovnou dále od retinotomie. Obávali jsme se narušení sítnice a ev. subretinálního krvácení při posouvání nosiče pinzetou nebo rozšiřování místa v sítnicovém „puchýři“ mechanickou cestou.

V roce 2014 Stanzel a kol. publikoval výsledky implantace lidských kmenových buněk RPE na polyesterové membráně u králíků využívající shodnou techniku[45, 58)]. V roce 2016 pak Al.Nawaiseh a kol. publikoval operační techniku ve formě krok-za-krokem detailně popisující operační protokol pro implantací nosiče u králíků. Studie se věnuje i předoperační a postoperační péči, stejně jako anesteziiliu.

V roce 2021 Liu a kol publikoval data úspěšné subretinální implantace lidských kmenových buněk pod sítnici primátů. Pro tyto účely bylo vybráno devět opic rodu cynomolgus, zástupce zvířecího modelu s velikým okem[47)]. V průběhu experimentu byla zvířata imunosuprimována pomocí sirolimu (2mg vstupně a pak 1mg každý den) a tetracyklinu (7.5 mg/kg) sedm dní před zákrokem a tři měsíce po zákroku. V obecné rovině byly operce prováděny dle protokolu popsaného Stanzlem a kol v roce 2012 a Al-Nawaisgemem v roce 2016. V našem souboru, v případě xenotransplantace, byla též použita imunosuprese pomocí subkutánní injekce mikrosfér postupně se uvolňujícího tacrolimu v depotní dávce 0.25mg/kg jako prevence odhojení štěpu.

V roce 2016 publikoval Koss a kol. Studii zaměřenou na bezpečnost a proveditelnost implantace subretinálního nevstřebatelného nosiče síťového charakteru (6.25x3.5 mm, tloušťky 0.4 µm) pokrytých hESC-RPE u 14 samic Yucatánských miniprasat[26)]. Imunosuprese byla navozena pomocí tacrolimu (dávka neuvedena) a dexamethasonu intravitreálně (depotní dexamethasone v léčivém přípravku Ozurdex). PPV byla provedena 20G přístupem za asistence triamcinolonu (Triesence) k obarvení ZSM. Při injektáži nosiče byl přechodně zvýšen nitrooční tlak na 60mmHg jako prevence krvácení. Po implantaci byl nosič přechodně fixován pomocí těžké vody. Následovala výměna za vzduch a následně silikonový olej. Další postup byl porovnatelný s naší metodou. Autoři publikovali úspěšnost zákroku v 91 % (úspěšnost je započítána jako úspěšná implantace s úspěšným následným sběrem dat). V porovnání s naší studií nepoužíváme kortikoidní látky k imunosupresi, pouze triamcinolon přechodně k zvýraznění ZSM a nelze posoudit efekt tohoto krátkodobého působení v roli imunosuprese. Nosič, který implantujeme je menší (5.2x2.1 mm vs. 6.25x3.5 mm) a během

nekomplikovaného zákroku nepoužíváme těžkou vodu a raději provádíme rovnou výměnu vody za vzduch.

Gandhi a kol. publikoval v roce 2019 poprvé studii s plně degradabilním nosičem pro různé typy buněk u Yorkshirských prasat[46)]. Tato studie se primárně zaměřovala na charakteristiku nosiče a jeho biologických vlastností (hydrogel pokrytý fibrinem). Autoři se zde zamýšlejí nad efektem agresivní imunosuprese (kterou ale nespecifikují) a její roli v degradaci nosiče. V průběhu operace provádějí sklerotomii přibližně 3.6 mm širokou cca 3.5 mm od limbu paralelní s limbem. K injektáži volí injektor napojený na pneumatický systém redukující nechtěné pohyby ruky a prstů chirurga[46)]. V našem souboru používáme sklerotomie umístěné do pars plicata cca 2.5-3.0 mm od limbu. Tato vzdálenost byla stanovena na základě sekčních nálezů na kadaverózním bulbu námi používaných prasat a minimalizujeme tak riziko poškození sítnice obzvláště u velkých sklerotomií. Hlavní sklerální řez má, s ohledem na velikost ústí implantační kanyly, 3 mm vodorovně jdoucí s limbem. Implantát vysunujeme pouze pomocí vlastní síly. Odstranění sklivce ve směru hlavního řezu, následné odstranění prolabujícího sklivce a kauterizace sklerálních cév v místě hlavního řezu se zdá být klíčové v prevenci odchlípení sítnice a rozsáhlého krvácení znemožňující další postup. Zvětšení implantátu s sebou může přinést další nevýhody. Jednak je třeba zvětšit rozsah sklerotomie, což nepochybně povede k vyšším peroperačním turbulencím intravitreálně, vyššímu riziku hypotonie, obtížnější sutuře skléry, vyššímu riziku prolapsu sklivce či sítnice. V neposlední řadě pak musíme zvážit míru imunitní reakce vůči implantovaným buňkám při vyšší implantované ploše a tím pádem počtu buněk. Gandhi a kol. používal velikost sklerotomie 3.6 mm[46)]. Stanzel a kol. měl na míru vyrobený injektor, který procházel skrz 20G sklerotomii, tzn. 0.8 mm[45)]. V naší studii je nutná sklerotomie o rozměrech 3.0 mm. Zde je nutno zmínit, že náš implantát, v průběhu vsazení do injektoru, není jakkoliv mechanicky namáhán. Pokud užíváme sklerotomii menší než velikost implantátu, tak to automaticky znamená, že implantát musí být nějakým způsobem „zabalen“. Tím pádem mechanicky trpí jak buňky na nosiči, tak nosič samotný, což v konečné fázi může vést k jeho poškození.

8. Závěr

Riziko perioperačních a postoperačních komplikací, jako např. odchlípení sítnice, sítnicové nebo sklerální krvácení, zánětlivé změny, zakalení čočky, proliferativní vitreoretinopatie nebo např. hypotonie bulbu mohou zásadním způsobem ovlivnit úspěšnost transplantace RPE. Při

dodržování jasně stanoveného protokolu (příprava, chirurgická technika, pooperační péče) jsme schopni minimalizovat četnost těchto komplikací a zachovat vysoký poměr úspěšných zákroků (93.1 % v našem souboru).

V naší práci nabízíme návod na implantaci RPE na nanovlákenném nosiči na zvířecím modelu s velkým okem. Miniprase se zdá, vzhledem k podobnostem s lidským okem, být do budoucna ideálním modelem pro experimenty přenositelné do humánní medicíny. Tyto podobnosti nám umožňují vyvíjet pokročilé chirurgické postupy pro implantaci subretinálních implantátů. Dalším důležitým faktem je možnost použití stejného instrumentária, které používáme u lidí a sítnicový chirurg je s těmito nástroji důvěrně seznámen.

8.1. Zhodnocení cílů a hypotéz

Hypotéza 1: Subretinální implantace nanovlákenného nosiče vede k mnohým peroperačním i pooperačním komplikacím.

Tato hypotéza byla vyvrácena – námi popsaný chirurgický výkon je vzhledem k rozsahu a náročnosti bezpečný a reprodukovatelný.

Hypotéza 2: Sítnice bude na subretinální nosič reagovat zánětlivými změnami

Tato hypotéza nebyla potvrzena. Na námi pořízených skenech OCT a histologických preparátech nebyla patrna prakticky žádná zánětlivá odpověď.

Cíl 1: Optimalizace tvaru subretinálního nosiče přizpůsobení implantační kanyly tvaru a vlastnostem nosiče bez ohledu na typ přenášených buněk.

Cíl byl splněn. Máme, z hlediska nosiče, dobře definovaný produkt.

Cíl 2: Optimalizace chirurgického zákroku s minimalizací nežádoucích událostí.

Úspěšnost operace přesahující 90 % je u takto komplikovaného výkonu solidním základem pro rozvoj operační techniky. Cíl považuji za splňený.

Cíl 3: Zhodnocení úspěšnosti operačního zákroku

Dle OCT i histologie se zdá, že je implantát dobře tolerován. Další výzkum bude zaměřen na konkrétní buněčné populace. Nutné je také doplnit funkční testy.

Cíl 4: Zhodnocení reaktivních změn sítnice po implantaci nosiče

Jednoznačné reaktivní změny sítnice nebyly detekovány.

10. Seznam použité literatury

1. Bressler, NM., Bressler, SB., Fine, SL.: Age-related macular degeneration. Surv Ophthalmol, 32; 1988: 375–413.

2. GBD 2019 Blindness and Vision Impairment Collaborators; Vision Loss Expert Group of the Global Burden of Disease Study. Causes of blindness and vision impairment in 2020 and

trends over 30 years, and prevalence of avoidable blindness in relation to VISION 2020: the Right to Sight: an analysis for the Global Burden of Disease Study. Lancet Glob Health. 2021 Feb;9(2):e144-e160. doi: 10.1016/S2214-109X(20)30489-7. Epub 2020 Dec 1. Erratum in: Lancet Glob Health. 2021 Apr;9(4):e408. PMID: 33275949; PMCID: PMC7820391.

3. https://ourworldindata.org/life-expectancy

4. Age-Related Eye Disease Study 2 Research Group. Lutein + zeaxanthin and omega-3 fatty acids for age-related macular degeneration: the Age-Related Eye Disease Study 2 (AREDS2) randomized clinical trial. JAMA. 2013 May 15;309(19):2005-15. doi: 10.1001/jama.2013.4997. Erratum in: JAMA. 2013 Jul 10;310(2):208. PMID: 23644932.

5. Miller JW, Schmidt-Erfurth U, Sickenberg M, Pournaras CJ, Laqua H, Barbazetto I, Zografos L, Piguet B, Donati G, Lane AM, Birngruber R, van den Berg H, Strong A, Manjuris U, Gray T, Fsadni M, Bressler NM, Gragoudas ES. Photodynamic therapy with verteporfin for choroidal neovascularization caused by age-related macular degeneration: results of a single treatment in a phase 1 and 2 study. Arch Ophthalmol. 1999 Sep;117(9):1161-73. doi: 10.1001/archopht.117.9.1161. Erratum in: Arch Ophthalmol 2000 Apr;118(4):488. PMID: 10496388.

6. Rosenfeld PJ, Rich RM, Lalwani GA. Ranibizumab: Phase III clinical trial results. Ophthalmol Clin North Am. 2006 Sep;19(3):361-72. doi: 10.1016/j.ohc.2006.05.009. PMID: 16935211.

7. Nanduri, D., Fine, I., Horsager, A., et al.: Frequency and am- plitude modulation have different effects on the percepts elicited by retinal stimulation. Invest Ophthalmol Vis Sci, 53; 2012: 205–214.

8. Lorach, H., Goetz, G., Smith, R., et al.: Photovoltaic resto- ration of sight with high visual acuity. Nat Med, 21; 2015: 476–482.

9. Ahuja, AK., Yeoh, J., Dorn, JD., et al.: Factors Affecting Per- ceptual Threshold in Argus II Retinal Prosthesis Subjects. Transl Vis Sci Technol, 2; 2013: 1.

10. Ho, AC., Humayun, MS., Dorn, JD., et al.: Long-Term Results from an Epiretinal Prosthesis to Restore Sight to the Blind. Ophthalmology, 122; 2015: 1547–1554.

11. Dudakova, L., Kousal, B., Kolarova, H., et al.: Gene the- rapy for inherited retinal and opticnerve disorders: current knowledge. Cesk Slov Oftalmol. 72; 2016; 128–136.

12. Bainbridge, JWB., Mehat, MS., Sundaram, V., et al.: Long- term effect of gene therapy on Leber's congenital amauro- sis. N Engl J Med, 372; 2015: 1887–1897.

13. Wang, D., Gao, G.: State-of-the-art human gene therapy: part II. Gene therapy strategies and clinical applications. Discov Med, 18; 2014: 151–161.

14. Kaufmann, KB., Buning, H., Galy, A., et al.: Gene therapy on the move. EMBO Mol Med, 5; 2013: 1642–1661.

15. Mali, S.: Delivery systems for gene therapy. Indian J Hum Ge- net, 19; 2013: 3–8.

16. Boye, SE., Boye, SL., Lewin, AS., et al.: A comprehensive re- view of retinal gene therapy. Mol Ther J Am Soc Gene Ther, 21; 2013: 509–519.

17. Maguire, AM., Simonelli, F., Pierce, EA., et al.: Safety and efficacy of gene transfer for Leber's congenital amaurosis. N Engl J Med, 358; 2008: 2240–2248.

18. Gu, SM., Thompson, DA., Srikumari, CR., et al.: Mutations in RPE65 cause autosomal recessive childhood-onset severe retinal dystrophy. Nat Genet, 17; 1997: 194–197.

19. Kousal, B., Ďuďáková, Ľ., Moravíková, J., et al.: Vzácná oční onemocnění v oftalmologické praxi. Oftalmol Praxi, 2018: 7–11.

20. Yue, L., Weiland, JD., Roska, B., et al.: Retinal stimulation strategies to restore vision: Fundamentals and systems. Prog Retin Eye Res, 53; 2016: 21–47.

21. Duebel, J., Marazova, K., Sahel, J-A.: Optogenetics. Curr Opin Ophthalmol, 26; 2015: 226–232.

22. Zeng, H., Sanes, JR.: Neuronal cell-type classification: challenges, opportunities and the path forward. Nat Rev Neurosci, 18; 2017: 530–546.

23. Simunovic, MP., Shen, W., Lin, JY., et al.: Optogenetic appro- aches to vision restoration. Exp Eye Res, 178; 2019: 15–26.

24. von Noorden, GK.: Application of basic research data to clinical amblyopia. Ophthalmology, 85; 1978: 496–504.

25. Kozak, I. et al. Safety and feasibility of new nanofiber subretinal delivery system with injector for RPE cell transplantation. Investigative Ophthalmology & Visual Science. 59 (9), 5670–5670 (2018).

26. Koss, M.J. et al. Subretinal implantation of a monolayer of human embryonic stem cell-derived retinal pigment epithelium: a feasibility and safety study in Yucatan minipigs. Graefe's archive for clinical and experimental ophthalmology = Albrecht von Graefes Archiv fur klinische und experimentelle Ophthalmologie. 254 (8), 1553–1565, doi: 10.1007/s00417-016-3386-y (2016).

27. Ghosh, F., Wong, F., Johansson, K., Bruun, A., Petters, R.M. Transplantation of full-thickness retina in the rhodopsin transgenic pig. Retina (Philadelphia, Pa.). 24 (1), 98–109, doi: 10.1097/00006982-200402000-00014 (2004).

28. Parolini, B., Di Salvatore, A., Pinackatt, SJ., et al.: Long-term results of autologous retinal pigment epithelium and cho- roid transplantation for the treatment of exudative and atrophic maculopathies. Retina, 2018.

29. Chen, FK., Patel, PJ., Uppal, GS., et al.: Long-term outcomes following full macular translocation surgery in neovascular age-related macular degeneration. Br J Ophthalmol, 94; 2010: 1337–1343.

30. Lee, E., MacLaren, RE.: Sources of retinal pigment epithe- lium (RPE) for replacement therapy. Br J Ophthalmol, 95; 2011: 445–449.

31. van Zeeburg, EJT., Maaijwee, KJM., Missotten, TOAR., et al.: A free retinal pigment epithelium-choroid graft in pati- ents with exudative age-related macular degeneration: results up to 7 years. Am J Ophthalmol, 153; 2012: 120-127.e2.

32. Ramsden, CM., Powner, MB., Carr, A-JF., et al.: Stem cells in retinal regeneration: past, present and future. Dev Camb Engl, 140; 2013: 2576–2585.

33. Carr, A-JF., Smart, MJK., Ramsden, CM., et al.: Develop- ment of human embryonic stem cell therapies for age-re- lated macular degeneration. Trends Neurosci, 36; 2013: 385–395.

34. Takahashi, K., Yamanaka, S.: Induction of pluripotent stem cells from mouse embryonic and adult fibroblast cultures by defined factors. Cell, 126; 2006: 663–676.

35. Kvanta, A., Grudzinska, MK.: Stem cell-based treatment in geographic atrophy: promises and pitfalls. Acta Ophthalmol (Copenh), 92; 2014: 21–26.

36. Tezel, TH., Kaplan, HJ., Del Priore, LV.: Fate of human re- tinal pigment epithelial cells seeded onto layers of human Bruch's membrane. Invest Ophthalmol Vis Sci, 40; 1999: 467–476.

37. Lee, E., MacLaren, RE.: Sources of retinal pigment epithe- lium (RPE) for replacement therapy. Br J Ophthalmol, 95; 2011: 445–449

38. Vodicka P, Smetana K, Jr., Dvorankova B, Emerick T, Xu YZ, Ourednik J, et al. The miniature pig as an animal model in biomedical research. Annals of the New York Academy of Sciences. 2005;1049:161-71.

39. Sevc, J. et al. Effective long-term immunosuppression in rats by subcutaneously implanted sustained-release tacrolimus pellet: effect on spinally grafted human neural precursor survival. Experimental neurology. 248, 85–99, doi: 10.1016/j.expneurol.2013.05.017 (2013)

40. Popelka S, Studenovska H, Abelova L, Ardan T, Studeny P, Stranak Z, et al. A frame-supported ultrathin electrospun polymer membrane for transplantation of retinal pigment epithelial cells. Biomedical materials. 2015;10(4):045022.

41. Eichhorn SJ, Sampson WW. Statistical geometry of pores and statistics of porous nanofibrous assemblies. Journal of the Royal Society, Interface. 2005;2(4):309-18

42. Binder, S., Stanzel, B.V., Krebs, I., Glittenberg, C. Transplantation of the RPE in AMD. Progress in retinal and eye research. 26 (5), 516–554, doi: 10.1016/j.preteyeres.2007.02.002 (2007).

43. Falkner-Radler, C.I. et al. Human retinal pigment epithelium (RPE) transplantation: outcome after autologous RPE-choroid sheet and RPE cell-suspension in a randomised clinical study. The British journal of ophthalmology. 95 (3), 370–375, doi: 10.1136/bjo.2009.176305 (2011).

44. Christiansen, A.T. et al. Subretinal implantation of electrospun, short nanowire, and smooth poly(epsilon-caprolactone) scaffolds to the subretinal space of porcine eyes. Stem cells international. 2012, 454295, doi: 10.1155/2012/454295 (2012).

45. Stanzel, B.V., Liu, Z., Brinken, R., Braun, N., Holz, F.G., Eter, N. Subretinal delivery of ultrathin rigid-elastic cell carriers using a metallic shooter instrument and biodegradable hydrogel encapsulation. Investigative ophthalmology & visual science. 53 (1), 490–500, doi: 10.1167/iovs.11-8260 (2012).

46. Gandhi, J.K. et al. Fibrin hydrogels are safe, degradable scaffolds for sub-retinal implantation. PloS one. 15 (1), e0227641, doi: 10.1371/journal.pone.0227641 (2020).

47. Liu, Z. et al. Surgical Transplantation of Human RPE Stem Cell-Derived RPE Monolayers into Non-Human Primates with Immunosuppression. Stem cell reports. 16 (2), 237–251, doi: 10.1016/j.stemcr.2020.12.007 (2021)

48. Al-Nawaiseh, S. et al. A Step by Step Protocol for Subretinal Surgery in Rabbits. (115), doi: 10.3791/53927. (2016).

49. Radtke, N.D., Aramant, R.B., Petry, H.M., Green, P.T., Pidwell, D.J., Seiler, M.J. Vision improvement in retinal degeneration patients by implantation of retina together with retinal pigment epithelium. American journal of ophthalmology. 146 (2), 172–182, doi: 10.1016/j.ajo.2008.04.009 (2008).

50. Maaijwee, K.J.M. et al. Histological evidence for revascularisation of an autologous retinal pigment epithelium--choroid graft in the pig. The British journal of ophthalmology. 91 (4), 546–550, doi: 10.1136/bjo.2006.103259 (2007).

51. Schwartz, S.D. et al. Human embryonic stem cell-derived retinal pigment epithelium in patients with age-related macular degeneration and Stargardt's macular dystrophy: follow-up of two open-label phase 1/2 studies. Lancet (London, England). 385 (9967), 509–516, doi: 10.1016/S0140-6736(14)61376-3 (2015). 3

52. Ghosh, F., Engelsberg, K., English, R.V., Petters, R.M. Long-term neuroretinal fullthickness transplants in a large animal model of severe retinitis pigmentosa. Graefe's archive for clinical and experimental ophthalmology = Albrecht von Graefes Archiv fur klinische und experimentelle Ophthalmologie. 245 (6), 835– 846, doi: 10.1007/s00417-006-0437-9 (2007).

53. Radtke, N.D., Seiler, M.J., Aramant, R.B., Petry, H.M., Pidwell, D.J. Transplantation of intact sheets of fetal neural retina with its retinal pigment epithelium in retinitis pigmentosa patients. American journal of ophthalmology. 133 (4), 544–550, doi: 10.1016/s0002-9394(02)01322-3 (2002).

54. Slijkerman RW., et al. The pros and cons of vertebrate animal models for functional and therapeutic research on inherited retinal dystrophies. Prog Retin Eye Res. 2015 Sep;48:137-59. doi: 10.1016/j.preteyeres.2015.04.004.

55. Shrader, S.M., Greentree, W.F. Göttingen Minipigs in Ocular Research. Toxicologic pathology. 46 (4), 403–407, doi: 10.1177/0192623318770379 (2018).

56. Vízina, M. Comparative ocular anatomy in commonly used laboratory animals. Ocular Toxicology in Laboratory Animals (A. B. Weir and M. Collins, eds.) pp. 9- 12. Humana Press, Totowa, NJ (2013).

57. Duarri A., et al. Transplantation of Human Induced Pluripotent Stem Cell-Derived Retinal Pigment Epithelium in a Swine Model of Geographic Atrophy. Int J Mol Sci. 2021 Sep 28;22(19):10497. doi: 10.3390/ijms221910497

58. Stanzel, B.V. et al. Human RPE Stem Cells Grown into Polarized RPE Monolayers on a Polyester Matrix Are Maintained after Grafting into Rabbit Subretinal Space. Stem Cell Reports. 2 (1), 64–77, doi: 10.1016/j.stemcr.2013.11.005 (2014).

11. Přílohy 1-5 (Publikace)

IOP Publishing Biomed. Mater. 10 (2015) 045022 doi:10.1088/1748-6041/10/4/045022

Biomedical Materials

PAPER

A frame-supported ultrathin electrospun polymer membrane for transplantation of retinal pigment epithelial cells

Štěpán Popelka[1], Hana Studenovská[1], Lucie Abelová[1], Taras Ardan[3], Pavel Studený[2], Zbyněk Straňák[2], Jiří Klíma[3], Barbora Dvořánková[4], Jiří Kotek[1], Jiří Hodan[1] and František Rypáček[1]

[1] Institute of Macromolecular Chemistry, v.v.i., Academy of Sciences of the Czech Republic, Heyrovsky Sq. 2, 162 06 Prague 6, Czech Republic
[2] 3rd Faculty of Medicine, Charles University in Prague, Vinohrady Teaching Hospital, Department of Ophthalmology, Šrobárova 1150/50, 100 34 Prague 10, Czech Republic
[3] Institute of Animal Physiology and Genetics, v.v.i., Academy of Sciences of the Czech Republic, Rumburská 89, 277 21, Liběchov, Czech Republic
[4] 1st Faculty of Medicine, Charles University in Prague, Kateřinská 32, 121 08 Prague 2, Czech Republic

E-mail: popelka@imc.cas.cz

RECEIVED
15 December 2014

REVISED
26 June 2015

ACCEPTED FOR PUBLICATION
29 June 2015

PUBLISHED
12 August 2015

Keywords: RPE transplantation, RPE carrier, age-related macular degeneration, electrospinning, porcine RPE

Supplementary material for this article is available online

Abstract

We report on the design and fabrication of a frame-supported nanofibrous membrane for the transplantation of retinal pigment epithelial (RPE) cells, which is a promising therapeutic option for the treatment of degenerative retinal disorders. The membranous cell carrier prepared from 640 nm-thick poly(DL-lactide) fibres uniquely combines high porosity, large pore size and low thickness, to maximize the nutrient supply to the transplanted cells in the subretinal space and thus to enhance the therapeutic effect of the transplantation. The carrier was prepared by electrospinning, which made it easy to embed a 95 μm-thick circular supporting frame 2 mm in diameter. Implantations into enucleated porcine eyes showed that the frame enabled the ultrathin membrane to be handled without irreversible folding, and allowed the membrane to regain its flat shape when inserted into the subretinal space. We further demonstrated that the minimum membrane thickness compatible with the surgical procedure and instrumentation employed here was as low as 4 μm. Primary porcine RPE cells cultivated on the membranes formed a confluent monolayer, expressed RPE-specific differentiation markers and showed transepithelial resistance close to that of the native RPE. Most importantly, the majority of the RPE cells transplanted into the subretinal space remained viable. The ultrathin, highly porous, and surgically convenient cell carrier presented here has the potential to improve the integration and the functionality of transplanted RPE cells.

1. Introduction

Retinal pigment epithelium (RPE) is a cellular monolayer of high metabolic activity that separates the outer part of the neuroretina from the choroid, the vascularized layer of the eye, and collaborates closely with the adjacent photoreceptors in maintaining visual function [1]. A number of degenerative retinal disorders, such as age-related macular degeneration (AMD) and Stargardt disease, impair the function of RPE, resulting in atrophy of choriocapillaris, loss of photoreceptors, and finally loss of vision [2]. Presently, no effective pharmacotherapy is available for the majority of patients affected by these visual disorders, so transplantation of RPE has been investigated as a viable treatment option which promises to halt the degeneration and maintain or improve the visual function [3, 4]. Early transplantations of RPE, either as an autologous RPE-choroid flap from the patient's eye periphery [5, 6], translocation of neuroretina [7] or allogeneic transplantations of fetal RPE sheet [8–10] have proven the beneficial effect of RPE replacement on the progression of the disease. Current experimental transplantation protocols employ RPE cells derived from stem cells [2], particularly from human embryonic stem cells (hESC-RPE) [11–13] and from induced pluripotent stem cells (iPSC-RPE) [14, 15]. Efforts to translate RPE transplantations based on stem cell therapy toward clinical application have recently advanced to the stage of clinical trials [2, 16–19].

© 2015 IOP Publishing Ltd

RPE cells are delivered into the subretinal space in the form of (i) a cell suspension [20], (ii) a self-supporting cell sheet [21], or (iii) a cell monolayer supported by an artificial membranous substrate [22]. Although injection of the cell suspension is surgically simpler, faster and less invasive than other techniques, cumulated experience from animal studies and from human clinical trials have revealed several drawbacks, which include reflux of the suspension into the vitreous cavity, limited adherence of RPE cells to the aged Bruch's membrane, incorrect apico–basal orientation, and failure to form a monolayer [23, 24]. The advantage of a self-supporting cell sheet and a cell monolayer supported by an artificial membranous substrate is that the cells are implanted in a highly differentiated state. They can therefore perform their metabolic activity immediately after implantation and can more easily retain their epithelial phenotype than cells in suspension [25]. The solid substrate in the third delivery technique (a cell monolayer supported by an artificial membranous substrate) in addition allows precise positioning of the RPE monolayer in the subretinal space and prevents the monolayer from folding and wrinkling, which is unavoidable without the support [21]. Transplantation of a supported polarized RPE monolayer can therefore result in improved survival and more efficient integration and function of the graft in comparison with cell suspension or a self-supporting RPE cell sheet. A disadvantage, however, is the need for more complex surgery involving larger sclerotomy and retinotomy, which, in turn, increase the risk of scarring, fibrosis and damage to the neuroretinal layers. Each of the techniques is currently being employed in separate ongoing clinical trials (WHO Nos. NCT01469832, NCT01691261 and JPRN-UMIN000011929).

The general structure of the artificial carrier for transplanting RPE cells is a membranous sheet of a porous biomaterial that serves two main functions: to support the formation and maintenance of a differentiated cell monolayer, and to facilitate surgical delivery. When designing the structure and the chemico-physical properties of the carrier, it is necessary to consider the physiological conditions of the subretinal space. RPE is separated from the choroid by Bruch's membrane, a pentalaminar structure of extracellular matrix that is 2–6 μm in thickness and that controls the diffusion of nutrients, signaling molecules and wastes between RPE and choroid [26]. Any additional separation of RPE and choroid by the RPE carrier, even if well permeable, will decrease the concentration gradient of the solutes and will slow down their diffusion fluxes proportionally to the separation. Therefore, carriers with high open porosity, large pore size and low thickness, lower than or comparable to the thickness of Bruch's membrane, may promote a higher rescue effect of the transplanted RPE layer on the photoreceptors and on the inner layers of the neuroretina.

Numerous biomaterials have been used in fabrication of carriers for RPE cell transplantation and they were reviewed by Hynes and Lavik [22]. These materials included biodegradable lactide-based polymers such as poly(DL-lactide-*co*-glycolide) and poly(L-lactide) that were among the first synthetic materials suggested for this purpose [27–32]. However, only two RPE carriers made of porous synthetic membranes were of about the same thickness as or thinner than Bruch's membrane, and their performance was also examined *in vivo*: a poly(ethylene terephthalate) (PET) track etched membrane 10 μm in thickness [33–35] and a Parylene C membrane 300 nm in thickness on a 6 μm-thick mesh frame [25, 36]. Both carriers were able to support the survival of a human stem cell derived-RPE monolayer *in vivo* but failed to preserve photoreceptors and inner layers of the retina above the RPE-carrier implant. Stanzel *et al* [35] suggested that one of the factors behind this detrimental effect was the low permeability of the carrier.

A fibrous membrane of submicron fibres (nanofibers) prepared by electrospinning has recently been suggested as a promising type of transplantation carrier for RPE cells. Such a carrier is, in general, highly permeable for solutes and displays a surface nanotopography mimicking the topography of the basement membrane [34, 37–40]. Nanofibrous membranes for RPE cell transplantation were prepared either from lactide-based polymers such as poly(L-lactide-co-glycolide) (PLGA) [40] and poly(L-lactide-*co*-ε-caprolactone) (PLCL) [37] or from a nondegradable polyamide [39]. RPE cells cultivated on this kind of substrate showed superior growth characteristics and enhanced differentiation in comparison with smooth surfaces [39, 40]. Moreover, electrospun fibrous membranes can be fabricated with low thickness, high porosity and large pore sizes. However, when the carrier thickness is decreased below ca 10 μm to enhance nutrient exchange between the transplanted RPE cells and the underlying tissue, such a thin carrier becomes too floppy to be handled without folding or curling, which in turn impairs the functionality of the transplant. Although the number of studies presenting a nanofibrous membrane for transplantation of RPE cells is increasing, none of them has so far presented implantation of the membrane into the subretinal space, neither *ex vivo*, nor *in vivo*.

The aim of this study was to develop a novel cell carrier for RPE transplantation based on an ultrathin (<6 μm) nanofibrous membrane with a supporting structure that would facilitate surgical manipulation and enable the carrier to regain a flat shape in the subretinal space. To this end we combined the electrospun membrane of poly(DL-lactide) (PDLLA) with a stiffer circular frame made of a poly(4-dioxanone) (PDS) monofilament suture fibre. We further aimed to find the minimal thickness of the nanofibrous membrane that would support *in vitro* cultivation of the RPE cells into an epithelium-like layer, would resist mechanical

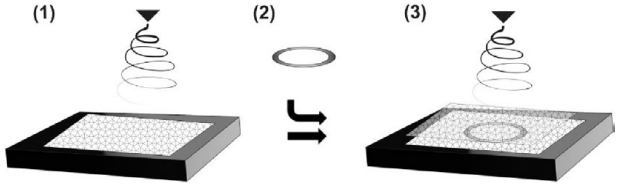

Scheme 1. Fabrication of the electrospun membrane with an embedded supporting circular frame. Step 1: deposition of the bottom half of the membrane, step 2: placement of the circular frame, step 3: deposition of the upper half of the membrane.

stress during transplantation and would enable safe transplantation of the cells.

2. Materials and methods

2.1. Electrospinning

2.1.1. Electrospinning apparatus

The custom-made electrospinning apparatus consisted of a dc high-voltage supply (Gamma High Voltage Research, Ormond Beach, FL 32174), an infusion pump (KD Scientific, USA), a syringe fitted with a stainless steel blunt-ended needle (20 G, ID/OD 0.584/0.902 mm) and a movable flat aluminium collector (11 × 19 cm) actuated by a PC-controlled linear actuator (Kolektor Synatec d.o.o.). A voltage of +5 kV was applied to the needle 10 cm distant from the surface of the grounded collector. The polymer solution was delivered at a flow rate of 125.5 μl h^{-1}. The formation and stability of the Taylor's cone was monitored with a video camera. The nanofibrous membranes with randomly oriented fibres were collected on 11 × 22 mm pieces of silicon wafer (one side polished silicon, thickness 450 μm, resistivity 5–22 Ω·cm, 50 nm thermal oxide overlayer, Siegert Consulting e.K.) placed on the movable collector. The speed of the collector in the range of 3.9–72 mm min^{-1} allowed the areal density of the nanofibrous mat to be controlled in the range of 10–180 μg cm^{-2} with the corresponding thickness between 0.9 μm and 6.2 μm. Electrospinning was performed at room temperature (24–26 °C).

2.1.2. PDLLA solution

Poly(DL-lactide) (PDLLA) (M_w 900 000 g mol^{-1}, PDI 1.9) was prepared by ring-opening polymerization of a racemic mixture of D and L-lactide (Aldrich) catalyzed by tin(II)octoate [41]. The polymer was dissolved in dimethylformamide at 11wt% under stirring 3 d before electrospinning.

2.1.3. Fabrication and embedding of the supporting frame

The circular frame 2 mm in diameter was prepared from monofilament poly(4-dioxanone) (PDS) surgical fibre (absorbable suture, PDS*II,7-0, kindly donated by Ethicon, Johnson and Johnson). The fibre was cut to the required length, was formed into a ring at 100 °C for 24 h, and finally its ends were glued together with a 9 wt% solution of poly(L-lactide) in dichloromethane. The thermally treated PDS fibre was 95 ± 5 μm in diameter with linear density of 98 dtex and Young modulus of 64 ± 15 cN/tex (ISO 5079), which was measured using an Instron 6025/5800 R tensile testing device. The circular frame was sandwiched between two successively deposited layers of the electrospun membrane (scheme 1). After drying at 50 °C in vacuum for 6 h, the sheets of the membrane were floated from the silicon wafers on the water surface by analogy with the preparation of specimen support films on transmission electron microscopy grids [42], and were collected on a larger supporting structure, e.g. an aluminium foil with a 5 mm-large circular opening or a commercial cell culture insert (Transwell Permeable Support, 3413, Corning Incorporated, USA) devoid of the original membrane. Finally, the membrane was affixed to these structures by neutral silicone glue.

2.2. Spin-cast polymer films

PDLLA coated glass cover-slips were prepared as a reference substrate for cultivation of RPE cells. PDLLA (M_w 900 000 g mol^{-1}) was dissolved in 1,4-dioxane to form 0.7 wt% solutions. Round glass cover-slips 12 mm in diameter were cleaned in methanol, followed by 15 s of air-plasma cleaning (Expanded plasma cleaner, Harrick Plasma), and were treated with (3-aminopropyl)triethoxysilane vapours prior to spin-casting. Films were spin-cast at a speed of 2000 rpm and at an acceleration of 1500 rpm s^{-1}. All films were held under vacuum for 1 h and at 120 °C to remove residual solvent and promote adhesion to the substrate. The polymer film thickness was 50 nm, as measured with a profiler (KLA-Tencor P-10 Surface Profiler).

2.3. Characterization of electrospun membranes

2.3.1. Areal density and thickness

The areal density of the fibrous membranes was calculated from the wafer area and the increase in the wafer mass (METTLER TOLEDO MX5 Microbalance) after fibre mat deposition. The membrane thickness was evaluated from profiler scans 500 μm in length taken at a scan speed of 20 μm s^{-1} over a groove made by a steel needle in the membrane. The membrane thickness was defined as the average of the ten highest peaks in the profile. The membrane samples were platinum sputtered before scanning.

2.3.2. Fibre width and pore size distribution

The morphology of the fabricated membranes was observed with the VEGA Plus TS 5135 scanning electron microscope (SEM) (Tescan, Czech Republic). The fibre width and pore diameter distribution were determined from SEM micrographs using ImageJ software [43]. The fibre width was recorded at 10 randomly chosen locations in 10 images. As the thickness of the fibrous networks described here is lower than the diameter of a dissociated RPE cell (12–20 μm, supporting information, figure S2) (stacks.iop.org/BMM/10/045022/mmedia), for the pore size analysis we neglected the structural component perpendicular to the network plane and modelled the electrospun mats as a two dimensional network. We extracted the polygonal pores from the SEM images by thresholding or tracing the pore borders manually (high areal densities). To determine whether a pore is permeable to a dissociated cell, we further extracted the diameter of the largest inscribed circle into a polygonal pore, which is equal to twice the maximum of the Euclidean distance map of a pore [44]. To acquire a representative sample of pores, 10 random images of the membrane of the same areal density were analyzed. The size of the scans was adjusted to cover as much of the pore size distribution body as possible. The pore size ranges and related characteristics that were detected from the images of the fibrous networks are given in supporting information, table S1 (stacks.iop.org/BMM/10/045022/mmedia). Further mathematical analysis (supporting information) (stacks.iop.org/BMM/10/045022/mmedia) made it possible to predict the critical value of the areal density below which the membrane structure could not support the formation of a confluent cell monolayer due to the presence of pores larger than the cell diameter.

2.3.3. Membrane porosity

The porosity of a porous structure is the fraction of voids within the structure volume, and can be calculated using the density of the porous structure d_s and the density of the structure material d as

$$\varepsilon = 1 - d_s/d \quad (1)$$

Here, the density of the membrane was calculated from the ratio of the areal density and the membrane thickness. PDLLA density of 1.248 g cm^{-3} was adopted from the literature [45]. For comparison, we also calculated 2D porosity as a fractional open area of the network from binarized SEM images.

2.3.4. Membrane stiffness

The stiffness of electrospun membranes was determined by a modified small-punch test. The small punch test is a miniature specimen mechanical testing technique which is widely used for evaluating mechanical behaviour of polymeric biomaterials [46]. Specimens of fibrous membranes with areal densities ranging from 10 μg cm^{-2} to 180 μg cm^2 were fixed on metal washers (18 mm outer diameter, inner diameter a = 6.6 mm, 1.6 mm thickness) and tested by indentation with a hemispherical head punch with a head radius of R = 1.5 mm (scheme 2). Taking into account small forces (<1 N), an ARES-G2 rheometer (TA Instruments) was used for the test. The tests were performed at room temperature and at a constant punch displacement rate of 1 mm . min^{-1}, until failure. During testing, the punch load and displacement were recorded. A commercial porous cell culture membrane made of PET 10 μm in thickness and 3 μm in pore diameter (Transwell permeable support 3462, Corning) was used as a reference material.

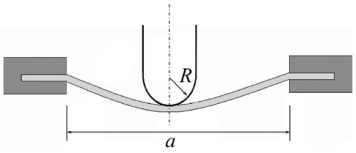

Scheme 2. Small punch test arrangement.

2.3.5. Resistance to surgical handling

The acellular fibrous carriers with different areal densities of the membrane were implanted into enucleated porcine eyes. After extraction, the carriers were washed in deionized water, placed on a microscope glass slide and allowed to dry. The damage to the membrane was assessed from the light microscope images (an Olympus SZ61 stereomicroscope equipped with a digital camera) as a fractional area within the circular frame without the membrane (figure 1) using ImageJ image analysis software.

2.4. Surgical procedure

To test the effect of the surgical handling on the integrity of the carrier and on the vitality of the RPE cells, we simulated the implantation procedure using enucleated porcine eyes and instruments for human eye surgery. The enucleated eyeballs from the cadavers of 2- to 3 year-old pigs were obtained from a local slaughter house. The experimental protocol was approved by the institutional animal ethics committee and complied with the association for research in vision and ophthalmology (ARVO) Statement for the Use of Animals in Ophthalmic and Vision Research. The eyes were affixed into an eye holder under the operating microscope (Carl Zeiss OPMI VISU 150 equipped with BIOM) and their cornea was covered with 2% methyl cellulose solution to improve the visibility of the rear segment. Standard 23 G vitrectomy ports were introduced in the pars-plana region with infusion at 4 o'clock and two ports at 2 o'clock and at 10 o'clock. The intraocular pressure was maintained at 25 mmHg. After vitrectomy using the Constellation Vision System (Alcon, Novartis), a bleb retinal detachment was created by injecting a small amount of balanced salt solution on

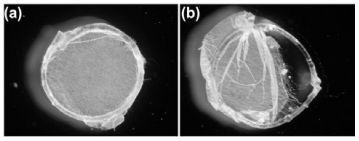

Figure 1. Microphotograph of the fibrous carrier (membrane thickness 1.6 μm) before implantation (*a*) and after implantation and subsequent extraction from the subretinal space (*b*). The damage to the membrane was assessed as an area fraction within the circular frame without the membrane.

the surface of the retina in the area centralis retinae. A retinotomy (ca 2PD) in the vicinity of the retinal bleb was formed using 23 G retinal scissors. The carrier, either acellular or with RPE cells, was punched along the embedded frame with a 3 mm circular biopsy punch. The punched carrier was loaded bi-manually, using retinal forceps, into an injector consisting of a Teflon tube (OD 1.97 mm, ID 1.32 mm) and a steel piston from a Hamilton syringe 1710 N (OD 1.309) (figure 2(*a*)). The inserted carrier adopted a rolled up shape in the injector. The injector was introduced into the vitreous cavity through a 4.1 mm sclerotomy at the 12 o'clock position. The carrier was displaced by a piston from the injector directly into the subretinal space through the retinotomy, and was positioned under the retina with the retinal forceps (figure 2(*b*)). When the injector was removed from the eye, the sclerotomy was sutured. The retina was then flattened against the host retinal pigment epithelium with perfluorodecalin (a mixture of cis and trans, 90%, Acros). After removal of the vitrectomy ports, the anterior segment of the porcine eye was cut off with scissors, perfluorodecalin was replaced by a balanced salt solution and the neuroretina was carefully removed to extract the carrier for further analysis (figure 2(*c*)). The placement of the carrier under the retina was characterized by Spectral Domain-Optical Coherent Tomography (SD-OCT, iVue 100, Optovue). The scans were taken after the anterior segment had been removed.

2.5. Primary porcine RPE cell culture

Freshly enucleated eyeballs of the same origin as those used in *ex vivo* surgery were liberated from the surrounding tissues and sterilized in 10% Betadine solution (EGIS Pharmaceuticals, Hungary) for 10 min. After washing with PBS, a circumferential section at ora serrata was made, and the anterior eye segment and vitreous were removed. The neural retina was gently loosened with forceps and separated from the optic nerve using scissors. The eyecup was then filled with PBS, supplemented with 0.025% Trypsin/EDTA solution and incubated at 37 °C for 20 min. After incubation, the trypsin solution was removed and the residual trypsin was inhibited by the addition of the culture medium consisting of DMEM/F12 (D6421, Sigma Aldrich), 10% FBS (F6178, Sigma Aldrich) and 2.5 mM GlutaMAX-1 (35050 038, Life Technologies). RPE cells in small multicellular aggregates were detached from the Bruch's membrane by gentle scraping with a pipette tip. Aspirated tissue was further triturated by pipetting, and the cell suspension was centrifuged for 5 min at 300 g at room temperature. Each cell pellet isolated from a single eye was resuspended in the culture medium and plated on two 35 mm culture plates. RPE cells were propagated in the culture medium, which was changed three times a week. After reaching confluence (usually in 10 d), the RPE cells were harvested (passage 0) by trypsinization for 5 min and finally washed with the culture medium.

2.5.1. *Cell seeding*

Primary RPE cells were seeded on PDLLA nanofibrous membranes fixed to 24-well inserts and on reference substrates PDLLA coated cover slides, at a density of 2000 cells mm^{-2}, providing the passage 1 cultures. The seeding area on the cover slides was delineated by means of a polypropylene O-ring (ID 5.3 mm, thickness 1 mm) that was affixed to the slide with neutral silicone glue. The volume of the inoculated suspension was 100 μl. Nanofibrous membranes with areal density of 100 μg cm^{-2} (thickness 3.5 μm) affixed to the bodies of Transwell permeable supports (3413, Corning) were immersed into the culture medium and were seeded with 150 μl of the cell suspension. The resulting confluent cell layers were cultured for 30 d with a culture medium that was changed twice a week.

2.5.2. *Immunocytochemistry*

Cultured primary cells either on cover slides or on nanofibrous membranes were washed twice with PBS. Monolayers were fixed in 4% paraformaldehyde in PBS (pH 7.4) at room temperature for 20 min. After one wash in PBS, the cells were permeabilized with 0.5% Triton X-100 in PBS at room temperature for 10 min. The samples were then immersed in a blocking solution (5% goat serum, 0.3% Tween 20, PBS) at room temperature for 30 min. Primary antibodies mouse monoclonal anti-ZO1 (1:100, cat. no. 33–9100, Life Technologies) and mouse monoclonal anti-RPE65 (1:200, cat. no. ab13826, Abcam) were diluted in fresh blocking solution, were applied to the specimens and incubated at room temperature for 90 min. The specimens were then washed 3 times in PBS. Primary antibodies were visualized by incubation for 45 min at room temperature with FITC-conjugated goat anti-mouse antibody (1:500, cat. no. A-11001, Life Technologies) diluted in a blocking solution at room temperature. After incubation, the monolayers were washed twice in PBS. The non-specific binding of primary target antibodies was assessed using isotype-matched antibody (1:200, mouse anti-CD117, Serotec) under the same staining conditions (supporting information, figure S4) (stacks.iop.org/BMM/10/045022/mmedia). Nanofibrous membranes with adherent cells were cut from the hanging inserts using a 4 mm biopsy punch

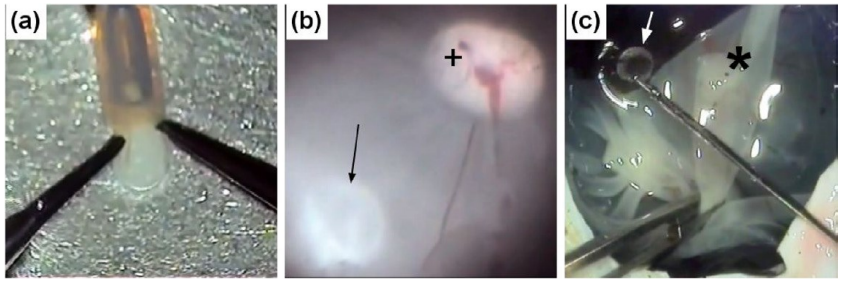

Figure 2. Implantation test into enucleated porcine eyes. (*a*) Insertion of the acellular carrier 2 mm in diameter into the implantation injector (OD/ID 1.97 mm/1.32 mm) using two retinal forceps, (*b*) carrier (black arrow) under the retina, optic disc (black cross), (*c*) extraction of the carrier (white arrow) from the posterior eye-cup after peeling the overlying neural retina (asterisk).

and were mounted with a DAPI containing medium. Cover slides with cultured cells were mounted directly on the microscope slide. Following the fixation and permeabilization steps, F-actin was visualized by staining with rhodamine labelled phalloidin (1:40, cat. no. R415, Life Technologies) in the blocking solution. After 40 min incubation at room temperature the specimens were washed twice with PBS and mounted as described above. Fluorescence microscopy was performed using a VS120 FL Virtual Slide Microscope (Olympus), and images were acquired and processed with VS-ASW FL software.

2.5.3. Transepithelial electrical resistance (TEER)
The TEER values were determined using a Millicell ERS-2 device equipped with STX01 Ag/AgCl electrodes (Merck Millipore). All measurements were performed in culture media at room temperature immediately after removing the insert from the incubator. To obtain the effective TEER, the blank resistance of the insert before cell seeding was subtracted from the resistance of the cell seeded one and the resulting value was multiplied by the effective area of the membrane.

2.6. Cell viability after implantation

The confluent RPE monolayer was prepared on fibrous membranes with an embedded frame and thickness of 3.7 μm as described in paragraph 2.5.1. The punched carrier was implanted into the subretinal space of an enucleated eye, and after removal of the anterior segment and extraction from beneath the neural retina, the carrier was washed with serum-free culture medium and incubated in 4 μM ethidium homodimer-1 (EthD-1, Invitrogen) solution for 30 min to stain the nuclei of dead cells only. Then the EthD-1 solution was removed and the carrier was mounted into a solution of Hoechst 33342 (Invitrogen) at a concentration of 5 μg ml^{-1} to stain all cell nuclei. The whole carriers were scanned with a VS120 FL Virtual Slide Microscope (Olympus) using 20 × objective and fluorescence filter sets for Cy3 and DAPI stains. For the cell viability three carriers before implantation and five carriers after implantation were evaluated.

3. Results

3.1. Fabrication and characterization of the frame-supported electrospun membranes

The proposed structure of the RPE carrier consisted of an electrospun membrane and an embedded supporting frame made of a fibre tens of microns in diameter. A simple three-step procedure was developed to incorporate the frame into the membrane (scheme 1). As a proof of concept, the carrier was fabricated from the membrane of the electrospun PDLLA and the frame of 95 μm-thick poly(4-dioxanone) monofilament suture fibre. The fibre was formed into a circular shape 2.0 to 2.3 mm in diameter, which corresponded to the size of the RPE carriers implanted into rabbits in other studies [33, 34]. Light microscopy and scanning electron microscopy images (figures 3(*a*) and (*b*)) provided evidence that the electrospun mesh has the same structure inside and outside the framed area, with the exception of a transition region 300 μm to 500 μm in width around the frame. In this transition region the fibres were aligned preferably perpendicular to the axis of the frame. Similarly to the mesh structure, the height profiles recorded across the embedded frame showed that the membrane thickness was the same on both sides of the transition region (figure 3(*c*)). The sheets of the membrane deposited on silicon wafers were floated on a water surface and were transferred to auxiliary supports, e.g. a sheet of aluminium foil with an opening (figure 3(*d*)) or the body of a cell culture insert (24-well) devoid of the original membrane (figure 3(*e*)). Both structures kept the membrane flat and allowed the membrane to be manipulated undisturbed in a cell culture dish. When the framed part of the membrane was punched, it could be handled with forceps without folding, in both dry and wet state (figure 3(*f*)).

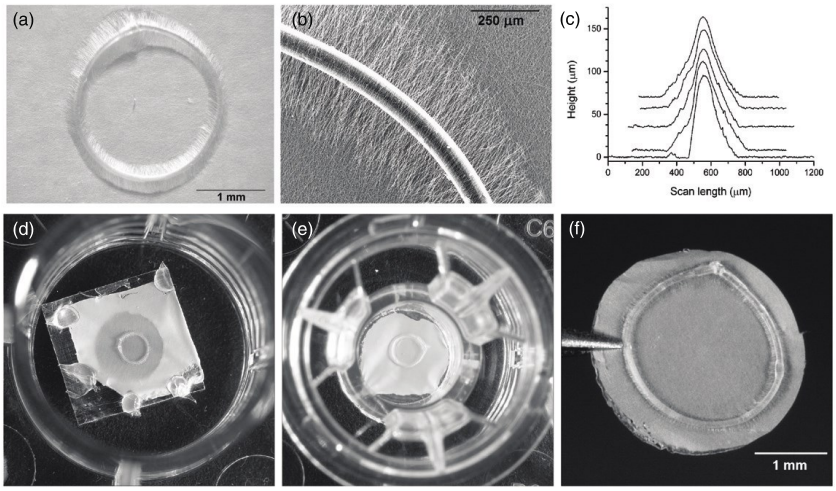

Figure 3. (*a*) Light microscopy image of the 5.3 μm-thick nanofibrous membrane with the embedded frame of 95 μm-thick monofilament fibre. (*b*) A detail of the frame recorded by SEM. (*c*) Height profiles across the frame (the curves were shifted along the *y* axis for clarity). A sheet of the nanofibrous membrane with the frame 2 mm in diameter was transferred and fixed to (*d*) an aluminium foil with an opening or (*e*) the body of a culture well insert (here in a 24-well culture dish), from which a framed part could be cut and easily handled with forceps (*f*).

3.2. Basic characteristics of the fibrous membranes

Electrospun membranes were prepared from 11 wt% PDLLA solution in DMF, and consisted of bead-free fibres with a mean diameter of 640 nm (standard deviation, SD 60 nm) (figure 4(*a*)). The target membrane thickness was achieved using the movable stage, which controlled the dwell time of the silicon wafers in the deposition zone. The thickness of the membranes was adjusted between 1.0 and 6.1 μm to be comparable to or lower than the thickness of the healthy Bruch's membrane [26]. The representative morphology of the thinnest and the thickest investigated membrane is shown in figures 4(*b*) and (*c*), respectively.

The membrane thickness was determined from profiler scans as the average of the 10 highest peaks along a 500 μm-long line scan the baseline of which was located on the surface of the supporting silicon substrate. Such thickness definition better represented the outer borders of the sparse membranes than the average height of the profile. Thickness measurement using a profiler was a destructive and relatively slow process, unlike the measurement of the membrane areal density (mass per unit of area). Therefore, the thickness was usually determined from the areal density using the calibration curve (figure 5). Due to the specific way of determining the thickness, the thickness extrapolated to zero areal density corresponded to the thickness of a single fibre.

The repeatability of the membrane preparation was characterized by the intra-batch relative standard deviation (RSD) of the areal density (supporting information, figure S3) (stacks.iop.org/BMM/10/045022/mmedia). The statistical nature of the fibre deposition resulted in RSD of 17% for the mean areal density of 8.5 μg cm^{-2}, and decreased down to 6% with increasing mean areal density up to 172 μg cm^{-2}.

3.3. Pore size distribution and critical membrane thickness

The pore size distribution of the electrospun fibrous membranes is a function of the two main adjustable processing parameters: areal density and fibre width [47]. At a constant fibre width, the general trend is that the mean pore size increases as the areal density or the membrane thickness decreases. When analyzing a 3D fibrous network as a scaffold for cell seeding, the network can be considered as a 2D projection to the plane of the network support if the network is thinner than the diameter of a single dissociated cell. This planar network has a polygonal structure. The pore size is then understood as the diameter of an inscribed circle in a polygon, and 2D porosity is understood as a fractional area of the openings.

In designing fibrous meshes for cultivating and transplanting RPE cells with the aim to identify the lowest applicable thickness or the corresponding areal density of the mesh, an obvious limitation is the fraction of pores exceeding the size of a dissociated cell. If this fraction is large enough, a part of the applied cell suspension will pass the membrane and will be lost for the formation of the cell monolayer. Moreover, the retained cells will possibly fail to bridge the large pores and to form a confluent layer. When specifying this criterion,

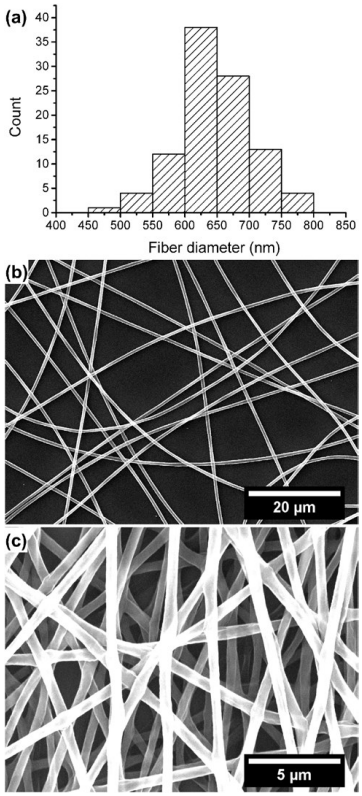

Figure 4. (*a*) Electrospun fibre diameter distribution with a mean diameter of 640 nm (SD = 60 nm) and representative scanning electron microscopy images of the electrospun meshes with the lowest and the highest investigated thickness of 1.0 μm (*b*) and 6.1 μm (*c*), respectively.

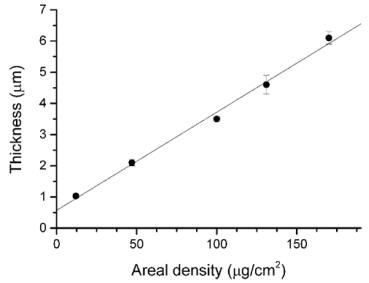

Figure 5. Thickness (mean ± SD, n =5) of the fibrous membrane as a function of the areal density. The slope and the increment of the linear fit were 0.032 μm • cm^2 μg^{-1} and 0.57 μm, respectively. The thickness was calculated from the height profiles as the average of the 10 highest peaks along a 500 μm-long scan by the profiler.

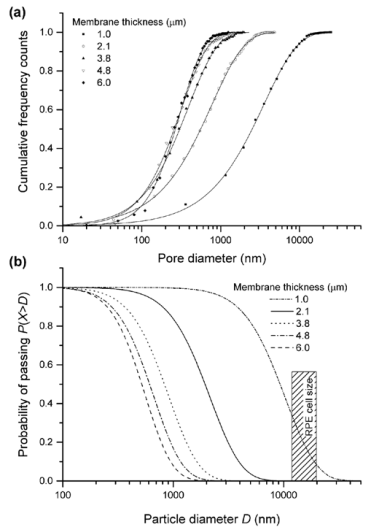

Figure 6. Analysis of the 2D pore size distribution of fibrous membranes of different thicknesses composed of 640 nm-thick fibres. (*a*) Cumulative frequency counts of the pore diameter acquired from image analysis of SEM images. The data were fitted to the cumulative gamma distribution function. (*b*) Probability (pore-area weighted) that a spherical particle with diameter D encounters a pore with a diameter larger than D, together with the depicted typical diameter range (12–22 μm) of freshly isolated porcine RPE cells.

we assumed that cell retention or passage was controlled only by the 'geometrical fitting' of a single cell to a pore, and that there were no other effects enhancing the retention, e.g. electrostatic forces, decreasing pore size by the retained cells, or the presence of multicellular aggregates in the cell suspension.

To determine the critical membrane thickness, the pore size cumulative distribution functions for different membrane thicknesses were compared with the minimal size of a dissociated RPE cell. The cumulative frequency counts of the pore sizes were acquired from SEM image analysis, and each set of data for a particular membrane thickness was fitted to the gamma cumulative distribution function (CDF) [48] (figure 6(*a*)). The distribution functions of the pore sizes were broad, with the distribution body covering the sizes of about two orders of magnitude. The fitted CDFs were further recalculated (supporting information) (stacks.iop.org/BMM/10/045022/mmedia) to provide the probability that a cell with diameter D or smaller will pass through the membrane by percolation [49] (figure 6(*b*)). This probability can also be interpreted as the fractional area of pores larger than cell size D. The smallest diameter of freshly isolated porcine RPE cells found in the suspension was 12 μm (supporting information, figure S2) (stacks.iop.org/BMM/10/045022/mmedia). A large proportion of the RPE cells would therefore pass through a mem-

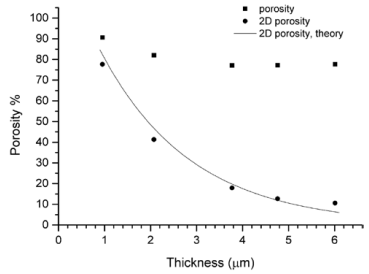

Figure 7. Porosity (squares) and 2D porosity (circles) of the PDLLA nanofibrous membranes (the mean fibre width of 640 nm) as a function of the membrane thickness. Porosity was calculated from equation (1), using fibre material density of 1.248 g . cm^{-3}, and the experimentally determined membrane thickness and areal density. 2D porosity was derived from SEM image analysis, and the data points were overlaid with the exponential function (supporting information, equation (4)) (stacks.iop.org/BMM/10/045022/mmedia) originating in the model of straight fibres positioned according to the Poisson line process in two dimensions.

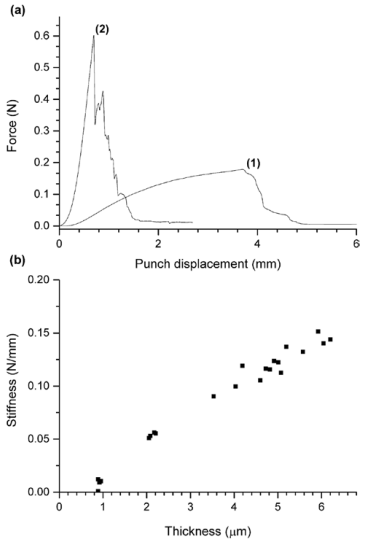

Figure 8. (*a*) Punch load-displacement curve from the small punch test performed on the nanofibrous PDLLA membrane 3.5 μm in thickness (1) and on a reference commercial PET membrane 10 μm in thickness (2). (*b*) Stiffness of the nanofibrous PDLLA membrane as a function of membrane thickness.

brane 0.95 μm in thickness, but the cells would be fully retained on membrane 2.1 μm in thickness. To further specify the critical thickness, we interpolated the CDF of the pore diameter as a function of the areal density to match the area fraction of larger pores $P(X > 12\ \mu m)$ equal to 1% (supporting information, equation (3)) (stacks.iop.org/BMM/10/045022/mmedia). The calculated areal density was 31 $\mu g\,cm^{-2}$, corresponding to a membrane thickness of 1.6 μm.

3.4. Membrane porosity

In addition to carrier thickness and pore size distribution, the porosity of the carrier is another design parameter that is essential for maintaining physiological flows of nutrients and for preserving the normal function and anatomy of the neuroretina [35]. The porosity of the investigated membranes decreased from 91% for the sparsest membrane 0.95 μm in thickness down to 77% for a thickness of 3.7 μm and higher (figure 7). For comparison, 2D porosity of the 2D model of the fibrous network was also plotted in figure 7. The 2D porosity represents the porosity fraction arising from the straight-through pores. The 2D porosity decreased from 79% for the 0.95 μm-thick membrane down to 11% for the 6.0 μm-thick membrane, and the data complied well with the theoretical negative exponential dependence (supporting information, equation (4)) (stacks.iop.org/BMM/10/045022/mmedia) originating in the arrangement of fibre axes according to the Poisson line process.

3.5. Membrane stiffness

Uniaxial stress-strain testing is a preferred method for mechanical testing of nanofibrous membranes [50]. However, in this case the membrane was thinner than 10 μm, and it was impossible to handle it in the large pieces necessary for the stress–strain test. We therefore used a small punch test, which is a biaxial mechanical test for miniature specimens. The advantage of this test is that the membrane undergoes a similar type of deformation as it does in the eye where it is pressed with the retina against the concave surface of the subretinal space. Figure 8(*a*) shows a typical punch load-displacement curve for the PDLLA nanofibrous membrane 3.5 μm in thickness (curve (1)). Following an initial toe-in region, the curves exhibited a linear region, from which the stiffness was calculated. The stiffness was determined as the slope of a line fitted to the linear part of the load-displacement curve. The stiffness of nanofibrous PDLLA membranes as a function of membrane thickness is plotted in figure 8(*b*). For comparison, we also measured stiffness of a commercial porous PET membrane 10 μm in thickness (figure 8(*a*), curve 2) that was employed by other researches as an RPE cell carrier in an *in vivo* study [34]. The stiffness of the PET membrane was 1.4 $\pm$ 0.2 N mm^{-1} (average from 3 measurements $\pm$ SD), while the stiffness of a nanofibrous PDLLA membrane of the same thickness would be 0.25 N mm^{-1}, as extrapolated from the plot in figure 8(*b*).

3.6. Resistance to mechanical stress during surgery

To test the resistance of the frame-supported PDLLA membranes to the mechanical stress during surgical handling and to investigate the effect of membrane thickness, the membranes were implanted into the enucleated porcine eyes under conditions that closely

Table 1. Damage to the frame-supported membrane due to the implantation surgery as a function of membrane thickness. The approximate damage was assessed from light microscope images of the explanted membranes as follows: +++ completely damaged membrane, ++ area of missing membrane of 10–20%, + area of missing membrane of <10%, '0' intact membrane. Four samples of the same membrane thickness were subjected to the implantation test.

	Membrane thickness			
Replicate	0.89 μm	1.8 μm	3.4 μm	4.0 μm
1	+ ++	+ +	+	0
2	+ +	+	+	0
3	+	0	0	0
4	+	0	0	0

simulated the human transplantation procedure. The injector was a cannula similar in size (OD 1.97 mm, ID 1.32 mm) to the injector used in transplanting retinal sheets into human eyes [51], and required a sclerotomy of 4.1 mm. The damage to the membrane as a function of thickness was assessed by the fraction of the missing membrane in the framed area of the carrier after implantation and extraction from the enucleated eye (table 1). All of the samples with the lowest thickness of 0.89 μm were at least partially damaged, while those with thickness of 1.8 μm and 3.4 μm showed minor damage or no damage. The membranes 4.0 μm in thickness were found to be microscopically intact after the procedure, and it was assumed that thicker membranes would be equally resistant.

An optical section of the retina by SD-OCT provided evidence that the 4 μm-thick membrane re-established an unfolded shape when implanted into the subretinal space (figure 9).

3.7. Porcine RPE cell culture

On the basis of the analysis presented above, a 3.7 μm-thick nanofibrous membrane was selected for the RPE cell culture. This membrane contained practically only pores smaller than the RPE cell size (figure 6(*b*)), and was sufficiently resistant to surgical handling when combined with the supporting frame (table 1). To evaluate the effect of the nanofibrous structure on the RPE cell culture, glass-cover slips covered with a PDLLA smooth film were used as a reference surface.

3.7.1. *Immunocytochemistry*

At passage 1, the primary porcine RPE cells seeded at a density of 2000 cell mm^{-2} attached to both PDLLA film and nanofiber surfaces within 2 d. During the 30 d of subsequent culture, regular RPE cell monolayers were formed with a density of 2000 $\pm$ 300 cell mm^{-2}, which was not much different from the seeding density. Phalloidin staining of F-actin revealed the polygonal morphology of the cells irrespective of the kind of surface used (figures 10(*a*) and (*d*)). The epithelial phenotype was further assessed by screening of tight junctions via ZO-1 protein and by screening of the RPE65 protein, which is involved in retinoid processing and is specific for RPE. ZO-1 was stained positive in cultures on both the PDLLA film and the nanofibrous membrane (figures 10(*b*) and (*e*)). However, in contrast to the cultures on a PDLLA film (figure 10(*b*)), the cells grown on nanofiber membranes (figure 10(*e*)) displayed a more distinct localization of ZO-1 immunofluorescence signal to cell–cell contacts. RPE65 was also stained positive on both types of surfaces (figures 10(*c*) and (*f*)).

3.7.2. *Transepithelial electrical resistance*

The functional properties of RPE monolayers on nanofibrous membranes were further evaluated by measuring the transepithelial electrical resistance (TEER), which indicates the maturation of cell-to-cell junctions [52]. After one month in culture, the RPE monolayers achieved (net) TEER values of 179 $\pm$ 59 Ω cm^2 ($n = 3$, 3 replicates).

3.7.3. *Cell viability after implantation*

To assess the survival of the RPE cells during the implantation procedure, we grew a cell monolayer on the 3.7 μm-thick nanofibrous membrane, cut the membrane along the embedded frame and implanted it into an enucleated porcine eye. The viability of the cells was determined using a two-colour test to stain dead cells (EthD-1, yellow fluorescence) and total cells (Hoechst 33342) at two stages in the implantation procedure: (i) before implantation just after cutting the carrier from the membrane and (ii) after implantation. The representative fluorescent images are shown in figure 11. The cutting of the membrane itself and the subsequent transfer of the carrier to the staining solution caused some cell detachment as well as cell death on the periphery of the carrier. The extent of cell loss and of cell death increased during implantation when the major contribution to the total mechanical stress was generated while the carrier was being loaded into the implantation injector and while the carrier was being inserted into the subretinal space. Extracting the carrier from the eye may also have generated additional cell loss. Nevertheless, after implantation, most of the cells on the carrier remained attached and alive, as indicated by the comparison of the above mentioned two-colour fluorescence staining. Dead cells and decellularized regions were located mainly on the periphery of the carrier, but they also appeared on the frame and also to some extent also inside the framed area. Unfortunately, some of the image fields of the virtual slide image were out of focus, due to the wavy surface of the carrier, and the cell nuclei could not be resolved. A quantitative evaluation by counting the nuclei was therefore not possible.

4. Discussion

4.1. Structure of the carrier: limitations, and possibilities for improvements

Nanofibrous electrospun meshes have been found to be a superior carrier material for preparing a

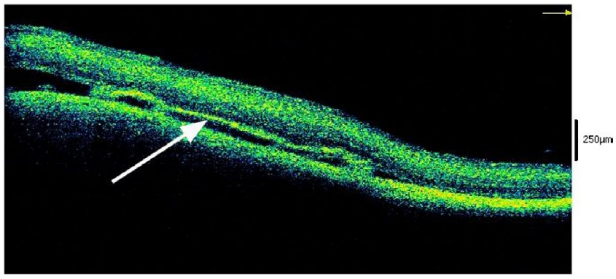

Figure 9. SD-OCT image of the frame-supported membrane (arrow) implanted *ex vivo* into the subretinal space.

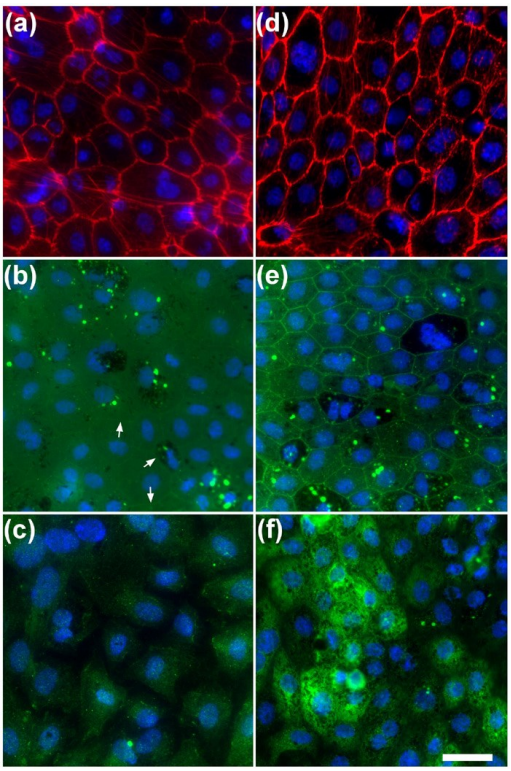

Figure 10. Immunofluorescence images of porcine primary RPE cultures on a smooth PDLLA film (*a*)–(*c*) and on a fibrous membrane (*d*)–(*f*) after a 30 d culture. The circumferential actin ring visualized by rhodamine-phalloidin staining (*a*, *d*) revealed the polygonal morphology characteristic of RPE. ZO-1, a marker of a tight junction complex, was present in cultures both on the PDLLA nanofibrous membrane (*e*) and on the smooth film (*b*). The localization of ZO-1 in cell–cell contacts was less distinct on the smooth film surface (arrows point to the cell–cell contacts). RPE65, a specific metabolic marker of RPE, was also stained positive on both types of surfaces. The bright punctate objects are staining artefacts. Scale bar 30 μm.

polarized RPE monolayer [34, 37–40, 53]. However, a wetted mesh thinner than 10 μm tends to be too floppy to allow subretinal implantation of the RPE cell layer without folding or wrinkling. Such behaviour would be even more critical for a large-scale RPE graft, e.g. 3 × 6 mm in size, which is intended for transplantation in the ongoing clinical trial WHO reg. no. NCT01691261.

In this study, we have designed and fabricated an ultrathin nanofibrous carrier equipped with a supporting frame that makes it feasible to transplant the RPE cell monolayer on the fine supporting structure. Benefiting from the flexibility of the electrospinning process, the supporting frame was sandwiched between two equally thick layers of the membrane successively deposited on the silicon wafer. Importantly, the frame was held by the nanofibers strongly enough so that no post-processing fixation was needed. In a simulated implantation using porcine cadaver eyes, we have demonstrated the mechanical stability of the carrier composed of a circular frame 2 mm in diameter made of a 95 μm-thick PDS fibre and a nanofibrous PDLLA mesh with thickness lower than 6 μm. Such a thickness corresponded to the upper value reported for the thickness of Bruch's membrane [26]. The frame prevented the membrane from collapsing during loading into the injector, and allowed the flat shape of the membrane to be re-established when implanted into the subretinal space (figure 9).

In line with the assumption that the success of RPE monolayer transplantation can be enhanced if the cell carrier is thinner than Bruch's membrane, we searched for the minimum membrane thickness that would still be compatible with both the surgical handling and the *in vitro* preparation of the RPE monolayer from the cell suspension. Using a simple tubular injector with an inner diameter of 1.32 mm, we showed that membranes assembled of 640-nm-thick PDLLA fibres resisted the mechanical stress of the implantation if the membrane was thicker than ca 3.5 μm. For thinner membranes, we observed that most of the damage to the membrane was generated during loading into the injector when the membrane was bent co-ordinately with two retinal forceps. Rather than puncturing of the membrane we observed disjoining of the supporting frame from the membrane. With decreasing membrane thickness, the strength of the clamping of the nanofibrous membrane around the frame decreased, and when the membrane was loaded into the injector the frame deformation resulted in fracture or disentanglement of the nanofibers and partial release of the frame. The compatibility of the 3.7 μm-thick nanofibrous membrane with the surgical handling was further examined by the *ex vivo* implantation of the RPE cell monolayer into an enucleated eye. The post-implantation analysis showed that most of the cells remained attached to the carrier and alive. However, on the periphery of the carrier behind the framed area an appreciable fraction of the cells was detached or dead (figure 11) as a result of the carrier punching from the membrane and loading into the injector. Such a transplant with the incomplete RPE monolayer may have lower transplantation efficacy. This problem could be overcome by a modification of the instrumentation that would allow the carrier to be cut and transferred more carefully.

Much lower mechanical stress might be imposed on the carrier if it was transferred with an advanced implantation tool similar to that reported by Stanzel *et al* [33]. This tool has an oval, flattened nozzle, and is equipped with a loading window that allows careful loading and transfer of a flat carrier without deformation. We can therefore envisage that the nanofibrous membrane might be considerably thinner than 4.0 μm. We also presume that the supporting frame could be thinner than 95 μm to retain sufficient stiffness for the manipulation. In a trial fabrication, we embedded a circular frame 2 mm in diameter made of 40 μm-thick monofilament suture fibre (Vicryl, 9-0, Ethicon) with a tensile modulus 7.5 times higher than that of PDS. This frame prevented the wetted carrier collapsing when it was lifted up using forceps. However, both PDS and Vicryl are resorbable materials that lose a large proportion of their initial tensile modulus in several weeks *in vivo*, as stated in the product specification. Softening of the carrier frame will also occur during *in vitro* preparation of an RPE cell monolayer, which typically takes 4 to 6 weeks to attain epithelial phenotype. To retain the mechanical response of the frame-supported carrier after culture, a nonresorbable frame or a more efficient culture protocol with a shorter culture period will have to be used. By reducing the mechanical stress during implantation with the aid of the advanced implantation tool the damage to transplanted cells would likely be also reduced.

4.2. Comparison with other carriers

Although numerous carriers for RPE transplantation have been proposed [22], few of them were thinner than or comparable to the thickness of Bruch's membrane and were tested at the same time in a preclinical animal study. Stanzel *et al* [35] implanted a continuous polarized layer of adult human RPE cells grown on a 10 μm-thick commercial PET membrane with 0.4 μm-large pores and nominal porosity of 0.5%. The RPE cells transplanted into rabbit eyes showed survival and retained polarized characteristics for 4 weeks. However, although the transplanted cells were alive and differentiated, the above-lying neuroretina degenerated within 1 week. The authors suggested that one of the factors causing the degeneration was the low permeability of the carrier. Similar degeneration of the neuroretina was reported for a hESC-RPE cell layer grown on a 300 nm-thick Parylene C membrane supported on a 6 μm-thick mesh frame that covered ca 43% of the membrane area [25]. The membrane material contained only nanosized pores that allowed hydrophilic tracers with a diameter smaller than 50 nm to pass [54]. The outer nuclear layer (ONL) above the implant disappeared in one third of the number of animals after 1 month, and in 92% of the animals after 6 months, although the implanted RPE cells survived for at least 12 months. Again, the failure of the implanted RPE in supporting the neuroretina could be explained by limited transport of nutrients to the photoreceptors. In this case, it was probably caused by a blockage of the carrier nanosized pores by the lipophilic deposits that

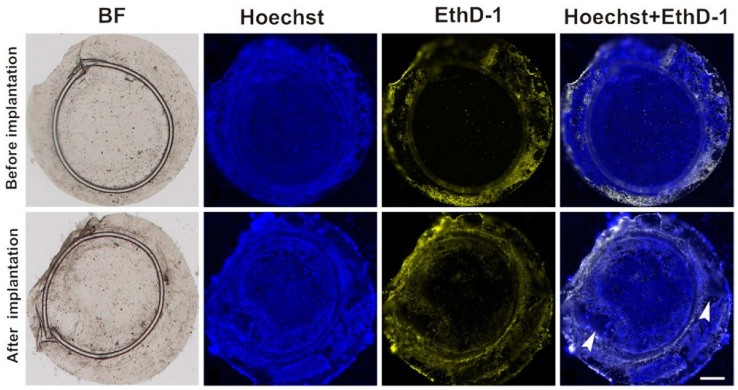

Figure 11. Bright field (BF) and fluorescent histochemical images of the whole RPE cell seeded nanofibrous carrier before and after implantation into the subretinal space. Hoechst 33342 stained nuclei of all cells (live and dead) while EtD-1 stained dead cells only. The regions free of fluorescence (arrows) indicated cell detachment. The BF and Hoechst images showed that most of the RPE cells present on the punched membrane remained attached after implantation although, there was an increase in the cell-free area, which was already present before implantation.. The most affected regions are located on the periphery of the carrier where the membrane came into contact with the punch and the tweezers. The number of dead cells increased after implantation, but they were less numerous than the live cells, and were found mostly in the peripheral region. Scale bar 400 μm.

are typical waste products of the RPE metabolism [1], or by an insufficient area fraction of the 300 nm-thick membrane in the carrier.

Another essential characteristic of the carrier is its stiffness. The implanted carrier has to have a sufficiently low stiffness to adapt to the curvature of the posterior eye and to establish a close contact with the adjacent tissue on the basal site. The pressure from the neuroretina against the carrier is low and possibly further reduced due to the malfunction of the RPE. However, no specific pressure value can be defined and the effect of the carrier stiffness can be only evaluated from the *in vivo* optical sections of the implanted carrier (i.e. OCT images). Commercial porous PET membrane 10 μm in thickness, which was used in several animal studies [33–35], had sufficiently low stiffness to conform to the curvature of the subretinal space. The stiffness of the presented PDLLA nanofibrous membrane with thickness of 4 μm was one order of magnitude lower than that of the commercial PET membrane (figure 8(*a*)), and shape adaptation of the PDLLA nanofibrous carrier should be therefore easier.

The RPE metabolic activity necessary for maintaining the above-lying neuroretina requires a carrier with lower barrier characteristics represented mainly by carrier thickness, porosity and pore size distribution. In these aspects, the nanofibrous PDLLA carrier presented here is superior to the PET and Parylene C carriers described above. Not only does it have a much higher pore size, with the dominating fraction between 100 and 1000 nm (figure 6(*a*)), but it also has much higher open porosity of 77% with a 17% fraction of porosity from the straight-through pores in the case of a 3.7 μm-thick membrane (figure 7). Furthermore, we anticipate that the thickness of the nanofibrous carrier could be reduced at least down to 2 μm without loss of resistance to surgical handling if an advanced implantation tool is used [33]. Further reduction may be limited by failure to support the cellular monolayer due to the presence of pores larger than the size of the individual cell (figure 6(*b*)).

4.3. Porcine RPE cell monolayer

Due to its anatomical and phylogenetic proximity, the porcine eye is in many aspects a powerful experimental model of the human eye [55] for studies of human retinal diseases and for developing surgical protocols [56, 57]. We therefore investigated the epithelialization of the primary porcine RPE cells on a nanofibrous membrane *in vitro* to enable future studies of RPE allotransplantation into the porcine animal model as a parallel to human RPE allotransplantations. We have demonstrated that an ultrathin (3.7 μm) PDLLA nanofibrous membrane can well support reconstitution of the epithelial phenotype of the porcine RPE cells while being mechanically resistant to the transplantation surgery. RPE cells attached reproducibly to the nanofibrous membrane and formed an epithelial-like monolayer. After one month culture, the RPE identity was proven by the detection of RPE65 and ZO-1 markers. In addition, the immunocytochemistry indicated an enhancing effect of the nanofibrous surfaces on the expression of ZO-1 over the smooth PDLLA surface. A similar enhancing effect of the nanofibrous surface was previously reported for the culture of human fetal cells [34] and human adult RPE cells [40]. This effect originates in the nanotopographical cues that are known to be potent modulators of cellular behaviour [58–60].

Although in most published protocols the RPE cells are seeded at a density in the range of 500 to 1000 cell mm^{-2}, we preferred to use a higher seeding den-

sity of 2000 cell mm^{-2}, for two reasons. First, in order to reach high RPE cell densities at least comparable to those in peripheral regions of the human fundus [61], and second, to preserve most of the differentiation markers, which are otherwise gradually lost during the extensive proliferation that occurs at the lower densities of adult RPE cells [62]. Toops *et al* [63] recently reported effective formation of tight and well differentiated primary porcine RPE monolayers when the cells were seeded at densities above 1500 cell mm^{-2}. The corresponding TEER was close to 100 Ω cm^2 after 21 d in culture, and increased with increasing seeding density up to 450 Ω cm^2 for a seeding density of 3000 cell mm^{-2}. In our *in vitro* cultivation of porcine RPE cells with a seeding density of 2000 cell mm^{-2} we found TEER of 179 ± 59 Ω cm^2, which provided evidence for the formation of impermeable tight junctions and a functional cell barrier, and was in accord with the values of Toops *et al* [63]. Taken together, the polygonal morphology, the presence of ZO-1 and RPE65 differentiation markers together with the high value of TEER found in the cultivated RPE cell layers on a nanofibrous membrane strongly indicate their differentiated status suitable for *in vivo* transplantation studies.

5. Conclusion

Ultrathin membranes assembled from nanofibers represent a promising carrier for the transplantation of RPE cells. RPE cells seeded onto this carrier benefit not only from the nanotopography that boosts reconstitution of their epithelial phenotype, but also from high porosity, large pore size and low thickness of the carrier, which all contribute to the high carrier permeability. In this study, we have presented a fabrication of the ultrathin nanofibrous PDLLA carrier supported by a peripheral frame. The frame makes it possible to surgically handle the carrier and to restore the flat shape of the carrier when inserted into the subretinal space. We have also demonstrated in an *ex vivo* test that most of the transplanted RPE cells on the carrier remained viable. The minimalistic supporting structure is assumed to enhance the therapeutic effect of RPE cell transplantations.

Acknowledgments

The authors would like to thank Ethicon Inc. for the kind gift of the suture material and Jatky Český Brod a.s. for providing enucleated porcine eyes. Dr Martina Nevoralová is acknowledged for her assistance with electron microscopy, Dr Hynek Beneš for taking the macro photos and Dr Jiří Czernek for the MATLAB calculations. The authors also thank MD Igor Kozák for helpful discussions concerning the transplantation surgery. This study was supported by the Czech Science Foundation (grant P108/12/1629) the Charles University in Prague (project GA UK No 203 62 14), the Ministry of Education, Youth and Sports of the Czech Republic (grant EE2.3.30.0029), the European Regional Development Fund ('BIOCEV—Biotechnology and Biomedicine Centre of the Academy of Sciences and Charles University' project, CZ.1.05/1.1.00/02.0109) and by the project ExAM (CZ.1.05/2.1.00/03.0124). Their financial support is gratefully acknowledged.

References

[1] Strauss O 2005 The retinal pigment epithelium in visual function *Physiol. Rev.* **85** 845–81
[2] Ramsden C M, Powner M B, Carr A J F, Smart M J K, da Cruz L and Coffey P J 2013 Stem cells in retinal regeneration: past, present and future *Development* **140** 2576–85
[3] Binder S, Stanzel B V, Krebs I and Glittenberg C 2007 Transplantation of the RPE in AMD *Prog. Retin. Eye Res.* **26** 516–54
[4] da Cruz L, Chen F K, Ahmado A, Greenwood J and Coffey P 2007 RPE transplantation and its role in retinal disease *Prog. Retin. Eye Res.* **26** 598–635
[5] Peyman G A, Blinder K J, Paris C L, Alturki W, Nelson N C and Desai U 1991 A technique for retinal-pigment epithelium transplantation for age-related macular degeneration secondary to extensive subfoveal scarring *Ophthalmic Surg. Lasers* **22** 102–8
[6] van Zeeburg E J T, Maaijwee K J M, Missotten T O A R, Heimann H and van Meurs J C 2012 A free retinal pigment epithelium-choroid graft in patients with exudative age-related macular degeneration: results up to 7 years *Am. J. Ophthalmol.* **153** 120–7
[7] Aisenbrey S *et al* 2002 Macular translocation with 360 degrees retinotomy for exudative age-related macular degeneration *Arch. Ophthalmol.* **120** 451–9
[8] Algvere P V, Gouras P and Kopp E D 1999 Long-term outcome of RPE allografts in non-immunosuppressed patients with AMD *Eur. J. Ophthalmol.* **9** 217–30
[9] Radtke N D, Aramant R B, Petry H M, Green P T, Pidwell D J and Seiler M J 2008 Vision improvement in retinal degeneration patients by implantation of retina together with retinal pigment epithelium *Am. J. Ophthalmol.* **146** 172–82
[10] Radtke N D, Aramant R B, Seiler M J, Petry H M and Pidwell D 2004 Vision change after sheet transplant of fetal retina with retinal pigment epithelium to a patient with retinitis pigmentosa *Arch. Ophthalmol.* **122** 1159–65
[11] Vugler A *et al* 2008 Elucidating the phenomenon of HESC-derived RPE: anatomy of cell genesis, expansion and retinal transplantation *Exp. Neurology* **214** 347–61
[12] Carr A J F, Smart M J K, Ramsden C M, Powner M B, da Cruz L and Coffey P J 2013 Development of human embryonic stem cell therapies for age-related macular degeneration *Trends Neurosci.* **36** 385–95
[13] Reynolds J and Lamba D A 2013 Human embryonic stem cell applications for retinal degenerations *Exp. Eye Res.* **123** 151–60
[14] Wright L S, Phillips M J, Pinilla I, Hei D and Gamm D M 2014 Induced pluripotent stem cells as custom therapeutics for retinal repair: progress and rationale *Exp. Eye Res.* **123** 161–72
[15] Kamao H, Mandai M, Okamoto S, Sakai N, Suga A, Sugita S, Kiryu J and Takahashi M 2014 Characterization of human induced pluripotent stem cell-derived retinal pigment epithelium cell sheets aiming for clinical application *Stem Cell Rep.* **2** 205–18
[16] Kvanta A and Grudzinska M K 2014 Stem cell-based treatment in geographic atrophy: promises and pitfalls *Acta Ophthalmol.* **92** 21–6
[17] Cyranoski D 2013 Stem cells cruise to clinic *Nature* **494** 413
[18] Schwartz S D, Hubschman J P, Heilwell G, Franco-Cardenas V, Pan C K, Ostrick R M, Mickunas E, Gay R, Klimanskaya I and Lanza R 2012 Embryonic stem cell trials for macular degeneration: a preliminary report *Lancet* **379** 713–20
[19] Schwartz S D *et al* 2015 Human embryonic stem cell-derived retinal pigment epithelium in patients with age-related macular degeneration and Stargardt's macular dystrophy: follow-up of two open-label phase 1/2 studies *Lancet* **385** 509–16

[20] Falkner-Radler C I, Krebs I, Glittenberg C, Povazay B, Drexler W, Graf A and Binder S 2011 Human retinal pigment epithelium (RPE) transplantation: outcome after autologous RPE-choroid sheet and RPE cell-suspension in a randomised clinical study *Br. J. Ophthalmol.* **95** 370–5
[21] Yaji N, Yamato M, Yang J, Okano T and Hori S 2009 Transplantation of tissue-engineered retinal pigment epithelial cell sheets in a rabbit model *Biomaterials* **30** 797–803
[22] Hynes S R and Lavik E B 2010 A tissue-engineered approach towards retinal repair: scaffolds for cell transplantation to the subretinal space *Graefes Arch. Clin. Exp. Ophthalmol.* **248** 763–78
[23] Sheridan C M, Mason S, Pattwell D M, Kent D, Grierson I and Williams R 2009 Replacement of the RPE monolayer *Eye* **23** 1910–5
[24] Stout J T and Francis P J 2011 Surgical approaches to gene and stem cell therapy for retinal disease *Hum. Gene Ther.* **22** 531–5
[25] Diniz B *et al* 2013 Subretinal implantation of retinal pigment epithelial cells derived from human embryonic stem cells: improved survival when implanted as a monolayer *Invest. Ophthalmol. Vis. Sci.* **54** 5087–96
[26] Ramrattan R S, van der Schaft T L, Mooy C M, de Bruijn W C, Mulder P G H and de Jong P T V M 1994 Morphometric analysis of Bruchs membrane, the choriocapillaris, and the choroid in aging *Invest. Ophthalmol. Vis. Sci.* **35** 2857–64
[27] Thomson R C, Giordano G G, Collier J H, Ishaug S L, Mikos A G, LahiriMunir D and Garcia C A 1996 Manufacture and characterization of poly(alpha-hydroxy ester) thin films as temporary substrates for retinal pigment epithelium cells *Biomaterials* **17** 321–7
[28] Giordano G G, Thomson R C, Ishaug S L, Mikos A G, Cumber S, Garcia C A and LahiriMunir D 1997 Retinal pigment epithelium cells cultured on synthetic biodegradable polymers *J. Biomed. Mater. Res.* **34** 87–93
[29] Lu L C, Garcia C A and Mikos A G 1998 Retinal pigment epithelium cell culture on thin biodegradable poly(DL-lactic-co-glycolic acid) films *J. Biomater. Sci. Polym. Ed.* **9** 1187–205
[30] Lu L C, Nyalakonda K, Kam L, Bizios R, Gopferich A and Mikos A G 2001 Retinal pigment epithelial cell adhesion on novel micropatterned surfaces fabricated from synthetic biodegradable polymers *Biomaterials* **22** 291–7
[31] Lu L C, Yaszemski M J and Mikos A G 2001 Retinal pigment epithelium engineering using synthetic biodegradable polymers *Biomaterials* **22** 3345–55
[32] Hadlock T, Singh S, Vacanti J P and McLaughlin B J 1999 Ocular cell monolayers cultured on biodegradable substrates *Tissue Eng.* **5** 187–96
[33] Stanzel B V, Liu Z, Brinken R, Braun N, Holz F G and Eter N 2012 Subretinal delivery of ultrathin rigid-elastic cell carriers using a metallic shooter instrument and biodegradable hydrogel encapsulation *Invest. Ophthalmol. Vis. Sci.* **53** 490–500
[34] Liu Z, Yu N, Holz F G, Yang F and Stanzel B V 2014 Enhancement of retinal pigment epithelial culture characteristics and subretinal space tolerance of scaffolds with 200 nm fiber topography *Biomaterials* **35** 2837–50
[35] Stanzel B V *et al* 2014 Human RPE stem cells grown into polarized RPE monolayers on a polyester matrix are maintained after grafting into rabbit subretinal space *Stem Cell Rep.* **2** 64–77
[36] Hu Y T *et al* 2012 A novel approach for subretinal implantation of ultrathin substrates containing stem cell-derived retinal pigment epithelium monolayer *Ophthalmic Res.* **48** 186–91
[37] Sorkio A, Porter P J, Juuti-Uusitalo K, Meenan B, Skottman H and Burke G 2015 Surface modified biodegradable electrospun membranes as a carrier for human embryonic stem cell derived retinal pigment epithelial cells *Tissue Eng.* A (doi:10.1089/ten.TEA.2014.0640)
[38] Xiang P *et al* 2014 A novel Bruch's membrane-mimetic electrospun substrate scaffold for human retinal pigment epithelium cells *Biomaterials* **35** 9777–88
[39] Thieltges F, Stanzel B V, Liu Z and Holz F G 2011 A nanofibrillar surface promotes superior growth characteristics in cultured human retinal pigment epithelium *Ophthalmic Res.* **46** 133–40
[40] Warnke P H, Alamein M, Skabo S, Stephens S, Bourke R, Heiner P and Liu Q 2013 Primordium of an artificial Bruch's membrane made of nanofibers for engineering of retinal pigment epithelium cell monolayers *Acta Biomater.* **9** 9414–22
[41] Kubies D, Rypacek F, Kovarova J and Lednicky F 2000 Microdomain structure in polylactide-block-poly(ethylene oxide) copolymer films *Biomaterials* **21** 529–36
[42] Sawyer L C and Grubb D T 1996 *Polymer Microscopy* 2nd edn (London: Chapman and Hall) p 85
[43] Schneider C A, Rasband W S and Eliceiri K W 2012 NIH Image to ImageJ: 25 years of image analysis *Nat. Methods* **9** 671–5
[44] Borgefors G 1986 Distance transformations in digital images *Comput. Vis. Graph. Image Process.* **34** 344–71
[45] Riedl B and Prud'Homme R E 1986 Thermodynamic study of poly(vinyl chloride)/polyester blends by inverse-phase gas chromatography at 120 °C *J. Polym. Sci.* B **24** 2565–82
[46] Kurtz S M, Foulds J R, Jewett C W, Srivastav S and Edidin A A 1997 Validation of a small punch testing technique to characterize the mechanical behaviour of ultra-high-molecular-weight polyethylene *Biomaterials* **18** 1659–63
[47] Eichhorn S J and Sampson W W 2005 Statistical geometry of pores and statistics of porous nanofibrous assemblies *J. R. Soc. Interface* **2** 309–18
[48] Dodson C T J and Sampson W W 1996 The effect of paper formation and grammage on its pore size distribution *J. Pulp Pap. Sci.* **22** J165–J9
[49] Castro J and Ostoja-Starzewski M 2000 Particle sieving in a random fiber network *Appl. Math. Modelling* **24** 523–34
[50] Nisbet D R, Rodda A E, Finkelstein D I, Horne M K, Forsythe J S and Shen W 2009 Surface and bulk characterisation of electrospun membranes: problems and improvements *Colloids Surf.* B **71** 1–12
[51] Radtke N D, Aramant R B, Seiler M and Petry H M 1999 Preliminary report: indications of improved visual function after retinal sheet transplantation in retinitis pigmentosa patients *Am. J. Ophthalmol.* **128** 384–7
[52] Madara J L 1998 Regulation of the movement of solutes across tight junctions *Annu. Rev. Physiol.* **60** 143–59
[53] Stanzel B V, Englander M, Strick D J, Sanislo S S, Huie P, Blumenkranz M S, Binder S and Marmor M F 2007 Perspective: tissue engineering for RPE transplantation in AMD *Spektrum Augenheilkd.* **21** 212–7
[54] Lu B, Zhu D, Hinton D, Humayun M S and Tai Y C 2012 Mesh-supported submicron parylene-C membranes for culturing retinal pigment epithelial cells *Biomed. Microdevices* **14** 659–67
[55] Sanchez I, Martin R, Ussa F and Fernandez-Bueno I 2011 The parameters of the porcine eyeball *Graefes Arch. Clin. Exp. Ophthalmol.* **249** 475–82
[56] Ghosh F, Wong F, Johansson K, Bruun A and Peters R M 2004 Transplantation of full-thickness retina in the rhodopsin transgenic pig *Retina* **24** 98–109
[57] Lassota N, Kiilgaard J F, Prause J U and la Cour M 2006 Correlation between clinical and histological features in a pig model of choroidal neovascularization *Graefes Arch. Clin. Exp. Ophthalmol.* **244** 394–8
[58] Biggs M J P, Richards R G and Dalby M J 2010 Nanotopographical modification: a regulator of cellular function through focal adhesions *Nanomed. Nanotechnol. Biol. Med.* **6** 619–33
[59] Sniadecki N J, Desai R A, Ruiz S A and Chen C S 2006 Nanotechnology for cell-substrate interactions *Ann. Biomed. Eng.* **34** 59–74
[60] Wang Y K, Yong T and Ramakrishna S 2005 Nanofibres and their influence on cells for tissue regeneration *Aust. J. Chem.* **58** 704–12
[61] Panda-Jonas S, Jonas J B and Jakobczyk-Zmija M 1996 Retinal pigment epithelial cell count, distribution, and correlations in normal human eyes *Am. J. Ophthalmol.* **121** 181–9
[62] Tamiya S, Liu L and Kaplan H J 2010 Epithelial-mesenchymal transition and proliferation of retinal pigment epithelial cells initiated upon loss of cell–cell contact *Invest. Ophthalmol. Vis. Sci.* **51** 2755–63
[63] Toops K A, Tan L X and Lakkaraju A 2014 A detailed three-step protocol for live imaging of intracellular traffic in polarized primary porcine RPE monolayers *Exp. Eye Res.* **124** 74–85

INNOVATIVE STRATEGIES FOR TREATING RETINAL DISEASES

Straňák Z.[1*], Kousal B.[2,3*], Ardan T.[4], Veith M.[1]

[1] Department of Ophthalmology, 3rd Faculty of Medicine, Charles University and Královské Vinohrady University Hospital, Chief Doctor: doc. MUDr. Pavel Studený, Ph.D., MHA
[2] Department of Ophthalmology, 1st Faculty of Medicine, Charles University and General University Hospital in Prague, Chief Doctor: prof. MUDr. Jarmila Heissigerová, Ph.D., MBA
[3] Department of Paediatric and Adolescent Medicine, 1st Faculty of Medicine, Charles University and General University Hospital in Prague, Chief Doctor: doc. MUDr. Tomáš Honzík, Ph.D.
[4] PIGMOD Centre, Institute of Animal Physiology and Genetics of the Czech Academy of Sciences, Centre Director: MVDr. Jan Motlík, DrSc.

**The first and second authors contributed to the article in an equal extent.*

Presented at the 19th congress of the Czech Young Ophthalmologists Society held in Železná Ruda, 21-22 June 2019

The authors of the study declare that no conflict of interest exists in the compilation, theme and subsequent publication of this professional communication, and that it is not supported by any pharmaceuticals company.

The study was supported by the grants SVV UJ 260367/2017, Czech Science Foundation 18-04393S and the National Sustainability Programme LO1609.

MUDr. Zbyněk Straňák
Oftalmologická klinika, 3. lékařská fakulta, UK a FN Královské Vinohrady
Šrobárova 50, 100 34 Praha 10
zbynekstranak@seznam.cz

Received: 1. 10. 2019
Accepted: 6. 11. 2019
Available on-line: 20. 5. 2020

SUMMARY

Objective: The aim of this comprehensive paper is to acquaint the readers with innovative approaches in the treatment of retinal diseases, which could in the coming years to get into clinical practice. Retinal prostheses, retinal pigment epithelial (RPE) transplantation, gene therapy and optogenetics will be described in this paper.

Methodology: Describing the basic characteristics and mechanisms of different types of therapy and subsequently literary minireview clarifying the current state of knowledge in the area.

Results: Retinal prostheses, RPE transplantation, gene therapy and optogenetics offer yet unexplored possibilities and are considered as the future of treatment of retinal diseases where classical pharmacotherapy or surgical treatment are no longer sufficient. However, all these methods challenge not only in the innovative technical implementation itself, but also for the ethical, administrative and economic demands.

Conclusion: There will be certainly interesting development in the treatment of retinal diseases, but it is not possible to fully estimate which modality of treatment will be dominant in the future.

Key words: optogenetics, induced pluripotent cells, retinal prostheses, gene therapy

Čes. a slov. Oftal., 75, 2019, No.6, p. 287–295

INTRODUCTION

The retina, due to its unique position and good accessibility for examination is a very popular target for innovative procedures, primarily of gene therapy, optogenetics, cell therapy and bionics. In the following text we shall present the principles of functioning of these therapeutic modalities and an overview of the current state of knowledge, using selected examples.

OBJECTIVE

To acquaint readers with innovative approaches in the treatment of retinal diseases. The article will describe retinal prostheses, transplantation of retinal pigment epithelium (RPE), gene therapy and optogenetics.

METHODS

Literary research on the given theme, with emphasis on the mechanisms of functioning of individual therapeutic modalities and ongoing clinical trials.

RESULTS

Cell therapy

Age related macular degeneration (ARMD), Stargardt's disease or for example retinitis pigmentosa. Although these are different clinical pathologies, in all of these cases we find damage to the retinal pigment epithelium (RPE) [5]. This concerns a single layer localised on the Bruch's membrane, which is responsible for maintaining homeostasis of the photoreceptors. Despite considerable advances in pharmacotherapy of retinal pathologies (e.g. vascular endothelial growth factor inhibitors), in many patients attempts have

failed to stabilise the condition of patients with affliction of the RPE. As a result, with regard to the substantial advances in cell therapy, methods of RPE transplantation are coming to the forefront. In recent years several research centres have focused on these procedures, and their proof-of-concept evidence is generally accepted.

The first isolation of the RPE was conducted almost fourteen years ago [12], and so the fundamental characteristics of the cells are now well known. Unlike other retinal cells, in the case of the RPE synaptic connection is not required for it to perform its function, and as a result and due to the easy possibility of examining the cells, for example with the aid of optical coherence tomography (OCT), RPE transplantation has become an attractive target for cell therapy.

At the beginning of the study there was an attempt to perform an autologous transplantation (e.g. autologous RPE-choroidal graft or subretinal injection of a suspension of autologous RPE cells) or macular translocation. Despite the fact that some authors have described a partial improvement of visual functions [30], in clinical practice these procedures are not widespread due to the high incidence of adverse complications (haemorrhage, proliferative vitreoretinopathy, retinal detachment, distorsion of image in macular translocation, poor apicobasal orientation in suspensions of cells) [16,21,40].

Thanks to advances in surgical techniques and cellular biology, we now have the option of transplantin also other than autologous cells. In the literature we most often encounter human embryonic stem cells (hESC-RPE) [32] and human induced pluripotent stem cells (iPSC-RPE) [6]. We obtain embryonic cells after the fertilisation of an oocyte by sampling from a blastocyte, whereas we obtain induced pluripotent cells by reprogramming of a somatic cell, typically a fibroblast [36]. In 2012 the Nobel Prize was awarded for this discovery (Shinya Yamanaka, Sir John B. Gurdon). The result in product of both methods is a pluripotent cell, which we can then direct toward development in the RPE. The main advantage upon use of iPSC-RPE is that it concerns an autologous source, and as a result it is not necessary to burden the patient with immune suppression. On the other hand, a disadvantage is the age of the cell (the source cell is the same age as the patient from whom it is taken), the same genetic makeup (persistence

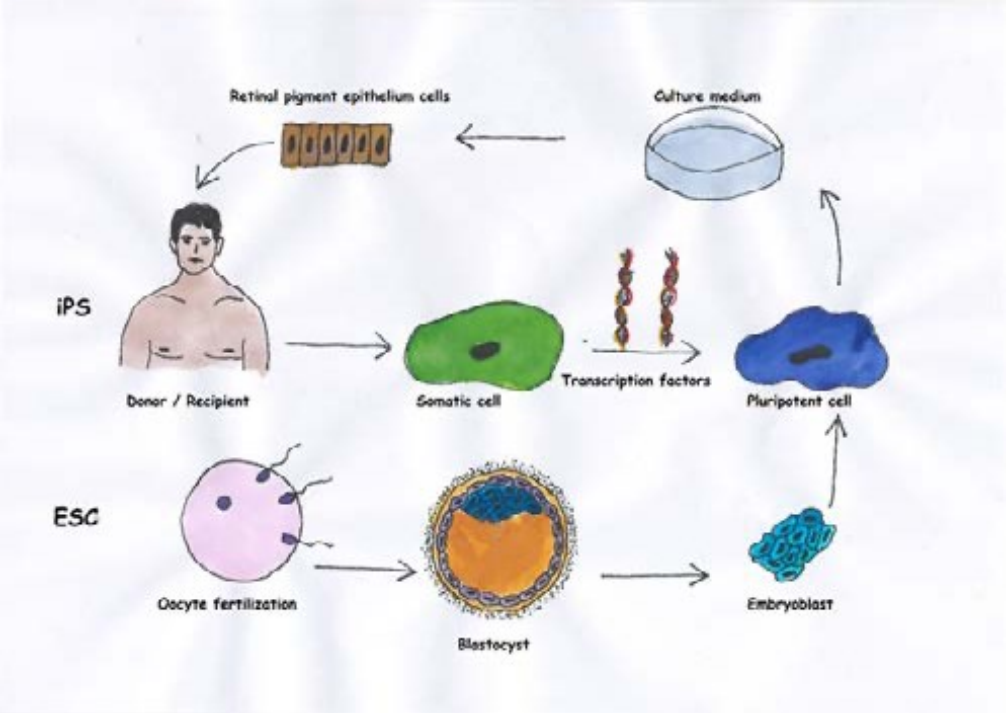

Fig. 1. Basic differences between cells of retinal pigment epithelium (RPE) from embryonic stem cells and induced pluripotent stem cells. Whereas we obtain induced pluripotent stem cells from somatic cells, typically mesenchymal cells from the skin of the donor (in the case of autologous transplantation the donor is also the recipient), we take embryonic cells from a blastocyte after fertilisation of the oocyte. Then we cultivate the pluripotent cells with the aid of appropriate growth mediators in a direction toward the RPE.

Table 1. Basic differences between embryonic stem cells and induced pluripotent stem cells (19)

	Embryonic stem cells	Induced pluripotent stem cells
Source of cells	Allogenic	Autologous
Age of cells	Embryonic	Same as donor
Risk of rejection	Slight	Low
Transmission of genetic mutation of recipient	No	Yes*
Risk of malignant proliferation	Low	Unknown
Potential of differentiation in RPE	Yes	Yes

** in the case of autologous transplantation of induced pluripotent stem cells*
RPE – retinal pigment epithelium

of any applicable genetic abnormalities) and the as yet uncertain teratogenic potential (lack of long-term data) [20]. The use of hESC-RPE is an advantage above all if it is desirable to transplant cells with a different genetic basis (genetically conditioned pathology, including mitochondrial), though naturally immune suppression is necessary. The main differences between iPSC and hESC are summarised by fig. 1 and table 1.

A second critical moment in cell therapy of the retina is surgical technique. Today there are three main directions in research: 1. subretinal injection of cellular suspension, 2. subretinal implantation of cell plate in form of epithelium, 3. subretinal injection of cell plate on supporting carrier (Fig. 2). Whereas injection of a cellular suspension is technically relatively simple, it is not possible to estimate entirely accurately whether the implanted cells will have the correct apicobasal orientation, and whether they will be capable of forming a functional monolayer with sufficient transepithelial resistance (TER, which indicates the resistance measured between the apical and basal side of the epithelium, in which the value is generally considered an indicator of the integrity of the epithelium). A role is played in this process among other factors by the Bruch's membrane, which is often pathologically altered in affected patients [37]. Subretinal implantation of a cell plate with or without a supporting carrier requires a demanding surgical technique, which however is balanced by correct apicobasal orientation and in vitro measurable TER, the values of which may help us in advance to determine the quality of the implanted cells. If we implant without a supporting carrier, the cell plate may roll up perioperatively and the cells peel off. If we use a supporting carrier, handling is easier [21], but it is necessary to select a sufficiently porous carrier so as not to form a barrier to the diffusion of nutrients and waste substances.

At present a number of clinical trials are currently under way, here we present one representative of each examined direction.

In 2016 Schwartz et al. published results of subretinal injection of hESC-RPE suspension into 18 eyes of 18 patients with dry form ARMD, Stargardt's disease or myopic macular degeneration. Cells were injected into a locality selected in advance on the interface of a healthy and pathological retina. Although pigment clusters were perceptible on the retina following application, increased autofluorescence from the baseline condition, which is considered activity of RPE, was determined in only one case. Despite the fact that this was a study primarily focused on safety, a gain of 14 letters of ETDRS (Early Treatment Diabetic Retinopathy Study) optotypes was recorded in treated eyes in the 12th month in comparison with a gain of 1 letter in the untreated eyes. The frequency of adverse effects was relatively low (1 endophthalmitis, 1 vitritis). It was necessary to use general immune suppression [33].

One year later, a study from Japan [26] was presented, accompanied by considerable media interest, in which iPSC-RPE were used for transplantation. Originally fibroblasts were taken from two patients with advanced wet form ARMD, and subsequently iPSC-RPE were cultivated from them. However, implantation was performed only on one of the patients. The second patient did not undergo the procedure due to the large amount of genetic mutations in the cultivated cells and fears of subsequent formation of a teratoma. One year after implantation the cell plate was stable, but visual acuity was unchanged. Immune suppression was not necessary [26].

In 2018 a study was presented within the framework of the still ongoing London Project to Cure Blindness. This concerned phase I, with the use of hESC-RPE on a coated synthetic carrier [8]. This study presented the results of implantation of

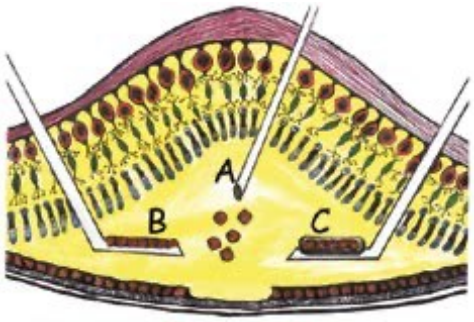

Fig. 2. Surgical technique of retinal pigment epithelium transplantation. Application of cellular suspension (A), self-supporting cell plate (B), cell plate on artificial supporting carrier (C)

2 eyes of 2 patients with extensive subretinal haemorrhage, in whom a subretinal carrier was implanted with monolayer hESC-RPE. In both cases there was an improvement of visual acuity (VA) by 29 and 21 letters of ETDRS optotypes respectively, however in one eye retinal detachment occurred, which required a further procedure, and in one patient decompensation of pre-existing diabetes mellitus occurred due to the influence of immune suppression.

As of today we do not have results available from larger clinical trials with the use of stem cells, nevertheless with regard to the initial results and large quantity of ongoing preclinical trials we can expect an advance in the coming years. With regard to surgical technique, the most advantageous appears to be a procedure with the use of a supporting carrier. Analogous experiments are taking place also in the Czech Republic, and following the phase of initial implantations [31], at the Institute of Animal Physiology and Genetics of Czech Academy of Sciences nanofibre carriers with dimensions of 2 x 5 mm [19] are being implanted, now also with iPSC-RPE or primary human RPE. The results shall be available within the following months.

Retinal prostheses

These are appliances that are capable of converting a light signal entering the region of the eye into an electrical stimulus via a device placed on the retina. The typical target of stimulation is not the photoreceptors, which are mostly lacking due to the influence of the pathology, but some of the higher embedded cells such as the retinal bipolar cells (RBCs) and retinal ganglion cells (RGCs). The processing of the signal by the retina itself is thus partially impaired, in which the transmission of the signal from the photoreceptor to the bipolar cell and subsequently the ganglion cell is modified by a large amount of further factors such as e.g. amacrine or horizontal cells (i.e. processing). Retinal prostheses are mostly divided according to location into epiretinal, subretinal and suprachorideal (Fig. 3). Epiretinal prostheses are an advantage with regard to their easier surgical access and easy activation of the ganglion cells. On the other hand, a disadvantage is their entirely uncontrollable processing of the image by the retina, in which in addition to the ganglion cells themselves, the surrounding axons are also activated and the signal does not appear as a luminous spot [28]. Subretinal prostheses are the opposite of epiretinal prostheses. Here we must be prepared for a demanding surgical technique, nonetheless the remaining photoreceptors are activated, or alternatively the RBCs, and the signal therefore does not circumvent processing in the retina [22]. Suprachoroideal implants are used less frequently, primarily due to the surgical demand factor and greater distance of the electrodes from the retina. Today the most commonly presented implants are Argus II (Second Sight, Sylmar, USA), Alpha AMS (Retina Implant AG, Reutlingen, Germany) and Photovoltaic Retinal Implant (PRIMA) Bionic Vision System (Pixium vision, Paris, France).

The most widespread implant is the Argus II, which has been implanted in more than 200 patients. This is an epiretinal implant with electrodes placed in six rows of ten. It is a camera attached to special glasses, generating a signal that is modulated in an external device. Subsequently the signal is transmitted by a radio frequency via a spool into a subconjunctivally implanted receiver, which is further transmitted transsclerally to the actual implant stimulating the retina [1]. The best documented visual acuity was only 20/1260, nonetheless the implant markedly improved the patient's spatial orientation or for example searching for objects on a table [15]. The most common adverse effects include erosion or dehiscence of the conjunctiva, presumed endophthalmitis or hypotonia of the eye. Cases of perceive discrepancy between the fixed image from the camera and eye movement outside of direct gaze have also been reported.

The PRIMA system uses a different principle. Special glasses with a camera record the image, which is subsequently modulated and with the aid of a projector in the glasses sent in the form of infrared rays to a subretinally implanted wireless photovoltaic plate, which converts photovoltaic energy into electrical energy stimulating nearby neurons [22]. It is theoretically possible to obtain visual acuity of 20/200 with this implant. Three-year clinical trials were commenced in Europe and the USA (always five patients) in 2017 and 2018 respectively, and the results can be expected in 2021.

The last representative is Alpha AMS. This subretinal implant detects light and at the same time electrically stimulates primarily the bipolar cells. Energy is supplied by a transscleral cable, which leads subcutaneously behind the ear and is reminiscent of a cochlear implant. Here it is charged via a spool. The advantage of this implant is that it respects ocular movements. Average visual acuity with this implant is 20/1200, even if values of 20/550 have been recorded [11,35,42]. The Alpha AMS is no longer available, since it did not meet the commercial requirements of the manufacturer.

The main differences and specifications of retinal implants are summarised in table 2 [3].

Gene therapy

The possibility of determining a diagnosis on the level of genes, and clinical testing of new targeted therapies has enabled the establishment of genetically focused clinical care in ophthalmology. Therapies based

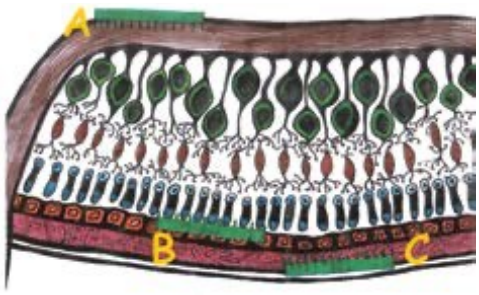

Fig. 3. Anatomical localisation of retinal prostheses. Retinal prostheses can be implanted epiretinally (A), subretinally (B) or suprachoroideally (C)

Table 2. Comparison of most commonly used retinal prostheses

	Argus II	Alpha AMS	PRIMA
Resolution	60 pixels	1600 pixels	142 pixels
Anatomical localisation	Epiretinal	Subretinal	Subretinal
External camera	Yes	No	Yes
Energy source	Yes	Yes	No
Intraorbital cabling	Yes	Yes	No

on knowledge of the genetic cause of the pathology represent an entirely new approach. With regard to its easy accessibility, small dimensions, immunological privilege, compartmentalisation and possibility of contralateral control, the eye is an ideal organ for clinical evaluation [9]. Gene therapy is a therapeutic procedure in which genetic material is introduced into the genome of cells, replacing or influencing the expression of the protein involved in the pathogenesis of a specific pathology. For the development and utilisation of gene therapy it is necessary to determine the gene responsible for the onset of the pathology and to know its function. If the cause of the pathology is a deficiency of a product of a mutated gene, it is sufficient to incorporate normal sequencing of the gene into the genome of the relevant cells (Fig. 4A), or to alleviate manifestations of the pathology by introducing a therapeutic gene (Fig. 4B). However, if an altered product of a mutated gene of the character of an aberrant protein has a pathological effect, it is necessary either to block the mutated gene (Fig. 4C) [2] or correct it (Fig. 4D) [9,38]. At the same time, treatment must not have negative impacts on the vitally important functions of the organism.

Gene therapy can be performed either in vivo, in which

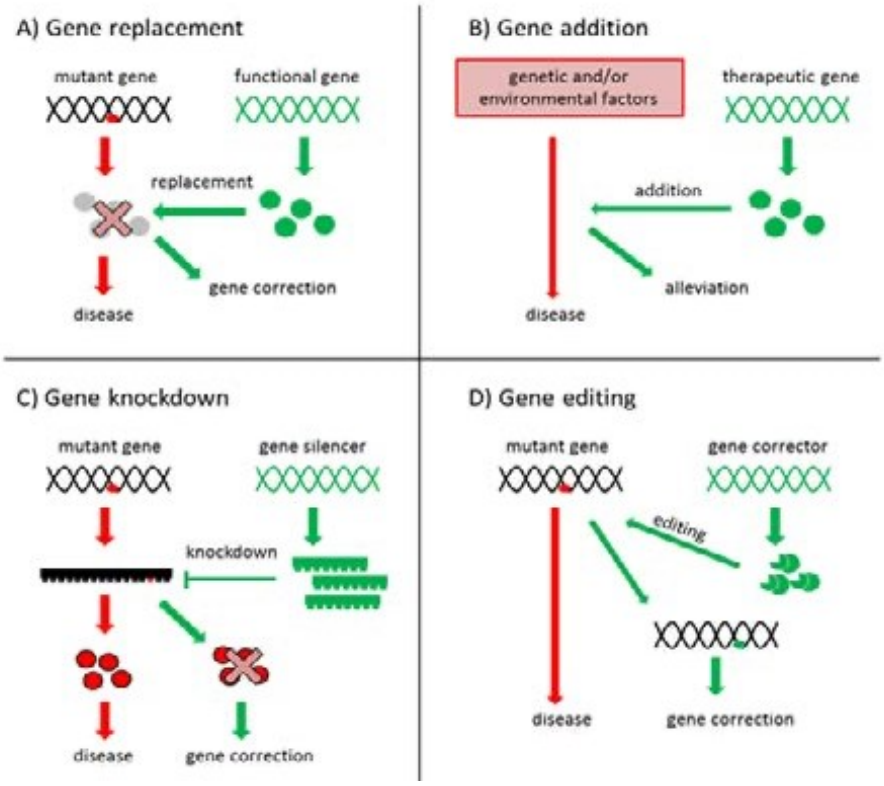

Fig. 4. Strategies used in gene therapy [8,37]

the target cells are a part of the organism throughout the entire period of treatment, or in vitro, in which the target cells are removed from the body of the organism, and following the performance of therapy are returned to their original location [17]. A condition for success is the application of treatment within the "therapeutic window", when irreversible damage to the tissue has not yet taken place.

Genetic information is transmitted into the target cells with the aid of carriers known as vectors. An ideal vector should penetrate into a large number of target cells and the expression of the introduced gene should take place for a sufficiently long period of time, in order accomplish the required therapeutic effect. In addition, the vector must not be toxic for the target cells or trigger adverse effects in the recipient such as viral infections or autoimmune reactions [25].

We divide vectors into viral and non-viral. Due to a range of disadvantages of physical and chemical vectors at present in clinical trials which are testing therapies for retinal pathologies in humans, viral vectors are used, in particular adenoviral and retroviral [25]. Genes in connection with the pathogenesis and reproduction of viruses are removed from viral particles. The genes are then replaced by an expression cassette prepared modification of DNA [9].

The risk of use of viral vectors consists in the fact that genetic information is inserted into the genome more or less at random. This may lead to a disturbance of the sequence of another gene with functional consequences. Another problem is the potential immunogenicity of viral vectors, causing inflammatory reactions [27]. Repeated application of therapeutics into the subretinal region also carries the risk of retinal damage or detachment [4]. Determination of the therapeutic dose and the amount of applied viral particles is also problematic.

In the treatment of retinal diseases, intravitreal and subretinal injections are most often used for the application of vectors. Although application into the vitreous body is less invasive for the retina, transmission of DNA takes place especially in the inner layers of the retina, thus in the Müller and ganglion cells. The membrana limitans interna and other retinal layers form a barrier to the penetration of vectors and pharmaceuticals into the deeper layers of the retina. Subretinal application is more suitable for the introduction of viral vectors into the layer of the photoreceptors and layer of RPE cells, in which the vector is injected into a vesicle between the aforementioned layers, and is thus in close contact with them [4].

Among the first cases proposed for gene therapy was Leber's congenital amaurosis 2 (LCA2), mainly due to the early manifestation of the pathology, the relatively long preserved structure of the retina and the availability of animal models [24]. LCA2 is an autosomal recessive disease originating upon a background of mutations in the gene RPE65 (retinal pigment epithelium-specific 65 kDa protein) [13]. This gene is virtually exclusively exprimated in the RPE, where it contributes to the recycling of opsin and rhodopsin. Insufficient function or absence of RPE65 subsequently leads to a degeneration of photoreceptors [7]. After 2007 the gene RPE65 was clinically tested in gene therapy trials [2,14], which culminated in 2017 in the approval of the first gene therapy for clinical ophthalmological practice by the American Food and Drug Administration, and in 2018 by the European Medicines Agency [18].

In the Czech Republic complex diagnosis and research into genetically conditioned ocular pathologies is the focus of the Centre for Clinical Ocular Genetics at the 1st Faculty of Medicine, Charles University and General University Hospital in Prague.

Optogenetics

In the broader sense of the word, optogenetics is defined as a technique in which a gene coding a photosensitive protein is introduced with the aid of a vector into a neuron cell, as a result of which the target cell is subsequently stimulated. In ophthalmology, this typically concerns the insertion of a photoreceptive protein into one of the sub-populations of retinal cells [39], which primarily do not have a photoreceptive function.

In practice it is first of all necessary to find an appropriate photosensitive protein, which we subsequently insert into a suitable vector (most commonly adenoviral), and target at the correct cell. The final step is a corresponding "illumination" of the treated retina.

It is possible to use two types of opsin as a photoreceptive protein: type 1 (microbial) or type two (animal). The most commonly used is type 1, which has several subtypes, but in principle always concerns an ion channel which can be activated by light (e.g. channelrhodopsin, halorhodopsin, archeorhodopsin) [10]. After activation of the ion channel there is a change in the polarisation of the cell and subsequently a transmission of the signal further. Type 2 is a photosensitive protein coupled with a G-protein. After activation an intracellular signal cascade of chemical conversions takes place, with a resulting opening of the coupled cation channel. The main advantage of type 1 as against type 2 is the simpler molecule directly containing an ion channel, while the disadvantage is the frequently higher de-

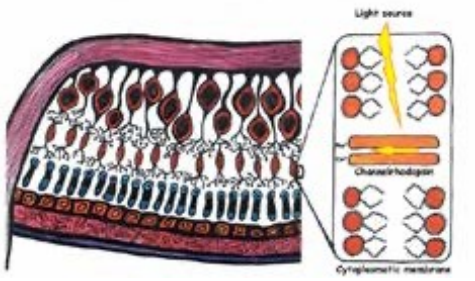

Fig. 5. Optogenetics targteted at retinal cells. Incorporation of photosensitive receptor, in this case channelrhodopsin, into the cell membrane of a bipolar cell

mands for light intensity necessary for a change of cell polarisation.

In the human retina we find more than one hundred different types of neuronal cells [41], which interreact to a certain degree and thereby ensure complex processing of the image before sending the signal further to the central nervous system by means of the axons of the ganglion cells. All attempts not to adhere to the natural procedure of photoreceptor-bipolar cell-ganglion cell therefore lead to a disruption of the retinal processing of the image, and thus to a reduction of its quality. As a result, our endeavour is always targeted at the outermost layers of the retina [34]. It is possible to use damaged photoreceptors which no longer have outer segments (here the preserved processing of the signal by the retina is an advantage), or upon circumventing this mechanism directly to use the bipolar or ganglion cells (Fig. 5).

The final step is the trapping of the light by the treated cell. Various channels are sensitive to different wavelengths of light. It is necessary to bear this in mind with regard to the possibility of phototoxicity. For example, channelrhodopsin is most sensitive in short wavelengths, and like the majority of type 1 channels requires a larger number of photon hits. This, together with the low proportion of blue light especially under worsened light conditions and the lower permeability of these wavelengths through the optical environments of the eye [29] requires higher light intensity at these wavelengths for correct functioning. This can be attained only with the aid of an external light source, which may have an adverse influence, resulting in phototoxicity.

Two ongoing studies are now registered in the international register of clinical trials https://clinicaltrials.gov.

Phase I/II, sponsored by the Allergan firm (NCT02556736), is designated for patients with advanced retinitis pigmentosa, by which a vector coding channelrhodopsin for the modulation of the retinal ganglion cells (substance RST-001) is injected intravitreally. At the time of writing of this article, recruitment of patients is still ongoing, with an envisaged total number of 21.

GenSight Biologics is currently recruiting patients for a study with substance GS030-DP (NCT03326336), which is a modified adenoviral vector for modified channelrhodopsin, with sensitivity shifted more to the red spectrum [23], thus theoretically guaranteeing a better safety profile with regard to phototoxicity. The Pixium Vision company is also involved in the project (see PRIMA system above), and it appears that a combination of optogenetics and glasses augmenting reality (i.e. the natural image is supplemented by a digital layer which enables for example the accentuation of certain predefined objects) represents a promising future pathway for reinforcing the effect.

DISCUSSION

Despite the fact that gene therapy, optogenetics, cell therapy and bionic eye are matters rather of the more or less distant future and bring with them a large number of unsolved questions, such as financing, effectiveness, indication criteria, ethical problems or technological demand factor, a number of initial commercial successes have already been achieved. The approval of vortigene neparvovec-ryzl as the first preparation for causal treatment of genetically conditioned disease has opened up a path for further promising products. It is therefore possible to assume that similar pharmaceutical preparation will progressively appear on the market and that treatment of an ever greater number of clinical units will be enabled.

Another good example is the implant Argus II, since though its resolution of 6 x 10 electrodes may not seem especially overwhelming today is nevertheless considered a prime mover and a “proof of concept” in the field. At the same time it has been demonstrated to be technologically very reliable, with no complications caused by a malfunction of the instrument appearing in the first three years of clinical practice [15]. This has led to a further development of more advanced systems, which are now in the phase of clinical evaluation (NCT03344848).

Great hopes have been invested in cell therapy, which is however more difficult to grasp in comparison with “exact” electronic implants, and there is immense variability of results with regard to the different quality of implanted cells and potential complications during the course of highly demanding surgical procedures. Uncertainty still predominates with regard to the safety profile of the cells, and there are also fears of possible teratogenicity. Ethical questions are also unclear. The implantation techniques are not uniform, and large discussions are taking place concerning artificial carriers for RPE, wherein on one hand manipulation of the cells is markedly improved upon the use of a carrier, while on the other this represents an artificial barrier which prevents the diffusion of substances into and out of the retina. A certain way out of this problem could be the use of nanotechnologies in the production of a carrier. A further issue that is as yet unclear is whether or not to drain off the original RPE cells perioperatively, and here there is a complete lack of data.

Optogenetics appears to be an interesting method, nonetheless we are still waiting for the first concrete results. A disadvantage is low photosensitivity, and it appears that this method will have to be supplemented by an external light source or e.g. glasses enabling the sending of an augmented reality image to the retina also in a wave spectrum other than visible light, on the precondition that photosensitive channels are sensitive to such a wavelength.

CONCLUSION

In the coming years we can expect fascinating developments in the treatment of retinal diseases, in which the greatest challenge shall perhaps not be technologies but rather correct indication for the selection of one of the above-described methods, which shall in their final consequence be supplemented, and thus offer an alternative for patients who cannot be helped at present.

LITERATURE

1. **Ahuja, AK., Yeoh, J., Dorn, JD., et al.:** Factors Affecting Perceptual Threshold in Argus II Retinal Prosthesis Subjects. Transl Vis Sci Technol, 2; 2013: 1.
2. **Bainbridge, JWB., Mehat, MS., Sundaram, V., et al.:** Long-term effect of gene therapy on Leber's congenital amaurosis. N Engl J Med, 372; 2015: 1887–1897.
3. **Bloch, E., Luo, Y., da Cruz, L.:** Advances in retinal prosthesis systems. Ther Adv Ophthalmol, 11; 2019: 1–16.
4. **Boye, SE., Boye, SL., Lewin, AS., et al.:** A comprehensive review of retinal gene therapy. Mol Ther J Am Soc Gene Ther, 21; 2013: 509–519.
5. **Bressler, NM., Bressler, SB., Fine, SL.:** Age-related macular degeneration. Surv Ophthalmol, 32; 1988: 375–413.
6. **Carr, A-JF., Smart, MJK., Ramsden, CM., et al.:** Development of human embryonic stem cell therapies for age-related macular degeneration. Trends Neurosci, 36; 2013: 385–395.
7. **Cideciyan, AV.:** Leber congenital amaurosis due to RPE65 mutations and its treatment with gene therapy. Prog Retin Eye Res, 29; 2010: 398–427.
8. **da Cruz, L., Fynes, K., Georgiadis, O., et al.:** Phase 1 clinical study of an embryonic stem cell-derived retinal pigment epithelium patch in age-related macular degeneration. Nat Biotechnol, 36; 2018: 328–337.
9. **Dudakova, L., Kousal, B., Kolarova, H., et al.:** Gene therapy for inherited retinal and opticnerve disorders: current knowledge. Cesk Slov Oftalmol. 72; 2016; 128–136.
10. **Duebel, J., Marazova, K., Sahel, J-A.:** Optogenetics. Curr Opin Ophthalmol, 26; 2015: 226–232.
11. **Edwards, TL., Cottriall, CL., Xue, K., et al.:** Assessment of the Electronic Retinal Implant Alpha AMS in Restoring Vision to Blind Patients with End-Stage Retinitis Pigmentosa. Ophthalmology, 125; 2018: 432–443.
12. **Flood, MT., Gouras, P., Kjeldbye, H.:** Growth characteristics and ultrastructure of human retinal pigment epithelium in vitro. Invest Ophthalmol Vis Sci, 19; 1980: 1309–1320.
13. **Gu, SM., Thompson, DA., Srikumari, CR., et al.:** Mutations in RPE65 cause autosomal recessive childhood-onset severe retinal dystrophy. Nat Genet, 17; 1997: 194–197.
14. **Hauswirth, WW., Aleman, TS., Kaushal, S., et al.:** Treatment of leber congenital amaurosis due to RPE65 mutations by ocular subretinal injection of adeno-associated virus gene vector: short-term results of a phase I trial. Hum Gene Ther, 19; 2008: 979–990.
15. **Ho, AC., Humayun, MS., Dorn, JD., et al.:** Long-Term Results from an Epiretinal Prosthesis to Restore Sight to the Blind. Ophthalmology, 122; 2015: 1547–1554.
16. **Chen, FK., Patel, PJ., Uppal, GS., et al.:** Long-term outcomes following full macular translocation surgery in neovascular age-related macular degeneration. Br J Ophthalmol, 94; 2010: 1337–1343.
17. **Kaufmann, KB., Buning, H., Galy, A., et al.:** Gene therapy on the move. EMBO Mol Med, 5; 2013: 1642–1661.
18. **Kousal, B., Ďuďáková, Ľ., Moravíková, J., et al.:** Vzácná oční onemocnění v oftalmologické praxi. Oftalmol Praxi, 2018: 7–11.
19. **Kozak, I., Stranak, Z., Popelka, S., et al.:** Safety and feasibility of new nanofiber subretinal delivery system with injector for RPE cell transplantation. Invest Ophthalmol Vis Sci, 59; 2018: 5670–5670.
20. **Kvanta, A., Grudzinska, MK.:** Stem cell-based treatment in geographic atrophy: promises and pitfalls. Acta Ophthalmol (Copenh), 92; 2014: 21–26.
21. **Lee, E., MacLaren, RE.:** Sources of retinal pigment epithelium (RPE) for replacement therapy. Br J Ophthalmol, 95; 2011: 445–449.
22. **Lorach, H., Goetz, G., Smith, R., et al.:** Photovoltaic restoration of sight with high visual acuity. Nat Med, 21; 2015: 476–482.
23. **Mace, E., Caplette, R., Marre, O., et al.:** Targeting channelrhodopsin-2 to ON-bipolar cells with vitreally administered AAV Restores ON and OFF visual responses in blind mice. Mol Ther J Am Soc Gene Ther, 23; 2015: 7–16.
24. **Maguire, AM., Simonelli, F., Pierce, EA., et al.:** Safety and efficacy of gene transfer for Leber's congenital amaurosis. N Engl J Med, 358; 2008: 2240–2248.
25. **Mali, S.:** Delivery systems for gene therapy. Indian J Hum Genet, 19; 2013: 3–8.
26. **Mandai, M., Watanabe, A., Kurimoto, Y., et al.:** Autologous Induced Stem-Cell-Derived Retinal Cells for Macular Degeneration. N Engl J Med, 376; 2017: 1038–1046.
27. **Misra, S.:** Human gene therapy: a brief overview of the genetic revolution. J Assoc Physicians India, 61; 2013: 127–133.
28. **Nanduri, D., Fine, I., Horsager, A., et al.:** Frequency and amplitude modulation have different effects on the percepts elicited by retinal stimulation. Invest Ophthalmol Vis Sci, 53; 2012: 205–214.
29. **von Noorden, GK.:** Application of basic research data to clinical amblyopia. Ophthalmology, 85; 1978: 496–504.
30. **Parolini, B., Di Salvatore, A., Pinackatt, SJ., et al.:** Long-term results of autologous retinal pigment epithelium and choroid transplantation for the treatment of exudative and atrophic maculopathies. Retina, 2018.
31. **Popelka, S., Studenovska, H., Abelova, L., et al.:** A frame-supported ultrathin electrospun polymer membrane for transplantation of retinal pigment epithelial cells. Biomed Mater Bristol Engl, 10; 2015: 045022.
32. **Ramsden, CM., Powner, MB., Carr, A-JF., et al.:** Stem cells in retinal regeneration: past, present and future. Dev Camb Engl, 140; 2013: 2576–2585.
33. **Schwartz, SD., Tan, G., Hosseini, H., et al.:** Subretinal Transplantation of Embryonic Stem Cell-Derived Retinal Pigment Epithelium for the Treatment of Macular Degeneration: An Assessment at 4 Years. Invest Ophthalmol Vis Sci, 57; 2016: ORSFc1-9.
34. **Simunovic, MP., Shen, W., Lin, JY., et al.:** Optogenetic approaches to vision restoration. Exp Eye Res, 178; 2019: 15–26.
35. **Stingl, K., Bartz-Schmidt, KU., Besch, D., et al.:** Arteficial vision with wirelessly powered subretinal electronic implant alpha-IMS. Proc Biol Sci, 280; 2013: 1–8.
36. **Takahashi, K., Yamanaka, S.:** Induction of pluripotent stem cells from mouse embryonic and adult fibroblast cultures by defined factors. Cell, 126; 2006: 663–676.
37. **Tezel, TH., Kaplan, HJ., Del Priore, LV.:** Fate of human retinal pigment epithelial cells seeded onto layers of human Bruch's membrane. Invest Ophthalmol Vis Sci, 40; 1999: 467–476.
38. **Wang, D., Gao, G.:** State-of-the-art human gene therapy: part II. Gene therapy strategies and clinical applications. Discov Med, 18; 2014: 151–161.

39. **Yue, L., Weiland, JD., Roska, B., et al.:** Retinal stimulation strategies to restore vision: Fundamentals and systems. Prog Retin Eye Res, 53; 2016: 21–47.
40. **van Zeeburg, EJT., Maaijwee, KJM., Missotten, TOAR., et al.:** A free retinal pigment epithelium-choroid graft in patients with exudative age-related macular degeneration: results up to 7 years. Am J Ophthalmol, 153; 2012: 120-127.e2.
41. **Zeng, H., Sanes, JR.:** Neuronal cell-type classification: challenges, opportunities and the path forward. Nat Rev Neurosci, 18; 2017: 530–546.
42. **Zrenner, E., Bartz-Schmidt, KU., Benav, H., et al.:** Subretinal electronic chips allow blind patients to read letters and combine them to words. Proc Biol Sci, 278; 2011: 1489–1497.

Many thank to Mgr. Štěpánek Eliška Straňáková for preparing Figures 1, 2, 3 and 5

Acta Ophthalmologica

Acta Ophthalmologica 2021

Advantages of nanofibrous membranes for culturing of primary RPE cells compared to commercial scaffolds

Lucie Tichotová,[1,2] Hana Studenovska,[3] Goran Petrovski,[4] Štěpán Popelka,[3] Yaroslav Nemesh,[1,2] Miroslava Sedláčková,[5] Saskia Drutovič,[1] Sonali Rohiwal,[1] Pavla Jendelová,[6] Slaven Erceg,[6,7] Anna Brymová,[1,2] Ana Artero-Castro,[7] Lyubomyr Lytvynchuk,[8] Zbyněk Straňák,[9,10] Zdeňka Ellederová,[1] Jan Motlík[1] and Taras Ardan[1]

[1]Institute of Animal Physiology and Genetics, Academy of Sciences of the Czech Republic, Libechov, Czech Republic
[2]Department of Cell Biology, Faculty of Science, Charles University, Prague, Czech Republic
[3]Institute of Macromolecular Chemistry, Academy of Sciences of the Czech Republic, Prague, Czech Republic
[4]Center for Eye Research, Department of Ophthalmology, Oslo University Hospital and Institute for Clinical Medicine, University of Oslo, Oslo, Norway
[5]Department of Histology and Embryology, Faculty of Medicine, Masaryk University, Brno, Czech Republic
[6]Institute of Experimental Medicine, Academy of Sciences of the Czech Republic, Prague, Czech Republic
[7]Stem Cell Therapies in Neurodegenerative Diseases Lab, Research Center 'Principe Felipe', Valencia, Spain
[8]Department of Ophthalmology, Justus-Liebig-University Giessen, University Hospital Giessen and Marburg, Giessen, Germany
[9]Ophthalmology Department of 3rd Faculty of Medicine, Charles University and University Hospital Kralovske Vinohrady, Prague, Czech Republic
[10]Third Faculty of Medicine, Charles University, Prague, Czech Republic

ABSTRACT.

Purpose: Dysfunction of the retinal pigment epithelium (RPE) causes numerous forms of retinal degeneration. RPE replacement is a modern option to save vision. We aimed to test the results of transplanting cultured RPEs on biocompatible membranes.

Methods: We cultivated porcine primary RPE cells isolated from cadaver eyes from the slaughterhouse on two types of membranes: commercial polyester scaffolds Transwell (Corning Inc., Kenneburg, ME, USA) with 0.4 μm pore size and prepared Poly (L-lactide-co-DL-lactide) (PDLLA) nanofibrous membranes with an average pore size of 0.4 μm.

Results: Five types of assays were used for the analysis: immunocytochemistry (ICC), phagocytosis assay, Western blotting, real-time qPCR (RT-qPCR) and electron microscopy. RT-qPCR demonstrated that RPEs cultured on nanofibrous membranes have higher expressions of BEST1 (bestrophin 1), RLBP1 (retinaldehyde-binding protein 1), RPE65 (retinal pigment epithelium-specific 65 kDa protein), PAX6 (transcription factor PAX6), SOX9 (transcription factor SOX9), DCT (dopachrome tautomerase) and MITF (microphthalmia-associated transcription factor). ICC of the RPEs cultured on nanofibrous membranes showed more intensive staining of markers such as BEST1, MCT1 (monocarboxylate transporter 1), Na^+/K^+ATPase, RPE65 and acetylated tubulin in comparison with commercial ones. Additionally, the absence of a-SMA proved the stability of the RPE polarization state and the absence of epithelial-to-mesenchymal transition. RPE possessed high phagocytic activity. Electron microscopy of both membranes confirmed a confluent layer of RPE cells and their genuine morphological structure, which was comparable to native RPEs.

Conclusions: Retinal pigment epitheliums cultured on polylactide nanofibrous membranes improved the final quality of the cell product by having better maturation and long-term survival of the RPE monolayer compared to those cultured on commercial polyester scaffolds. PDLLA-cultured RPEs are a plausible source for the replacement of non-functioning RPEs during cell therapy.

Key words: AMD – eye – nanofibrous membrane – retina – retinal pigment epithelium – RPE

Special thanks to Hana Říhová and Irena Dejlová for technical support and the slaughterhouse 'Kohout a synové' for providing us with cadaverous porcine eyes.

The Czech Science Foundation (Project Number 18-04393S), Norway Grants and Technology Agency of the Czech Republic (KAPPA Programme, Project Number TO01000107), Czech Science Foundation (Project Number 19-09628J) and AFM-Telethon (Project number 22258) supported this study.

Acta Ophthalmol.

[a] 2021 Acta Ophthalmologica Scandinavica Foundation. Published by John Wiley & Sons Ltd

doi: 10.1111/aos.15034

Introduction

Retinal pigment epithelial (RPE) cells form a monolayer of pigmented cells in the retina (Bok 1993). Their apical side communicates with the light-sensitive outer segments of photoreceptors, while their basolateral segments face the highly specialized multilayered Bruch's membrane (BM), a connective tissue that separates the RPEs from the choriocapillaris and provides a barrier between RPEs and the blood flow in the fenestrated vessels of the choroid (Hogan et al. 1971; Guymer et al. 1999). The RPE monolayer plays a key role in the metabolic pathway between photoreceptors and choroid (Maitz 2015). The morphology of the RPEs is cuboidal, hexagonal. The RPEs are surrounded by an extracellular space, called subretinal space. Specialized microvilli of the RPEs project into the subretinal space and communicate with the photoreceptors (Holan et al. 2015). The number of photoreceptors invaginating into an RPE cell varies by retinal location and age. It is estimated to be 20–55 photoreceptors per one RPE cell (Rodriguez-Crespo

et al. 2014). The RPEs form a monolayer connected by tight junctions, which is part of the blood–retina barrier (Bok 1993), which efficiently isolates the inner retina from the blood of the choroid.

The functions of the RPEs are diverse and include photoreceptor development, homeostasis and many other physiological processes (Sheridan et al. 2010). RPEs absorb light energy and transport ions, water and metabolic end products from the subretinal space to the blood (Duan et al. 2013). Furthermore, RPEs take up glucose, retinol and fatty acids from the blood back to the photoreceptors. The apical microvilli of the RPEs are long, thin and formed by actin, with the function to absorb the outer segments of photoreceptors and facilitate phagocytosis (Lerit & Abaño, 2012; Lakkaraju et al. 2020).

Dysfunction of the RPEs affects the extracellular environment for photoreceptors and the BM, which can result in a variety of degenerative retinal disorders, such as age-related macular degeneration (AMD) and Stargardt´s disease (Ramsden et al. 2013). The most modern and promising option to save the vision for prospective future use in a clinic is to transplant new RPE cells, which are capable to replace the non-functional epithelium. For this purpose, cultured RPEs can be delivered into the subretinal space in the form of (1) a cell suspension (Falkner-Radler et al. 2011), (2) a self-supporting cell sheet (Yaji et al. 2009) or (3) a cell monolayer supported by an artificial membranous carrier (Hynes & Lavik 2010; Stout & Francis 2011). Although injection of the cell suspension is surgically simpler, faster and less invasive than the other techniques, the cumulated experience has revealed several disadvantages, which include regress of the suspension into the vitreous cavity, limited adherence of RPE cells to the aged BM, incorrect apicobasal orientation and failure to form a monolayer (Sheridan et al. 2009). The advantage of a self-supporting cell sheet and a cell monolayer supported by an artificial substrate is that the cells are implanted in a highly differentiated state (Diniz et al. 2013). In the nineties, several authors tried to replace damaged cells with a patch of cultured human foetal RPEs, but they were not successful (Lindner et al. 2010). The last delivery technique includes a tissue-engineered scaffold supporting RPEs. Since the monolayer organization and correct polarization of the RPE layer are critical for the renewal of the functioning epithelium (Maitz 2015), the implantation of RPE cells seeded on a membranous carrier mimicking BM represents a promising direction in the transplantation of RPE cells. BM, which is the innermost layer of the choroid, is 2–6 μm thick. Thus, the thickness of the transplanted membrane should adopt similar dimensions. One of the most important factors for the successful functioning of a solid carrier with RPEs is the porosity of the membrane. The retina is a metabolically very active site of the eye; thus, high open porosity and large pore size are some of the key factors in RPE production and transplantation.

Numerous solid carriers have been presented in the literature, and their ability to support the formation of RPE monolayer *in vitro* has been demonstrated (Hynes & Lavik 2010). However, only a few of these carriers have been porous enough or comparably thin or thinner than the actual BM (Hu et al. 2012; Stanzel et al. 2012, 2014; Diniz et al. 2013; Liu et al. 2014; Ilmarinen et al. 2015). These carriers have been able to support the survival of human stem cell-derived RPE monolayer *in vivo* but failed to preserve the photoreceptors and the inner retinal layers (da Cruz et al. 2018; Fernandes et al. 2017). It was suggested that one of the factors behind this detrimental effect was the low permeability of those carriers (Stanzel et al. 2014).

Nanofibrous membranes prepared by electrospinning can combine the advantages of high porosity, large pore size and low thickness. There are a number of polymers used for electrospun membrane preparation for tissue engineering, from which the more biocompatible and biodegradable polylactide-based ones have belonged to the leading group. Polymers for electrospun membrane fabrication include, for example poly (L-lactide) (Surrao et al. 2017), poly(L-lactide-co-D,L-lactide) (PDLLA) (von Burkersroda et al. 2002), poly(L-lactide-co-glycolide) (Warnke et al. 2013) or poly(L-lactide-co-caprolactone) (Sorkio et al. 2015; Hotaling et al. 2016).

The aim of this study was to compare the quality of the primary porcine RPE cultured on the commercial polyester membrane to those cultured on electrospun PDLLA nanofibrous membrane using cell, molecular and morphological/electron microscopy analysis. Additionally, transepithelial electrical resistance (TEER) and phagocytosis capacity of the RPEs were evaluated to show the functional activity of the cultured RPEs.

Methods and Materials

Nanofibrous membranes

The nanofibrous membranes were prepared as described previously (Popelka et al. 2015) with some minor modifications. PDLLA (ratio of LLA/DLLA 90/10, Mw 868 270 g/mol, PDI 2.3) was dissolved in dry pyridine at a concentration of 11 wt% with the addition of 2.2 μl of formic acid/g. The solution was electrospun using a single needle nozzle (20 G blunt-ended needle) at 7 kV of applied voltage, 250 μl/h of feeding rate and a 10 cm gap. The membranes were dried at 75°C in a vacuum overnight. The sheets of the membrane were floated from the silicon wafers on the water surface and fixed by silicon glue to commercial polyester cell culture insert Transwell (Corning Inc.) devoid of the original membrane. The fibre width was measured from microphotographs taken with scanning electron microscope VEGA Plus TS 5135 (Tescan, Brno, Czech Republic). The nanofibrous membrane was sputter-coated with platinum before visualization. The membrane thickness was measured using KLA-Tencor P-10 Surface Profiler from the height step of the groove made in the membrane. The areal density of the membrane was measured by weighing the membrane of the known area (METTLER TOLEDO MX5 Microbalance). The pore size distribution of the nanofibrous membranes was calculated from the microphotographs using IMAGEJ software (NIH, USA). The porosity of the membrane was calculated as described earlier (Eichhorn & Sampson, 2005) using experimentally determined membrane thickness, area density and fibre material density of 1.248 g/cm^3. Samples were air-plasma treated for 30 s at the power of 7 W (Expanded plasma cleaner, Harrick Plasma, Ithaca, NY, USA) before RPE cultivation.

Commercial membranes

The commercial membranes used were Corning® Transwell® polyester mem-

brane cell culture inserts (Corning Inc.), and the manufacture number was Corning 3460. Such a membrane is 10 μm thick and is made from transparent polyester. The membranes are sterilized by gamma radiation after production. The inserts and membranes are round in shape and 12 mm in diameter. The cell growth area is 1.12 cm^2. The pore size on membranes is 0.4 μm, and the nominal pore density is 4×10^6 pores per cm^2. The surface is TC-treated. This membrane is non-degradable.

Isolation and culturing

All experiments complied with the research standards of the Declaration of Helsinki and the Association for Research in Vision and Ophthalmology (ARVO) for experiments on animals. RPE cells were isolated from porcine eyes from a nearby slaughterhouse. Isolation and culturing of the cells were performed at the Department of Cell Regeneration and Plasticity of the Institute of Animal Physiology and Genetics AS CR, v. v. i. Extracted eyes from pigs were transported to the cell culture laboratory from the slaughterhouse within 2 h after enucleation in a thermobox at 4°C, followed by washing in water, leaching in 0.2% betadine for 15 min and 1% penicillin/streptomycin for 20 min (Penicillin–Streptomycin (10 000 U/ml); Gibco, Thermo Fisher Scientific, Waltham, MA, USA). The eyes were then dissected in an equatorial line with a blade, and the whole anterior segment and vitreous were removed. Consequently, the neural retina was removed. The RPEs were obtained by using 0.25% trypsin applied for 20 min, and then, a 10% RPE medium – commercial medium (DMEM, high glucose, GlutaMAX™ Supplement, pyruvate; Gibco, Thermo Fisher Scientific, Waltham), supplemented with 10% FBS (Foetal Bovine Serum F7524; Sigma-Aldrich, Saint Louis, MO, USA), 1% NEAA (MEM Non-Essential Amino Acids Solution 100X; Gibco, Thermo Fisher Scientific, Waltham), 0.1% gentamicin (Gentamicin (50 mg/ml); Gibco, Thermo Fisher Scientific, Waltham) and epithelial growth factor 50 ng/ml (EGF Recombinant Human Protein; Gibco, Thermo Fisher Scientific, Waltham) were added. The suspension of trypsin and 10% RPE medium was pelleted by centrifugation for 3 min at 1200 rpm, the supernatant removed and the pellet dissolved in 2 ml of new 10% RPE medium. The suspension was then placed into a cell culture plate (Tissue Culture Test Plates with 12 wells; TPP Techno Plastic Products AG, Trasadingen, Switzerland) and incubated at 37°C in a humidified 5% CO_2 incubator. The 10% RPE medium was changed 3 times per week. All experiments were performed using cultured RPE cells at 80–95% confluence. Growth was maintained for 10–14 days, and after that, the cells were transferred to membranes.

Cell transferring to PDLLA nanofibrous membranes and commercial scaffolds

After the cells had grown sufficiently in a culture dish, and they were collected by 0.5% trypsin and seeded 3000 cells per square millimetre on both membranes – manufactured PDLLA nanofibrous membranes with porosity of 72% (IMC, Prague, Czech Republic), and commercial polyester scaffold Transwell with porosity of 20% (Corning Inc.). The sterilization of the nanofibrous membranes was performed by air-plasma treatment followed by immersion in 70% ethanol. The surface of both membrane types was not covered by any compound. Due to the absence of significant differences between coated (fibronectin coating was tested) and uncoated membranes, only uncoated membranes were used further in the study. Moreover, in the case of uncovered membranes, we could exclude any effects other than that from the material itself on cell growth and cultivation. The cells were seeded in a 10% RPE medium as described above. Usually, after 10 days of cultivation in higher FBS-containing medium, the cells were continued in lower FBS-containing medium (2% RPE medium – commercial medium, 2% FBS, 1% NEAA, 0.1% gentamicin). The RPEs were matured on membranes for 4 weeks, and the medium was changed 3 times per week.

Transepithelial electrical resistance (TEER)

Millicell ERS-2 device equipped with STX01 Ag/AgCl electrodes (Merck Millipore, Darmstadt, Germany) was used to determine the TEER values (Ω cm^2). Both types of membranes were used for the measurement in culture media at room temperature after being removed from the incubator. Both types of membranes without cultured cells (blank) demonstrated values of TEER around 0–5 Ω/cm^2, and these values were deducted from the values measured on membranes seeded with RPE cells.

Immunocytochemistry

Commercial scaffolds and nanofibrous scaffolds were fixed in cold 4% paraformaldehyde for 5 min and washed three times in PBS (Phosphate Buffered Saline). Consequently, treatment by freshly prepared 0.1% Triton x100 for 10 min was performed, which was twice washed in PBS and incubated in 5% goat serum for 45 min. Primary antibodies were added for 2 h at room temperature. The following primary antibodies were used: anti-BEST1 antibody (1:200 mouse monoclonal IgG; Abcam, Cambridge, UK), anti-Na^+/K^+ATPase antibody (1:100 rabbit polyclonal IgG; Biorbyt, Cambridge, UK), anti-RPE65 antibody (1:200 mouse monoclonal IgG; Antibodies-Online Inc., Atlanta, GA, USA), anti-MCT1 antibody (1:100 mouse polyclonal IgG; Abcam), anti-tubulin antibody (1:500 mouse monoclonal IgG; Sigma-Aldrich, Saint Louis), anti-ZO1 antibody (1:100 mouse monoclonal IgG; Thermo Fisher Scientific, Rockford, IL, USA), anti-ezrin antibody (1:500 mouse monoclonal IgG; Abcam), anti-SMA (1:200 mouse monoclonal IgG; Santa Cruz Biotechnology, Santa Cruz, CA, USA). After washing in PBS, the samples were incubated in secondary antibodies or mouse IgG kappa binding protein (1:200 m-IgGκ BP-CFL 647; Santa Cruz Biotechnology) for the detection of anti-SMA for 45 min in dark. Secondary antibodies were goat anti-mouse antibody (1:500 polyclonal IgG Alexa Fluor 488; Invitrogen, Carlsbad, CA, USA), goat anti-rabbit antibody (1:500 polyclonal IgG, Alexa Fluor 488; Invitrogen) and goat anti-mouse antibody (1:500 polyclonal IgG Alexa Fluor 647; Invitrogen). For the detection of colocalization of ZO1 and F-actin in the RPE cells, a mix of goat anti-mouse antibodies (1:500 polyclonal IgG Alexa Fluor 488; Invitrogen) and Phalloidin-iFluor 647 Reagent (1:1000 Abcam) was prepared. After staining, the samples were mounted with DAPI and evaluated under a fluorescent

microscope and a histological scanner VS120 (Olympus, Tokyo, Japan). The staining of the selected markers for RPEs cultured on the nanofibrous and commercial membranes was investigated using Leica TCS SP5 microscope (Leica, Wetzlar, Germany). We assessed 20–24 images per marker. The images were observed and graded according to the staining intensity of marker expression. The images with the best intensity of staining were selected for the figures. For the objective comparison of fluorescent signal intensity, we used the same light properties (light intensity or exposure time) during the image acquiring of a particular marker staining. For the quantification of differences of immunofluorescent staining, we employed the image analysis method where the evaluation and quantification of immunoreactivity were performed using a densitometry measurement of staining by image analysis software VS-Desktop (Olympus).

Real-time quantitative Polymerase Chain Reaction (RT-qPCR)

Isolation of RNA was made according to the instructions of the RNeasy Plus Mini Kit (Qiagen, Hilden, Germany). RNA concentrations of each sample were measure and diluted accordingly to the same concentration (10 ng/μl). Luna Universal One-Step RT-qPCR Kit (New England Biolabs Inc., Ipswich, MA, USA) was used; 6 samples were used for each marker for both types of membranes. The results were evaluated using a Bio-Rad detection system (CFX96 Touch Real-Time PCR Detection System; BIO-Rad, Hercules, CA, USA). The annealing temperature was 60°C. The specifications of all primers used in this study are stated in Table 1.

Electron microscopy

Cells in the monolayer adherent on both types of membranes (PDLLA nanofibrous membranes or commercial scaffolds) were processed for electron microscopy. Altogether, we assessed 47 images, 29 images for TEM and 18 images for the SEM. TEM images were graded according to the ultrastructure of membranes (total porosity and size of pores) and the presence of typical cell structures such as zonula occludens or melanin granules. The evaluation of SEM images was based on the presence of the microvilli, pigment granules.

Transmission electron microscopy (TEM)
Samples were fixed with 300 mmol/l glutaraldehyde in 100 mmol/l cacodylate buffer and postfixed in 40 mmol/l osmium tetroxide in 100 mmol/l cacodylate buffer, then embedded in LR White resin (Sigma-Aldrich, Saint Louis, MO, USA). Ultrathin sections (60–90 nm) were made on Leica EM UC 6 (Leica Microsystems) ultramicrotome. After staining with uranyl acetate and lead citrate, the sections were examined in TEM FEI Morgagni 268D (FEI Company, Hillsboro, OR, USA).

Scanning electron microscopy (SEM)
Samples were fixed in the same way as for TEM. After dehydration by increasing the concentration of ethanol, the samples were dried to the critical point of the drying process on CPD 300 (BAL-TEC, Balzers, Liechtenstein), prepared on mounting tables, coated by gold on sputter unit SCD 040 (Balzers Union, Pfäffikon, Switzerland) and examined in Vega 3 (Tescan) SEM.

Phagocytosis assay

The phagocytic activity of RPE cells was assessed using pHrodo™ Deep Red E. coli BioParticles™ Conjugate for phagocytosis (Invitrogen). In the first step, we dissolved BioParticles™ with PBS, pH 7.4 to a final concentration of 1 mg/ml, and subsequently vortexed and sonicated solution for 10 min in a bath sonicator (Elma, Singen, Germany). The 2% RPE medium in the wells containing RPE cells seeded on commercial and PDLLA nanofibrous membranes was replaced by the complete medium with 100 μg/ml of the BioParticles™. Cells were incubated at 37°C in a humidified incubator with a 5% CO2 level for 1 h 30 min. As a negative control, we incubated cells with BioParticles™ at 4°C on the ice to inhibit phagocytic activity. RPE cells were washed once in PBS for 5 min and then fixed in freshly prepared 2.5% glutaraldehyde solution for 10 min. RPE cells were rinsed with PBS 3 times for 5 min and mounted with DAPI, then imaged by Leica TCS SP5 microscope (Leica). The relative fluorescence units (RFU) were measured with OLYMPUS VS-DESKTOP 2.9 (Olympus). The phagocytosis activity (% Change) was calculated as a ratio of the difference between the average RFU of the sample and the average RFU of the blank to the RFU of the sample. The net phagocytosis was calculated by subtracting % change of negative control from the % change of experimental sample.

SDS-PAGE and Western-Blot

Cells lysates were obtained from trypsinized cells using Pierce RIPA Buffer (Thermo Fisher Scientific, Rockford) with Halt™ Protease and Phosphatase Inhibitor Cocktail (Thermo Fisher Scientific, Rockford), sonicated for 15 min at 4°C and centrifuged at 20 000 g for

Table 1. Primers and their sequences used for real-time qPCR. The primer B2 M was used as a housekeeping gene.

Primer name	Primer sequence 5′- 3′
RPE65 - fwd	CTGCAGTGACCGATTCAAGC
RPE65 – rev	GCCAAACCCCCATGGTTTCA
BEST1 - fwd	GACCGTCACCTACTCAAGCC
BEST1 – rev	TAGAAGCCCAGCACGAAGGA
RLBP1 – fwd	GCCATCCACTTCATCCACCA
RLBP1 – rev	CTCCGTGGACAAAGACCCTC
MITF - fwd	TTACTCAGAATACAGGAACTT
MITF - rev	CTGCTTGATGATCCGATT
SOX9 - fwd	GGCAAACTCTGGAGACTGCTG
SOX9 - rev	ATGGCGTTGGGAGAGATGTG
PAX6 - fwd	GAATTCTGCAGGTGTCCAACG
PAX6 - rev	CACTCCCGCTTATACTGGGC
DCT - fwd	TCAAGTGATGAGCCTTCA
DCT - rev	GATCATTGGCAGCAGAAT
B2M - fwd	AAACGGAAAGCCAAATTACCTGA
B2M - rev	ATCTCTGTGATGCCGGTTAGTG

15 min at 4°C. We transferred supernatants to new tubes and measured protein concentration via Pierce BCA Protein Assay Kit (Thermo Fisher Scientific, Rockford). 10 µg of total protein per sample was loaded onto NuPAGE 4–12% Bis-Tris Gel (Invitrogen) and run at 150 V. Gel was transferred onto nitrocellulose membrane (Bio-Rad) and blocked in 5% nonfat milk, Tris-buffered saline-Tween 20 (TBS-T; 1.5 M NaCl; Lach-Ner, Neratovice, Czech Republic), 0.5% TWEEN 20 (Sigma-Aldrich, Burlington, MA, United States), 200 mM Tris (Roth, Karlsruhe, Germany), pH 7.6 and incubated overnight with primary antibodies diluted in 5% nonfat milk: anti-BEST1 antibody (1:1000 mouse monoclonal IgG; Abcam), anti-Na^+/K^+ATPase (1:1000 mouse monoclonal IgG; Abcam), anti-RPE65 (1:1000 rabbit monoclonal IgG; Abcam) at 4°C. After washing in TBS-T, membranes were incubated in secondary antibodies conjugated with horseradish peroxidase (1:10 000 anti-mouse, or 1:10 000 anti-rabbit, Jackson ImmunoResearch, Philadelphia, PA, USA). The signal was revealed by chemiluminescence using ECL Reagent (Amersham, UK) and detected by the ChemiDoc XRS+ system (Bio-Rad). The volume intensity was measured by IMAGE LAB 6.1.0. software (Bio-Rad).

Statistical analysis

Unpaired *t*-test or a one-way ANOVA test with Bonferroni's (or Tukey's) multiple comparison post-test was used from the GRAPHPAD PRISM software (GraphPad Software, San Diego, CA, USA) for all analyses.

Results

Characterization of the PDLLA nanofibrous membranes

The design of the insert with the fixed nanofibrous membrane is presented in Fig. 1A. The diameter of the bead-free fibres was 380nm (standard deviation, SD: 10 nm), and it is shown in Fig. 1B in comparison with the commercial membrane shown in Fig. 1C. In our previous study[26], we found that the optimal area density of the nanofibrous membrane which complies with a safe surgical manipulation should be as low as 90 µg/cm^2. In this study, we prepared membranes with an area density of 130 µg/cm^2 (SD 10 µg/cm^2). Membrane thickness measured from the profiler scans was 3.7 µm accordingly.

The average pore size of the PDLLA nanofibrous membranes was 0.4 µm (SD 0.2 µm), and it was calculated from 3 micrographs, the total number of evaluated pores being 170. The pore size was obtained as the diameter of an inscribed circle into a visible pore. The pore size distribution is depicted in Fig. 2.

The porosity of the nanofibrous membrane is the fraction of voids within the structure volume. The calculated porosity of the 3.7 µm thick fibrous membrane with a fibre diameter of 380 nm was 72%.

Culturing of RPE cells

Cultured RPEs reached 85% confluence by the second week on both membranes. The first 3–5 days the cells formed dendrite-like extensions on the oblong morphological structure trying to make contact with the surrounding cells. After 1 week, they demonstrated a morphological change from elongated to round-shaped cells as they turned into a monolayer. These changes were observed in both types of membranes on the same day.

Transepithelial electrical resistance (TEER) measurements on RPE cells

Measuring the TEER indicates a maturation of the cells on the membranes covered by RPEs and shows the presence of cell–cell connection (tight junctions). Cell monolayers were measured after 3 weeks of culturing on both types of membranes. The TEER values of PDLLA nanofibrous membranes were 176 ± 15 Ω/cm^2 (n = 6), while that of commercial membranes were 161 ± 26 Ω/cm^2 (n = 6). The TEER values of non-cellularized nanofibrous and commercial membranes fluctuated in the range of 0–5 Ω/cm^2 (n = 6).

Immunocytochemistry (ICC) on cultivated RPE cells on membranes

Based on the immunocytochemical findings, all of the tested proteins were found on both membranes after 4 weeks in culture. We recognized and confirmed the expression of markers in different fields of view and various Z-planes (Figs 3 and 4) in the bright-field and confocal microscopy respectively. PDLLA nanofibrous membrane-cultivated RPEs demonstrated a higher intensity of immunofluorescence of each marker compared to those on

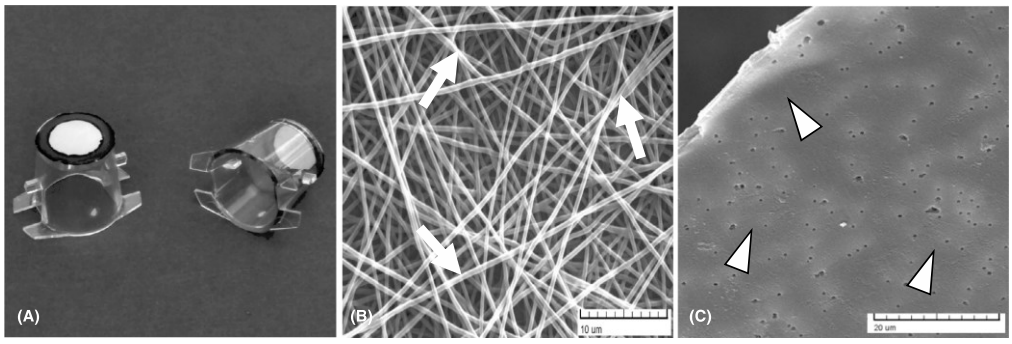

Fig. 1. The morphological features of the nanofibrous membrane (A). The polylactide nanofibrous membrane (B) is made from individual fibres (white arrows) in comparison with a commercial membrane (C) which is a PET commercial track-etched (white arrowheads). Depending on the scale, it is possible to state that the pores on the nanofibrous membrane (B) are significantly larger than the ones found on the commercial membrane (C).

commercial membranes. The only exception was ezrin (Fig. 3K,L), which showed comparable or weaker fluorescence signals on nanofibrous compared to commercial membranes. The most visible difference with a higher level of expression on nanofibrous membranes in comparison with the commercial membranes was detected for the retinal pigment epithelium-specific 65 kDa protein (RPE65) (Figs 3N and 4J) and Na^+/K^+ATPase (Figs 3D and 5H) markers. Enzyme RPE65, an esters convertor, was found in most Z-planes, so we assumed that this protein is located in the cytoplasm of the entire cell (Fig. 4I,J). The Na^+/K^+ATPase was stained preferentially in the upper optical focussed planes (Fig. 4G,H). The expression of acetylated tubulin (Figs 3H and 4B), zonula occludens 1 (ZO1) (Figs 3P and 4L), bestrophin 1 (BEST1) (Figs 3F and 4D) and monocarboxylate transporter 1 (MCT1) (Figs 3J and 4F) demonstrated moderately higher immunosignals in RPE cells cultured on nanofibrous membranes. A peripheral membrane protein ZO1 was found between the cells in the place of tight junctions and colocalized with apically occurring actin (Fig. 4K, L). BEST1 was located in the lower and middle focal planes of analysis (Fig. 4C,D). MCT1 was found on both the higher and bottom parts of the focal planes (Fig. 4E,F). Acetylated tubulin was demonstrated intracellularly in the apical parts of RPE cells (Fig. 4A,B). The image analysis of RPE immunostaining showed significantly increased expression of bestrophin 1 and Na^+/K^+ATPase in RPE cells cultured on the nanofibrous membrane (Fig. 4M).

Real-time quantitative polymerase chain reaction analysis on RPE cells cultivated on membranes

RT-PCR was used to investigate the expression of different markers related to RPE cells (Fig. 5). The list of all primers used in the assay is shown in Table 1. PDLLA nanofibrous membranes in all cases showed higher relative normalized expressions of the tested markers compared to the commercial membranes. The transcription factor SOX 9 (SOX9) was highly expressed with a statistically significant difference ($p = 0.0314$) on nanofibrous membranes compared to commercial ones. Furthermore, dopachrome tautomerase (DCT) was upregulated with a statistically significant difference ($p = 0.0028$) on the nanofibrous membranes as well. Despite visibly higher expressions of the transcription factor *PAX6* (*PAX6*), *BEST1*, retinaldehyde-binding protein 1 (*RLBP1*), *RPE65* and microphthalmia-associated transcription factor (*MITF*) on the nanofibrous membranes, their results were not significantly different for both membranes.

Electron microscopy of RPE monolayer

SEM showed a difference between the PDLLA nanofibrous membrane- and commercial membrane-cultivated RPEs, confirming the better surface covering in a monolayer on the nanofibrous membranes (Fig. 6). Furthermore, cells on the nanofibrous membrane showed typical RPE morphology including the presence of microvilli and tight junctions (Fig. 6A, B). This corresponds to the natural organization of the RPEs in a functional monolayer structure with accurate polarization of the apicobasal surfaces. The magnified cells on the PDLLA nanofibrous membrane displayed well visible microvilli (Fig. 6A–C) of better quality (density and orientation) compared to cells on the commercial membrane (Fig. 6F–H).

TEM revealed the structure of both the polylactide-based nanofibrous- and polyester-based commercial membranes. The very thick commercial membrane (Fig. 6I,J) was more visible compared to the nanofibrous membrane. Only thin fibres of polylactide from the nanofibrous membrane (Fig. 6D,E) could be observed under the RPE cells. Moreover, the nanofibrous membrane demonstrated a more permeable structure with vertical and horizontal pores compared to the commercial membranes.

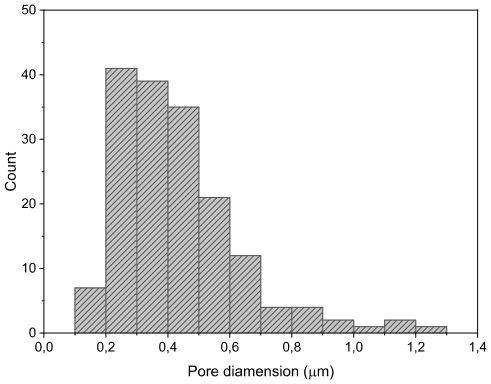

Fig. 2. Pore size distribution in the nanofibrous membranes (mean fibre width of 380 nm).

Phagocytosis assay and epithelial-to-mesenchymal transition (EMT)

To test the functional activity of cultivated RPE cells, the phagocytosis assay was carried out. The confocal microscopy showed a high amount of pHrodo™ Deep Red BioParticles™ within the RPEs on both the nanofibrous and commercial membranes after 1 h 30 min of incubation time (Fig. 7D,F) and its very low concentration in controls (Fig. 7E,G). The relative quantification of phagocytosis using an image analysis technique confirmed the results of immunostaining where we found values 75% and 72% for nano- and commercial membranes respective 16% (nano-) and 7% (commercial) for their controls on the ice.

Additionally, we investigated whether cultured RPEs express the epithelial-to-mesenchymal transition (EMT) marker α-SMA (Fig. 7A,B). The NIH-3T3 fibroblast cell line was used as a positive control for the alpha-smooth muscle actin (α-SMA) (Fig. 7C). There was no observed signal in cultured RPE cells on both types of membranes in comparison with α-SMA, presented in the NIH-3T3 fibroblasts.

Western blot analysis (WB)

WB analysis with a densitometric evaluation confirmed results of the

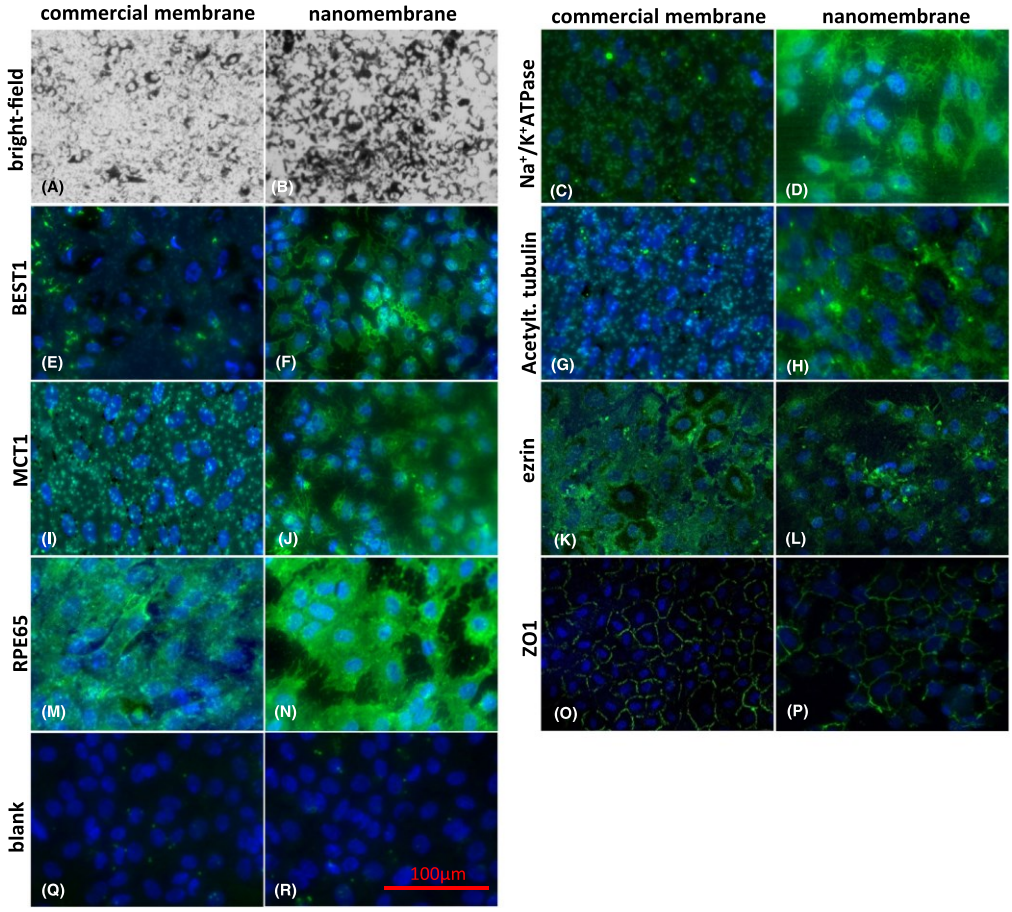

Fig. 3. Representative images of the RPE cells cultured on polyester commercial and nanofibrous membranes without staining (bright-field microscopy) or stained by immunocytochemistry (ICC). The first images A, B show cultured RPE cells without staining using bright-field microscopy. We can detect more melanin in the cells cultured on nanofibrous membranes (B). ICC results demonstrate the expression of the following proteins: Na^+/K^+ATPase (C, D), BEST1 (E, F), tubulin (G, H), MCT1 (I, J), ezrin (K, L), RPE65 (M, N), ZO1 (O, P), and the last two images represent the blanks on the commercial membrane (Q) and nanofibrous membrane (R). The Na^+/K^+ATPase (D) and RPE65 (N) demonstrated a higher intensity of immunofluorescence on the nanofibrous membranes compared to commercial membranes. The proteins BEST1 (F), acetylated tubulin (H), MCT1 (I) and ZO1 (P) showed moderate immunoexpression on nanofibrous membranes. Marker ezrin (L) indicated weak fluorescent signals on the nanofibrous membrane compared to that found on the commercial membranes (K).

immunocytochemical examination where we found a higher concentration of Na^+/K^+ATPase, bestrophin 1 and RPE65 in RPE cells cultured on a nanofibrous membrane (Fig. 8).

Discussion

Retinal pigment epithelium cell replacement therapy belongs to the very modern and promising treatment modalities for retinal neurodegenerative diseases such as AMD, retinitis pigmentosa (Falkner-Radler et al. 2011; da Cruz et al. 2018) and Stargardt´s disease (Ramsden et al. 2013). In these diseases, RPE dysfunction or their cell loss leads to the damage of photoreceptors and eventually blindness.

The flat surface of commercial membranes with track-etched porosity enables the formation of an RPE monolayer on them. However, the fewer pores with a manufactured-specified pore size of 0.4 µm seem not to be sufficient to mimic the real BM properties. In contrast to commercial membranes with flat 2D surface and low porosity, the electrospun membranes offer three-dimensional surroundings, providing a continuous flow of nutrients for the seeded cells (Shokoohmand et al. 2017). The important properties of both membranes are summarized in Table 2.

In this comparative study, we employed scaffolds with two types of membranes: polylactide-based nanofibrous membranes and commercial

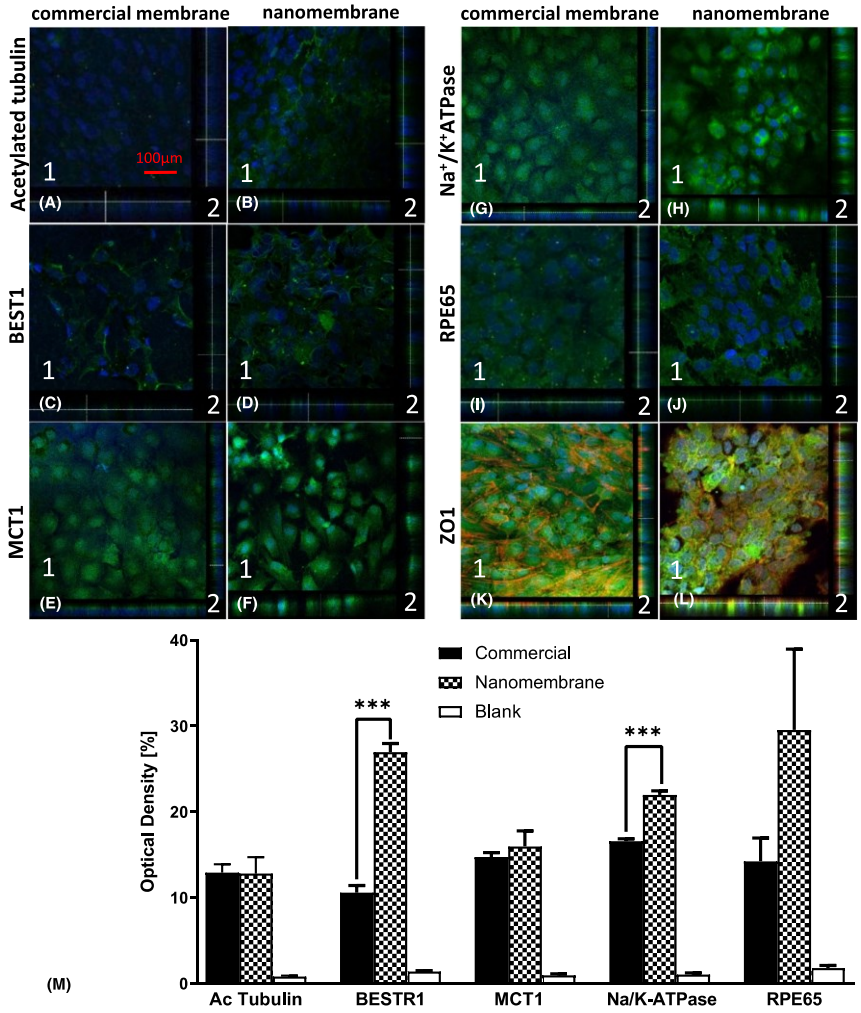

Fig. 4. Images of RPE cells cultured on commercial and nanofibrous membranes stained by immunocytochemistry. The confocal microscope was used for visualization of the following markers: acetylated tubulin (A, B), bestrophin 1 (C, D), monocarboxylate transporter 1 (E, F), Na^+/K^+ATPase (G, H), retinal pigment epithelium-specific 65 kDa protein (I, J) and zonula occludens 1 (K, L). Only samples K and L (ZO1) were stained by two markers – ZO1 (green) and actin (red). Each staining (A-L) includes a front view (1) and an orthogonal view (2). The image analysis of the immunohistochemical staining demonstrated significantly increased bestrophin 1 and Na^+/K^+ATPase expressions in RPE cells cultured on the nanofibrous membrane (M), ***($p < 0.0001$).

polyester-based rigid membranes with track-etched pores and thickness of 10 µm. We manufactured the nanofibrous membranes with respect to the properties of supporting RPE cells. The commercial polyester membrane is commonly used for culturing various types of cells including RPEs (Jiang et al. 2013; Damasceno et al. 2015). The surface of the tested membranes did not need modification by coating substrates (laminin, collagen, fibronectin) to potentially increase the cell adhesion to the substrate surface. The membranes without coating have an exactly defined chemical structure, which interacts directly with the cultured RPE cells during their growth, differentiation and maturation. Moreover, for future clinic use, it is better to decrease or eliminate the infectious risks associated with the use of proteins of animal origin.

The prepared ultrathin membranes with a thickness of 3.7 µm corresponded very well with the dimensions of the healthy BM. The average pore

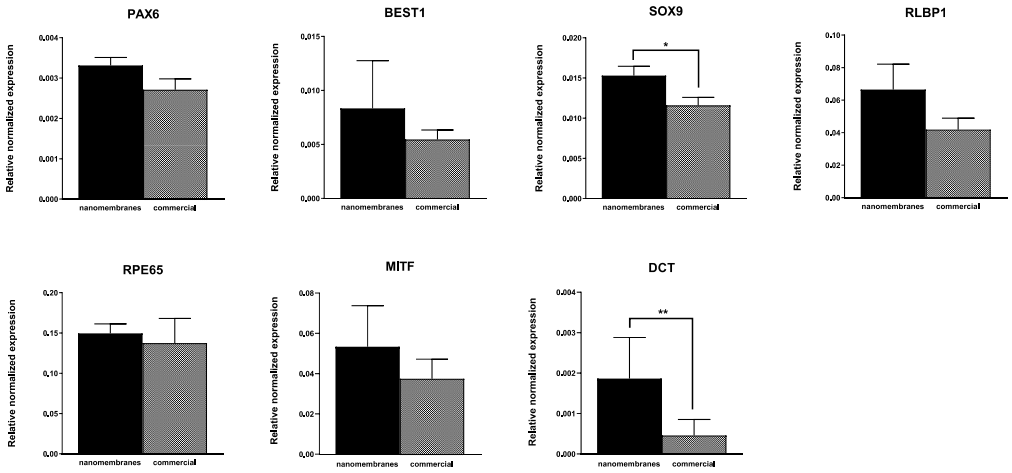

Fig. 5. RT-qPCR analysis of seven typical RPE markers: *PAX6*, *BEST1*, *SOX9*, *RLBP1*, *RPE65*, *MITF*, *DCT*. The results of the RT-qPCR related to the B2M housekeeping gene showed higher normalized expression of markers on the nanofibrous membranes (black column) in comparison with commercial membranes (light grey column). Two markers – *SOX9* and *DCT*, demonstrated significantly higher expressions, * (n = 6, p = 0.0314) and ** (n = 6, p = 0.0028).

size of 0.4 μm found in nanofibrous membranes is comparable to those of the commercial membranes. However, the 72% porosity of the nanofibrous carrier is almost four times higher than that in commercial membranes. Thus, ultrathin nanofibrous membranes can better support the physiological flow of nutrients and preserve the normal function and anatomy of the neuroretina. Furthermore, a recent study (Sharma et al. 2019) showed that native basal infoldings (Hayes et al. 2019) of human iPSC-derived RPE cells were formed only on the nanofibrous membrane, while other characteristics such as morphology, electrical properties and expression of RPE markers were found similar between the nanofibrous and track-etched membranes. Stanzel et al. (2014) suggested that lower porosity with small pores (0.4 μm) of cell carriers could affect the long-term survival of the RPE cells and subsequent neuroretina degeneration. Primary RPE cells (Johnson et al. 2011), as well as stem cell-derived RPEs, tend to produce extracellular deposits on their basal side. These deposits have been shown to fill up the 0.4 μm large pores of the Transwell inserts during a 6 months period of RPE culturing (Pilgrim et al. 2017). In this regard, the PDLLA nanofibrous support would probably be more resistant to the blockage or clogging up by the sub-RPE deposits, not only because of the more open structure but also due to the nanofibre degradation. A semi-crystalline polymer such as PDLLA with a high molecular weight could provides overall mechanical strength to the delicate nanofibrous membrane with a degradation lifetime of at least 5 months and more (Zhang et al. 1994; Landes et al. 2006; Lehtonen et al. 2013), and no adverse effects known during the polymer degradation (Weir et al. 2004). Such a period could be sufficient for a typical 2–6 months long cultivations of RPE cells *ex vivo* (Stanzel et al. 2014), followed by mechanical manipulation during surgery. The degradable nature of the nanofibrous membrane seems to be also advantageous in supporting *de novo* synthesis of a Bruch's membrane equivalent by the donor RPE cells, and their integration into the host's Bruch's membrane as shown in an animal study by previously (Sharma et al. 2019). The only disadvantage of the thin nanofibrous membrane compared to the commercial track-etched membrane is the lower stiffness. To be implantable with a clinically relevant size of 3 × 6 mm (Fernandes et al. 2017), additional mechanical support, for example a peripheral frame (Popelka et al. 2015), has to be incorporated around the nanofibrous membrane.

In our *in vitro* culturing of porcine primary RPE cells, the measured TEER of 176 ± 15 Ω/cm^2 confirmed the formation of tight junctions and the functional cell barrier between the RPEs, which results were in agreement with the previous study described by Toops et al. (2014) and Manlin et al (Jin et al. 2002). Moreover, the RPE cells cultured on the PDLLA nanofibrous membranes showed a higher level of TEER in comparison with another TEER measurement performed on bovine (Hartnett et al. 2003) and human primary RPEs (Blaauwgeers et al. 1999), as well as APRE-19 cell cultures (Ablonczy & Crosson 2007; Huang et al. 2015).

In this study, we used RPE-specific markers to characterize the various morphological and functional properties of these cells including differentiation and maturation processes. RPE65 is a typical marker of the visual cycle, and it had an increased expression both at gene and protein levels in RPE cells cultured on PDLLA nanofibrous membranes. The presence of this protein in the RPE cells is essential for the 11-cis retinal synthesis and confirms the maturity of the RPE cell cultures (Seo et al. 2004).

PAX6 is known for its ability to reprogram RPE cells into a state of multipotency without imposing danger of undergoing myofibroblastic differentiation (Vareilles et al. 1977; Casco-Robles et al. 2016). The gene expression of this retinal marker showed a

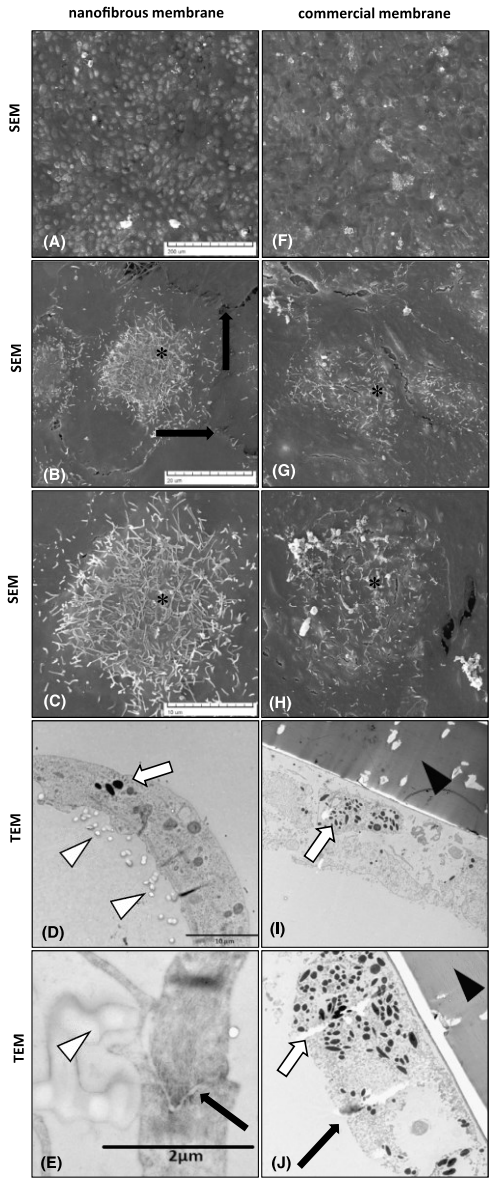

Fig. 6. Scanning electron micrographs (SEM) of the difference between a nanofibrous membrane (A–E) and commercial membrane (F–J). Nanofibrous membrane (A) is better covered by very nicely visible rounded RPE cells containing visible microvilli as compared to the commercial membrane (F). A cell from the nanofibrous membrane (B, C) shows the presence of microvilli (*) which are of better quality (density, orientation) than those on the commercial membrane (G, H). In picture B, we can see the presence of tight junctions under the black arrows. Transmission electron microscopy (TEM) shows nanofibrous membrane (D, E) from polylactide fibres (white arrowheads) and thick commercial membrane (I, J) from polyester (black arrowheads). White arrows show granules of melanin in pictures D, I and J. The TEM also shows the presence of tight junctions in the cultured RPEs (B, E, J; black arrows).

slight increase in RPE cells cultured on the nanofibrous membrane, indicating the possibility of such reprogramming in these cells without the risk of myofibroblastic differentiation.

ZO1 is a very important marker for the maintenance of the RPE monolayer, and for making tight junctions between RPEs, as previously shown in RPEs cultured on various scaffolds such as an amniotic membrane or porous polycaprolactone (Stanzel et al. 2005; McHugh et al. 2014). In the present study, we found a high expression of ZO1 protein in RPE cells cultured on both types of membranes without any visible differences using immunocytochemical analysis.

The next three markers evaluated in this study participate in the RPE ion transport mechanisms. BEST1 is a very important protein that associates with the Ca^{2+}/Cl^{-} ion-exchange in retinal cells, while mutations in this gene cause a group of retinal diseases known as bestrophinopathies (Bakall et al. 2003; Hariprasad & Singh 2011; Jun et al. 2012). Na^{+}/K^{+}ATPase participates in the turnover of cations important for the polarization/depolarization of the apical part of the RPE membrane upon receiving photons by photoreceptors (Marmorstein et al. 1998, 2000; Marmorstein 2001). The third ion exchanger, MCT1, is responsible for the symport of H^{+}-lactate and water and thus has an important role in maintaining intracellular pH and water homeostasis (Batman et al. 2008). Elevated levels of BEST1, Na^{+}/K^{+}ATPase in our cultured RPE cells determined by gene and protein analysis (WB) demonstrated a highly polarized state of our epithelial monolayer. Indeed, the ICC expression of BEST1, Na^{+}/K^{+}ATPase including their protein levels detected by WB, and MCT1 was higher in RPE cells cultured on the PDLLA nanofibrous membranes compared to commercial membranes and thus can denote the better functional support the nanofibrous membranes provide in form of ion transport in the polarized RPE monolayer.

Acetylated tubulin, F-actin and ezrin play the main role in cell shape, division, migration, adhesion and transport of organelles (Fuchs et al. 1991; Lerit & Abaño, 2012). Previously, acetylated tubulin was colocalized with claudin 1 in RPE cilia (Amaral et al. 2016). Ezrin is the actin-binding

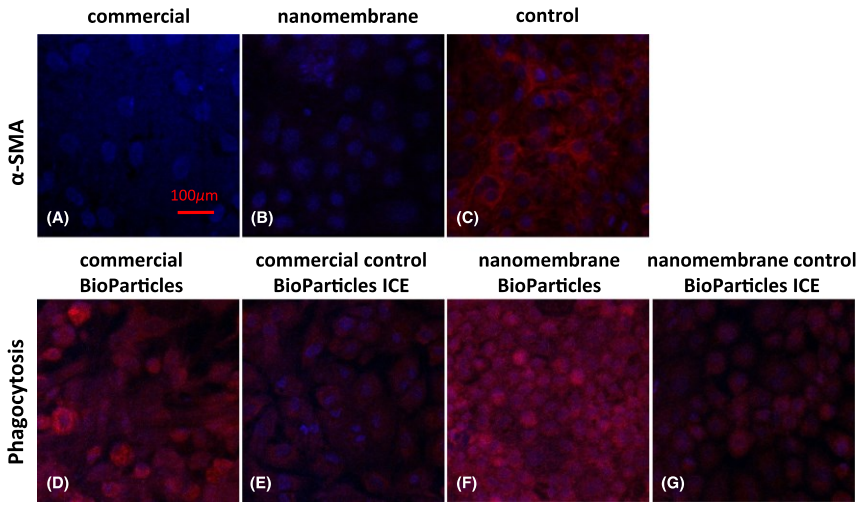

Fig. 7. Confocal microscopy visualization of the alpha-smooth muscle actin (α-SMA) in the cultured RPE cells on commercial (A) and nanofibrous (B) membranes a comparison is shown of the expression of this marker to that in NIH-3T3 fibroblasts (C). Representation of the internalized fluorescent pHrodo™ BioParticles™ (red) and the stained nuclei (blue) in the cultured RPE cells on both commercial (D) and nanofibrous membranes (F) reveals the phagocytic capacity of the cultured RPEs. The control phagocytosis on both types of membranes was done at 4°C (E, G).

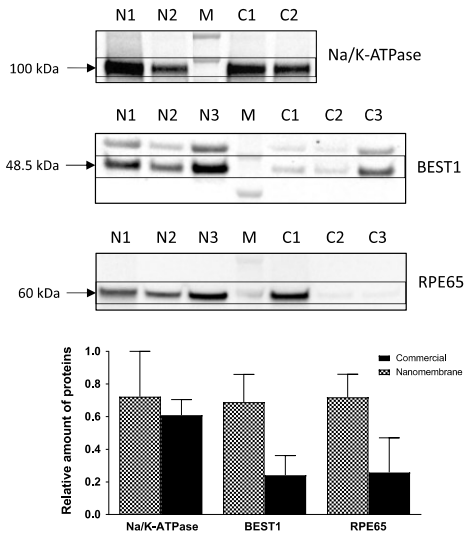

Fig. 8. The difference in the protein level of RPE cell markers in primary RPE cells cultivated on the nanofibrous (N1, N2, N3) and commercial membranes (C1, C2, C3). Western blot detected signals of Na^+/K^+ATPase, BEST1, and RPE65 in RPE cell lysates. There is higher volume intensity of BEST1 and RPE65 in the RPE cells cultivated on the nanofibrous membranes in comparison with RPE cells cultivated on the commercial membranes. There is a smaller difference in volume intensity of the Na^+/K^+ATPase signal on the both types of membranes. M, Novex Sharp Pre-Stained Protein Standard (Invitrogen). The relative amount of proteins was measured using a densitometric evaluation.

protein, which is localized along actin filaments in RPE microvilli and basal infoldings (Bednarz et al. 2000; Sparrow et al. 2000; Valtink et al. 2008). It participates in processes of retinal pigment regeneration (Guo et al. 2016; Pfeiffer et al. 2016). In our study, increased expressions of proteins (tubulin, ezrin) and mRNA of *RLBP1* with moderate prevalence in the case of tubulin and RLBP1 in RPE cells cultured on nanofibrous membranes were observed. The immunocytochemical and biochemical analysis of these markers further confirmed the high polarization and differentiation state of the cultured RPE monolayer.

The transcription factor SOX9 is a key player in transcriptional upregulation of a group of many visual cycle genes such as *RLBP1* and *RPE65* (Bharti 2015; Lee et al. 2016). Masuda and Esumi (2010) described the involvement of SOX in the regulation of the *BEST1* promoter in the RPEs. Even though we found a relatively high expression of *SOX9* in the RPE cells cultured on both scaffolds, the cells on the nanofibrous membranes revealed significantly higher *SOX9* expression than the commercial ones. These results confirmed the presence of

Table 2. Comparison of the polylactide nanofibrous membrane to the polyester commercial membrane, with shown advantages and disadvantages of both.

Nanofibrous membrane	Commercial membrane
Degradable	Non-degradable
Vertical and horizontal pores	Only vertical pores
80% porosity	20% porosity
Polylactide membrane	Polyester membrane
More permeable	Less permeable

mature cells, which possess mechanisms of the visual cycle and *BEST1* gene regulation in the cultured RPE.

Microphthalmia-associated transcription factor (MITF) has been reported to play an important role in RPE physiology, including melanogenesis, anti-oxidant functions, regulation of trophic factor expression, the visual cycle (Kawaguchi et al. 2009; Barca et al. 2014; Joshi et al. 2016) and cell proliferation (Gong et al. 2008; Vossmerbaeumer et al. 2009). Our RPEs cultured on PDLLA nanofibrous membranes revealed higher expression of this marker in comparison with the polyester commercial scaffolds. This would make the nanofibrous membrane-cultivated RPEs to better fulfil the essential role MITF has in melanogenesis and suppression of cell proliferation during the late stages of RPE maturation. Furthermore, the significant increase in the DCT expression in RPE cells cultured on PDLLA nanofibrous membranes indicates the presence of advanced melanogenesis and differentiation of these cells. Our results correspond well with the results of the phase-contrast microscopy analysis, where we found a slight increase of melanin in the porcine RPE cells cultured on nanofibrous membranes.

It occurs that primary RPE cells may undergo EMT during cell cultivation. Several different cellular markers participate in the EMT process. Particularly, an increase in the α-SMA expression is observed under such conditions in the RPEs, which translates into lost polarization, tight junctions and functionality accordingly (Li et al. 2020; Zhou et al. 2020). The absence of the α-SMA was confirmed using immunocytochemistry in the cultured RPE cells on both the nanofibrous and commercial membranes, in comparison with a NIH-3T3 fibroblast culture used as a positive control. According to these results, we assumed that our cultured RPEs remained in a differentiated and polarized state and were able to maintain their physiological functions.

Such physiological function was further examined by a phagocytosis ability of the culture RPE cells. The results revealed a high level of phagocytic particle positive signal inside the cells.

To better reveal the ultrastructural properties of the cultured RPEs, TEM and SEM were performed of the RPE monolayer on both membranes. The electron microscopy confirmed the presence of typical structures found on RPE cells such as microvilli, pigmented granules, tight junctions and well-developed rough-surfaced and smooth-surfaced endoplasmic reticulum.

In summary, the RPE cells cultured on PDLLA nanofibrous membranes reveal more intensive staining of all-important markers for these cells in comparison with those cultured on commercial ones. The RT-qPCR analysis revealed that RPEs cultured on nanofibrous membranes demonstrate a higher expression of RPE-specific genes. Electron microscopy of both membranes confirmed a confluent layer of RPE cells and their correct morphological structure and orientation, which was comparable to that found in cells of the native retina. Particularly, the nanofibrous scaffolds appeared to be a better substrate for the development of RPE microvilli as revealed by the SEM.

Conclusion

The functional and morphological properties of RPEs cultured on PDLLA nanofibrous membranes confirm the better quality of this epithelial monolayer including proper differentiation, correct polarization, high phagocytic activity, good confluence and long-term survival in comparison with commercial membranes. These nanofibrous scaffolds seeded with cultured RPE cells appear to be a suitable carrier for cell therapy based on the replacement of diseased RPE.

Acknowledgment

The project was supported by The Czech Science Foundation(Project Number 18-04393S), Norway Grants and Technology Agency of the Czech Republic (KAPPAProgramme, Project Number TO01000107) and Czech Science Foundation (Project Number 19-09628J) supportedthis study. Special thanks to Hana Říhová and Irena Dejlová fortechnical support and the slaughterhouse "Kohout a synové" for providing uswith cadaverous porcine eyes.

References

Ablonczy Z & Crosson CE (2007): VEGF modulation of retinal pigment epithelium resistance. Exp Eye Res **85**: 762–771.

Amaral J, Campos M, Maminishkis A, Khristov V, Zhou R, Charles ST, Stanzel BV, Jha B, Bunea I, Miller SS & Bharti K (2016): A porcine model of retinal pigment epithelium (RPE) injury to test the efficacy of human induced pluripotent stem cell–derived RPE (hiPSC--RPE) transplants. Invest Ophthalmol Vis Sci **57**: 258.

Bakall B, Marmorstein LY, Hoppe G, Peachey NS, Wadelius C & Marmorstein AD (2003): Expression and localization of bestrophin during normal mouse development. Invest Ophthalmol vis Sci **44**: 3622–3628.

Barca F, Caporossi T & Rizzo S (2014): Silicone oil: different physical proprieties and clinical applications. Biomed Res Int **2014**: 1–7.

Batman C, Ozdamar Y, Mutevelli S, Sonmez K, Zilelioglu G & Karakaya J (2008): A comparative study of tissue glue and vicryl suture for conjunctival and scleral closure in conventional 20-gauge vitrectomy. Eye **23**: 1382–1387.

Bednarz J, Teifel M, Friedl P & Engelmann K (2000): Immortalization of human corneal endothelial cells using electroporation protocol optimized for human corneal endothelial and human retinal pigment epithelial cells. Acta Ophthalmol Scand **78**: 130–136.

Bharti K (2015): Induced to cure: engineering iPS cell derived RPE scaffolds to treat degenerative eye diseases. Acta Ophthalmol **93**: ABS15-0109.

Blaauwgeers HG, Holtkamp GM, Rutten H et al. (1999): Polarized vascular endothelial growth factor secretion by human retinal pigment epithelium and localization of vascular endothelial growth factor receptors on the inner choriocapillaris. Evidence for a trophic paracrine relation. Am J Pathol **155**: 421–428.

Bok D (1993): The retinal pigment epithelium: a versatile partner in vision. J Cell Sci Suppl **17**: 189–195.

Casco-Robles MM, Islam MR, Inami W et al. (2016): Turning the fate of reprogramming

cells from retinal disorder to regeneration by Pax6 in newts. Sci Rep **6**: 33761.

da Cruz L, Fynes K, Georgiadis O et al. (2018): Phase 1 clinical study of an embryonic stem cell–derived retinal pigment epithelium patch in age-related macular degeneration. Nat Biotechnol **36**: 328.

Damasceno E, Damasceno N, Hossy BH, Rio AC & Miguel NC (2015): Scleral wound healing and crosslink technique. Influence on sclerotomy cicatrization on the rabbit eyes. Evaluation with Histological and Morphological Analysis in the Scleral Tissue. A Pilot Study. Invest Ophthalmol Vis Sci **56**: 371.

Diniz B, Thomas P, Thomas B et al. (2013): Subretinal implantation of retinal pigment epithelial cells derived from human embryonic stem cells: improved survival when implanted as a monolayer. Invest Ophthalmol Vis Sci **54**: 5087–5096.

Duan P, Xu H, Zeng Y, Wang Y & Yin ZQ (2013): Human bone marrow stromal cells can differentiate to a retinal pigment epithelial phenotype when co-cultured with pig retinal pigment epithelium using a transwell system. Cell Physiol Biochem **31**: 601–613.

Eichhorn, SJ & Sampson, WW (2005): Statistical geometry of pores and statistics of porous nanofibrous assemblies. J R Soc Interface **2**: 309–318.

Falkner-Radler CI, Krebs I, Glittenberg C, Povazay B, Drexler W, Graf A & Binder S (2011): Human retinal pigment epithelium (RPE) transplantation: outcome after autologous RPE-choroid sheet and RPE cell-suspension in a randomised clinical study. Br J Ophthalmol **95**: 370–375.

Fernandes RAB, Stefanini FR, Falabella P et al. (2017): Development of a new tissue injector for subretinal transplantation of human embryonic stem cell derived retinal pigmented epithelium. Int J Retina Vitreous **3**: 41.

Fuchs U, Kivela T & Tarkkanen A (1991): Cytoskeleton in normal and reactive human retinal-pigment epithelial-cells. Invest Ophthalmol Vis Sci **32**: 3178–3186.

Gong L, Wu Q, Song B, Lu B & Zhang Y (2008): Differentiation of rat mesenchymal stem cells transplanted into the subretinal space of sodium iodate-injected rats. Clin Exp Ophthalmol **36**: 666–671.

Guo X, Zhu D, Lian R, Han Y, Guo Y, Li Z, Tang S & Chen J (2016): Matrigel and Activin A promote cell-cell contact and anti-apoptotic activity in cultured human retinal pigment epithelium cells. Exp Eye Res **147**: 37–49.

Guymer R, Luthert P & Bird A (1999): Changes in Bruch's membrane and related structures with age. Prog Retin Eye Res **18**: 59–90.

Hariprasad SM & Singh A (2011): Polyethylene glycol hydrogel polymer sealant for vitrectomy surgery: an in vitro study of sutureless vitrectomy incision closure. Arch Ophthalmol **129**: 322–325.

Hartnett ME, Lappas A, Darland D, McColm JR, Lovejoy S & D'Amore PA (2003): Retinal pigment epithelium and endothelial cell interaction causes retinal pigment epithelial barrier dysfunction via a soluble VEGF-dependent mechanism. Exp Eye Res **77**: 593–599.

Hayes MJ, Burgoyne T, Wavre-Shapton ST, Tolmachova T, Seabra MC & Futter CE (2019): Remodeling of the basal labyrinth of retinal pigment epithelial cells with osmotic challenge, age, and disease. Invest Ophthalmol Vis Sci **60**: 2515–2524.

Hogan MJ, Alvarado JA & Weddell JE (1971): Histology of the human eye; an atlas and textbook. Philadelphia, PA: Saunders.

Holan V, Trosan P, Cejka C, Javorkova E, Zajicova A, Hermankova B, Chudickova M & Cejkova J (2015): A comparative study of the therapeutic potential of mesenchymal stem cells and limbal epithelial stem cells for ocular surface reconstruction. Stem Cells Transl Med **4**: 1052–1063.

Hotaling NA, Khristov V, Wan Q et al. (2016): Nanofiber scaffold-based tissue-engineered retinal pigment epithelium to treat degenerative eye diseases. J Ocul Pharmacol Ther **32**: 272–285.

Hu YT, Liu L, Lu B et al. (2012): A novel approach for subretinal implantation of ultrathin substrates containing stem cell-derived retinal pigment epithelium monolayer. Ophthalmic Res **48**: 186–191.

Huang C, Wang JJ, Jing G, Li J, Jin C, Yu Q, Falkowski MW & Zhang SX (2015): Erp29 attenuates cigarette smoke extract-induced endoplasmic reticulum stress and mitigates tight junction damage in retinal pigment epithelial cells. Invest Ophthalmol Vis Sci **56**: 6196–6207.

Hynes SR & Lavik EB (2010): A tissue-engineered approach towards retinal repair: scaffolds for cell transplantation to the subretinal space. Graefes Arch Clin Exp Ophthalmol **248**: 763–778.

Ilmarinen T, Hiidenmaa H, Koobi P et al. (2015): Ultrathin polyimide membrane as cell carrier for subretinal transplantation of human embryonic stem cell derived retinal pigment epithelium. PLoS One **10**, e0143669.

Jiang X, Sui X, Lu Y, Yan Y, Zhou C, Li L, Ren Q & Chai X (2013): In vitro and in vivo evaluation of a photosensitive polyimide thin-film microelectrode array suitable for epiretinal stimulation. J Neuroeng Rehabil **10**: 48.

Jin M, Barron E, He S, Ryan SJ & Hinton DR (2002): Regulation of RPE intercellular junction integrity and function by hepatocyte growth factor. Invest Ophthalmol Vis Sci **43**: 2782–2790.

Johnson LV, Forest DL, Banna CD et al. (2011): Cell culture model that mimics drusen formation and triggers complement activation associated with age-related macular degeneration. Proc Natl Acad Sci USA **108**: 18277–18282.

Joshi R, Mankowski W, Winter M, Saini JS, Blenkinsop TA, Stern JH, Temple S & Cohen AR (2016): Automated measurement of cobblestone morphology for characterizing stem cell derived retinal pigment epithelial cell cultures. J Ocul Pharmacol Ther **32**: 331–339.

Jun EJ, Kim JH, Purcell TL & Schanzlin DJ (2012): Comparison of bursting pressure after scleral tunnel incision sealed with sutures or an adherent ocular bandage in human globes. J Int Med Res **40**: 756–760.

Kawaguchi T, Kobayashi K, Osa M & Yoshizaki T (2009): Is a "Cloud-Point Curve" in Aqueous Poly(N-isopropylacrylamide) Solution Binodal? J Phys Chem B **113**: 5440–5447.

Lakkaraju A, Umapathy A, Tan LX, Daniele L, Philp NJ, Boesze-Battaglia K & Williams DS (2020): The cell biology of the retinal pigment epithelium. Prog Retin Eye Res **78**: 100846.

Landes CA, Ballon A & Roth C (2006): Maxillary and mandibular osteosyntheses with PLGA and P(L/DL)LA implants: a 5-year inpatient biocompatibility and degradation experience. Plast Reconstr Surg **117**: 2347–2360.

Lee DY, Lorach H, Huie P & Palanker D (2016): Implantation of modular photovoltaic subretinal prosthesis. Ophthalmic Surg Lasers Imaging Retina **47**: 171–174.

Lehtonen TJ, Tuominen JU & Hiekkanen E (2013): Resorbable composites with bioresorbable glass fibers for load-bearing applications. In vitro degradation and degradation mechanism. Acta Biomater **9**: 4868–4877.

Lerit SJT & Abaño JMR (2012): Comparison of tensile strength of fibrin glue, 2-octyl cyanoacrylate, liquid ocular bandage, and conventional nylon 10–0 sutures in corneal laceration repair in an animal model. Philipp J Ophthalmol **37**: 52–58.

Li X, Zhao M & He S (2020): RPE epithelial-mesenchymal transition plays a critical role in the pathogenesis of proliferative vitreoretinopathy. Ann Transl Med **8**: 263.

Lindner U, Kramer J, Rohwedel J & Schlenke P (2010): Mesenchymal stem or stromal cells: toward a better understanding of their biology? Transfus Med Hemother **37**: 75–83.

Liu Z, Yu N, Holz FG, Yang F & Stanzel BV (2014): Enhancement of retinal pigment epithelial culture characteristics and subretinal space tolerance of scaffolds with 200 nm fiber topography. Biomaterials **35**: 2837–2850.

Maitz MF (2015): Applications of synthetic polymers in clinical medicine. Biosurf Biotribol **1**: 161–176.

Marmorstein AD (2001): The polarity of the retinal pigment epithelium. Traffic **2**: 867–872.

Marmorstein AD, Finnemann SC, Bonilha VL & Rodriguez-Boulan E. (1998): Morphogenesis of the retinal pigment epithelium: toward understanding retinal degenerative diseases. In: Fleischmajer R, Timpl R & Werb Z (eds) Morphogenesis: cellular Interactions. New Jersey: John Wiley & Sons, Ltd 1–12.

Marmorstein AD, Marmorstein LY, Rayborn M, Wang X, Hollyfield JG & Petrukhin K

(2000): Bestrophin, the product of the Best vitelliform macular dystrophy gene (VMD2), localizes to the basolateral plasma membrane of the retinal pigment epithelium. Proc Natl Acad Sci USA **97**: 12758–12763.

Masuda T & Esumi N (2010): SOX9, through interaction with microphthalmia-associated transcription factor (MITF) and OTX2, regulates BEST1 expression in the retinal pigment epithelium. J Biol Chem **285**: 26933–26944.

McHugh KJ, Tao SL & Saint-Geniez M (2014): Porous poly(epsilon-Caprolactone) scaffolds for retinal pigment epithelium transplantation. Invest Ophthalmol Vis Sci **55**: 1754–1762.

Pfeiffer RL, Marc RE & Jones BW (2016): Müller cell metabolic chaos during retinal degeneration. Exp Eye Res **150**: 62–70.

Pilgrim MG, Lengyel I, Lanzirotti A et al. (2017): Subretinal pigment epithelial deposition of drusen components including hydroxyapatite in a primary cell culture model. Invest Ophthalmol Vis Sci **58**: 708–719.

Popelka S, Studenovska H, Abelova L et al. (2015): A frame-supported ultrathin electrospun polymer membrane for transplantation of retinal pigment epithelial cells. Biomed Mater **10**: 045022.

Ramsden CM, Powner MB, Carr AJF, Smart MJK, da Cruz L & Coffey PJ (2013): Stem cells in retinal regeneration: past, present and future. Development **140**: 2576–2585.

Rodriguez-Crespo D, Di Lauro S, Singh AK, Garcia-Gutierrez MT, Garrosa M, Pastor JC, Fernandez-Bueno I & Srivastava GK (2014): Triple-layered mixed co-culture model of RPE cells with neuroretina for evaluating the neuroprotective effects of adipose-MSCs. Cell Tissue Res **358**: 705–716.

Seo JM, Kim SJ, Chung H, Kim ET, Yu HG & Yu YS (2004): Biocompatibility of polyimide microelectrode array for retinal stimulation. Mater Sci Eng C Biomim Supramol Syst **24**: 185–189.

Sharma R, Khristov V, Rising A et al. (2019): Clinical-grade stem cell-derived retinal pigment epithelium patch rescues retinal degeneration in rodents and pigs. Sci Transl Med **11**: eaat5580.

Sheridan CM, Mason S, Pattwell DM, Kent D, Grierson I & Williams R (2009): Replacement of the RPE monolayer. Eye **23**: 1910–1915.

Sheridan CM, Pattwell D, Thompson S, Mason S, Kent DL & Grierson I (2010): Differentiation potential of mesenchymal stem cells to RPE cells. Invest Ophthalmol Vis Sci **51**: 502.

Shokoohmand A, Jeon JE, Theodoropoulos C, Baldwin JG, Hutmacher DW & Feigl B (2017): A novel 3D cultured model for studying early changes in age-related macular degeneration. Macromol Biosci **17**: 1700221.

Sorkio A, Porter PJ, Juuti-Uusitalo K, Meenan B, Skottman H & Burke G (2015): Surface modified biodegradable electrospun membranes as a carrier for human embryonic stem cell derived retinal pigment epithelial cells. Tissue Eng Part A **21**: 2301–2314.

Sparrow JR, Nakanishi K & Parish CA (2000): The lipofuscin fluorophore A2E mediates blue light-induced damage to retinal pigmented epithelial cells. Invest Ophthalmol Vis Sci **41**: 1981–1989.

Stanzel BV, Espana EM, Grueterich M, Kawakita T, Parel J-M, Tseng SCG & Binder S (2005): Amniotic membrane maintains the phenotype of rabbit retinal pigment epithelial cells in culture. Exp Eye Res **80**: 103–112.

Stanzel BV, Liu Z, Brinken R, Braun N, Holz FG & Eter N (2012): Subretinal delivery of ultrathin rigid-elastic cell carriers using a metallic shooter instrument and biodegradable hydrogel encapsulation. Invest Ophthalmol Vis Sci **53**: 490–500.

Stanzel BV, Liu Z, Somboonthanakij S et al. (2014): Human RPE stem cells grown into polarized RPE monolayers on a polyester matrix are maintained after grafting into rabbit subretinal space. Stem Cell Rep **2**: 64–77.

Stout JT & Francis PJ (2011): Surgical approaches to gene and stem cell therapy for retinal disease. Hum Gene Ther **22**: 531–535.

Surrao DC, Greferath U, Chau YQ et al. (2017): Design, development and characterization of synthetic Bruch's membranes. Acta Biomater **64**: 357–376.

Toops KA, Tan LX & Lakkaraju A (2014): A detailed three-step protocol for live imaging of intracellular traffic in polarized primary porcine RPE monolayers. Exp Eye Res **124**: 74–85.

Valtink M, Gruschwitz R, Funk RH & Engelmann K (2008): Two clonal cell lines of immortalized human corneal endothelial cells show either differentiated or precursor cell characteristics. Cells Tissues Organs **187**: 286–294.

Vareilles P, Conquet P & Le Douarec J-C (1977): A method for the routine intraocular pressure (IOP) measurement in the rabbit: range of IOP variations in this species. Exp Eye Res **24**: 369–375.

von Burkersroda F, Schedl L & Gopferich A (2002): Why degradable polymers undergo surface erosion or bulk erosion. Biomaterials **23**: 4221–4231.

Vossmerbaeumer U, Ohnesorge S, Kuehl S, Haapalahti M, Kluter H, Jonas JB, Thierse H-J & Bieback K (2009): Retinal pigment epithelial phenotype induced in human adipose tissue-derived mesenchymal stromal cells. Cytotherapy **11**: 177–188.

Warnke PH, Alamein M, Skabo S, Stephens S, Bourke R, Heiner P & Liu Q (2013): Primordium of an artificial Bruch's membrane made of nanofibers for engineering of retinal pigment epithelium cell monolayers. Acta Biomater **9**: 9414–9422.

Weir NA, Buchanan FJ, Orr JF & Dickson GR (2004): Degradation of poly-L-lactide. Part 1: in vitro and in vivo physiological temperature degradation. Proc Inst Mech Eng H **218**: 307–319.

Yaji N, Yamato M, Yang J, Okano T & Hori S (2009): Transplantation of tissue-engineered retinal pigment epithelial cell sheets in a rabbit model. Biomaterials **30**: 797–803.

Zhang XC, Wyss UP, Pichora D & Goosen MFA (1994): An investigation of poly(lactic acid) degradation. J Bioact Compat Polym **9**: 80–100.

Zhou M, Geathers JS, Grillo SL, Weber SR, Wang W, Zhao Y & Sundstrom JM (2020): Role of epithelial-mesenchymal transition in retinal pigment epithelium dysfunction. Front Cell Dev Biol **8**: 501.

Received on February 4th, 2021.
Accepted on September 22nd, 2021.

Correspondence:
Taras Ardan, MD, PhD
Institute of Animal Physiology and Genetics
Academy of Sciences of the Czech Republic
Rumburska 89
27721 Libechov
Czech Republic
Tel: +420 315 639 570
Fax: +420 315 639 510
Email: ardan@iapg.cas.cz

tom sin vivo CT) ost mortem peanut agglutining (PNA) (marker); PKCα (ntin, GFAP (markers);(**Results:** The hRPEs assumed cobblestone morphology, persistent pigmentation and measurable trans-epithelial electrical resistance on the nanofibrous PDLLA carrier. The surgical delivery of the implants in the subretinal space of the immunosuppressed minipigs was successfully achieved and monitored by fundus imaging and OCT. The implanted hRPEs were positive for HNAA and STEM121 and located between the minipig's neuroretina and RPE layers at week 2 post-implantation, which was gradually attenuated till week 8. The neuroretina over the implants showed rosette or hypertrophic reaction appearance at week 6. The implanted cells expressed the typical RPE marker bestrophin throughout the whole observation period, and a gradual diminishing of the CRALBP expression in the area of implantation at week 8 post-implantation was observed . The transplanted hRPEs appeared not to form a confluent layer and were less capable of keeping the inner and outer retinal segments intact. The cone photoreceptors adjacent to the implant scaffold were unchanged initially, but underwent a gradual change in structure after hRPE implantation; the retina above and below the implant appeared relatively healthy. The glial reaction of the transplanted and host retina showed Vimentin and GFAP positivity from week 1 onward. Microglial activation appeared in the retinal area of the transplant early after the surgery, which seemed to move into the transplant area over time. sfully achieved and monitored by fundus imaging and OCT. The implanted hRPEs were positive for HNAA and STEM121 and located between the minipig's neuroretina and RPE layers at week 2 post-implantation, which was gradually attenuated till week 8. The neuroretina over the implants showed rosette or hypertrophic reaction appearance at week 6. The implanted cells expressed the typical RPE marker bestrophin throughout the whole observation period, and a gradual diminishing of the CRALBP expression in the area of implantation at week 8 post-implantation was observed . The transplanted hRPEs appeared not to form a confluent layer and were less capable of keeping the inner and outer retinal segments intact. The cone

photoreceptors adjacent to the implant scaffold were unchanged initially, but retina above and below the implant **Conclusions:** The differentiated hRPEs can serve as an alternative cell source for RPE replacement in animal studies. These cells can be cultivated on nanofibrous PDLLA and implanted subretinally into minipigs using standard 23-gauge vitrectomy an implantation injector. The hRPE-laden scaffolds show relatively good incorporation into the host retina over an 8 weeks observation period, with some indication of a gliotic scar formation, and a likely neuroinflammatory response in the transplanted area in site of the use of immunosuppression. an implantation injectora in site of

Keywords: retinal pigmented epithelium, subretinal implantation, nanofibrous membrane, minipigs, age-related macular degeneration (AMD)

Introduction

Age related macular degeneration (AMD) is one of the most prevalent forms of irreversible visual impairment with multifactorial etiology. Its pathogenesis is characterized by early appearance of drusen, followed by functional anomalies in the retinal pigmented epithelium (RPE) and geographic atrophy followed by photoreceptor degeneration affecting the macular region (1).

There are multiple reasons for the photoreceptor dysfunction and degeneration including ionization of photosensitive retinoids upon light exposure, generation of reactive oxygen species and inflammatory cascade leading to photoreceptor cells death. Among the major factors leading to photoreceptor cell death are those associated with increased permeability of RPE, aberrant choroidal neovascularization (2), altered RPE phagocytosis (3), as well as sub-retinal recruitment of resident and monocytic microglial cells (4). Functional, as well as structural changes in the RPEs are thought to drive the onset of the disease. RPEs are specialized pigmented cells arranged in a compact monolayer between the neural retina and the choriocapillaris. Loss or degeneration of the RPEs results in vision loss due to their important function in supplying nutrients to the photoreceptors (rods and cones), and phagocytosis and maintenance of the blood-retina barrier among others (5). The cause of degeneration of the RPEs has not been fully deciphered to date. There are no therapeutic interventions that can reverse AMD (6, 7). However, treatment modalities like injection of anti-vascular andothelial growth factors (VEGFs) or laser-based coagulation or photodynamic therapy have been used to reduce the severity of the wet form of AMD (8). The cell therapy-based regenerative approach offers a solution in treating and reversing AMD (9). Stem cell-derived sources can be used for derivation of allogenic or autologous induced RPEs (iRPE) that can be injected into the subretinal space to regenerate the lost RPE monolayer and thus reduce the symptoms of AMD including vision loss (10-13). However, recent studies have suggested that injection of RPEs in the subretinal space leads to incomplete epithelization of the degenerated RPE monolayer, as well as suboptimal cell engraftment and diminished reversibility of vision loss. This could be attributed to various reasons like improper attachment of the RPEs on the Bruch's membrane, loss of cell-to-cell contact between the RPEs, change in functional behaviour of transplanted RPEs in the diseased environment, and de-differentiation of transplanted RPEs leading to loss of functionally mature cells (7). To overcome this limitation, RPEs seeded on a bioscaffold have been transplanted and have shown to improve the integration, regeneration and functional behaviour *in vivo* upon transplantation, as compared to the cell-injection methods of delivery. Such knowledge further accentuates the need for newer scaffold-based delivery approaches, where RPEs pre-seeded patches could be directly transplanted into the subretinal space (14). This would overcome some of the limitations observed in cell delivery modalities including the de-differentiation of RPEs, and help the proper engraftment of the transplanted RPEs, with eventual complete degradation of the scaffold and monolayer cellularization of the RPE layer. The aforementioned strategies are clinically viable, if a reproducible, efficient and faster way of deriving already dedicated RPEs exists from human cadaver donors. So far, most studies have focused on *in vitro* development of iPSCs involved in spontaneous derivation of RPE-like cells during culturing of ectoderm-committed embryonic stem cells (ESCs). This process usually takes 4-6 months to achieve, giving sufficient number of cells for *in vivo* studies (7, 11, 13). Furthermore, the process is spontaneous and factors like efficiency, gene and functional level of RPE remain elusive and may vary from batch to batch.

In order to increase and maintain the differentiation state, strategies and improvements have been made to achieve better yield of RPEs derived from ESCs and iPSCs using either biphasic or triphasic methods (7, 14-16), however, still in a rather complex and tedious manner. Alternatively, differentiated human primary RPEs (hRPEs) from cadaver donors can offer the potential source to derive cellular therapy modalities and applications in disease modelling, as well as *in vitro* development for drug testing. Development of hRPEs for transplantation purposes on biodegradable scaffolds for human transplantation is therefore indispensable. Herein, we present the initial methodology and results of such an approach.

Trans-epithelial e lectrical resistance (TEER)

Nanofibrous membranes were coated using 5 µ g/mL laminin overnight to assist cell attachment. The following day, hRPE cells were seeded at passage 1 onto the membranes at a density of 2000 cells / mm^2 and cultured on the membranes for up to 6 weeks until TEER measurements took place. A Millicell® ERS-2 Voltohmmeter (Merck, Darmstadt, Germany) was used to determine membrane resistance values. Cultured cells were provided with a fresh, serum-free medium and an internal control electrode was used to calibrate the device prior to measurement. The electrodes, small enough to fit between the trans-well inserts, were dipped into the wells following the manufacturer's guidelines and the data was recorded.

Implantation injector

The custom-made injector consisted of a rectangular plastic capillary (outer diameter 2.8 × 0.8 mm) and a stainless steel blade plunger. The length of the plastic capillary was 6 cm. The carrier was loaded into the injector through a loading window located 6 mm from the distal end of the capillary in sterile conditions in the experimental department of laboratory facility. The injector with preloaded carriers was prepared separately for every case. The injectors were transferred to the operating theatre in a sterile container shortly before the implantation stage of the surgery in order to avoid drying up of the carrier that could cause the adhesion of the carrier to the inner surface of the capillary. Before the implantation stage of the surgery the injector was taken out of the container. After the surgeon performed the injection of the carrier into the subretinal space by a pushing of the plunger, the injector was withdrawn out of the eye.

Animals used for the experimental study

"Libechov" minipigs that were 12–36 months old and of both sexes were used in the study (19). General anaesthesia of the minipigs was induced by intramuscular injection of TKX mixture consisting of Tiletamine (2 mg/kg, Zoletil 100, Virbac), Zolazepam (2 mg/kg, Zoletil 100, Virbac), Ketamine (2 mg/kg, Narketan 10, Vetoquinol), and Xylazine (0.4 mg/kg, Xylapan, Vetoquinol). After induction of sedation, an ear vein cannula was introduced and the animal intubated for inhalation maintenance of anaesthesia (Isoflurane 1.5%). During eye surgery, intramuscular injection was given to the animals by Eficur (1ml/16kg BW, Hipra) and Depo-Medrol 120 mg (Pfizer, New York, USA). Eficur was repeatedly injected 24 and 48 hours after surgery, followed by a 72 hours injection of the animals by Draxxin (1ml/40 kg BW, Zoetis) as a secondary bacterial infection prevention. Postoperatively, Ophthalmo-Framycoin ointment (Zentiva, Prague, Czech Republic) was applied into the conjunctival sac of the animals 5 times per day during 1 week. Animals were sacrificed by exsanguination in deep general anaesthesia 1, 2, 6, and 8 weeks after RPE cell graft implantation.

Immunosuppression of minipigs

Survival of the donor cells was supported by tacrolimus immunosuppressive therapy of the recipient animals. The immunosuppressive therapy was administered by a subcutaneous injection of tacrolimus-eluting polymer microspheres which were successfully used in rats (20). We used tacrolimus in a dose of 0.05 mg/kg/day. The first injection of tacrolimus microspheres was done six days before the implantation surgery. The protocol used in all minipigs is shown in **Figure 2**.

Figure 2. Immunosuppression protocol used throughout the experimental studies in minipigs. The concentration of tacrolimus in the blood was examined on Days 5, 14, and 23 after initial application.

Implantation of hRPEs on a nanofibrous carrier into minipigs

Five immunocompromised minipigs were used throughout the experiment and followed up to 8 weeks (**Table 1**).

Table 1. Experimental setup and timeline.

Surgical technique

All surgeries were performed in the operating room of the Institute of Animal Physiology and Genetics, Academy of Sciences of the Czech Republic (Libechov, Czech Republic) by three experienced vitreoretinal surgeons (L.L., G.P., Z.S.) who previously accomplished a training course and obtained a certificate, which allows for performing eye microsurgeries on pigs with experimental aim. Every surgical procedure was performed under general anaesthesia with implementation of standard aseptic and antiseptic measurements. A microsurgical approach was facilitated by using ophthalmic surgical microscope Hi-R NEO 900A (Haag-Streit Surgical, Wedel, Germany), vitrectomy machine R-Evolution CR (Optikon, Rome, Italy) and a non-contact indirect viewing system MERLIN BIOM (Volk, Mentor, OH, USA). After the skin and the conjunctival sac were disinfected using 10% and 5% solution of povidone-iodine (Betadine), respectively, the speculum was inserted. The conjunctiva was opened nasally 2.5 mm from the limbus and was 5 mm long. Episcleral vessels were cauterized. A standard three port vitrectomy was done with 23-gauge (G) trocars, which were inserted 2.5-3 mm from the limbus in a standard position (**Supplementary Figure 1**). Core pars plana vitrectomy (PPV) was performed with removal of the vitreous centrally and anterior to the equator at the site of the future insertion of the injector. Posterior vitreous detachment was assisted by intravitreal injection of the triamcinolone acetonide (TA) crystals. Creation of subretinal bleb was facilitated through subretinal injection of balanced salt solution (BSS®, Alcon Laboratories, Inc., Fort Worth, TX, USA) with subretinal PolyTip cannula 25/38 gauge (MedOne Surgical, Inc. Sarasota, FL, USA), which was connected through a Luer lock adapter to the syringe filled with BSS®. Subretinal fluid application was performed from the nasal side toward the centre of the retina to avoid formation of a bleb in the periphery. Caution was given to avoid injection of BSS under the RPEs with detachment of the choroid. During subretinal application of BSS the intraocular pressure settings on the vitrectomy machine were decreased from 25 to 15 mmHg. After the episcleral vessels were cauterized with exodiathermy, a 3 mm long limbal parallel sclerotomy between the two nasal trocars was performed 2.5 mm from the limbus with bevelled angled Phaco Slit Knife 2.2 mm (D.O.R.C. Zuidland, The Netherlands). After removal of the prolapsed vitreous an injector was introduced into the vitreous cavity and the carrier was injected into the subretinal space through the retinotomy. Following withdrawal of the injector, the 3 mm sclerotomy was sutured with Vicryl 8.0 (Johnson & Johnson, New Jersey, USA). A fluid-air exchange was performed under visual control with injection of endotamponade with silicone oil 1000 cSt (D.O.R.C. Zuidland, The Netherlands). The position of the implanted carrier was documented using fundus photography. Trocars were removed, and the sclerotomies and the conjunctival wound were sutured with Vicryl 8.0. The conjunctival sac was washed with Betadine and subconjunctival injection of gentamicin 20 mg and dexamethasone 2 mg was performed at the end of the surgery. All surgeries were

documented by drawing the fundus scheme and recording in video format (video and snapshot modes).

In vivo optical coherence tomography

The retina of all animals was examined by spectral-domain optical coherence tomography (SD-OCT) system iVue (Optovue, Fremont, CA, USA).

Euthanasia and tissue processing

Euthanasia was performed under general anesthesia with i.m. T61 (Embutramidum 200 mg/kg, Mebezonii iodidum 50 mg/kg, Tetracaine hydrochloride 5 mg/kg, Intervet International B.V, AN Boxmeer, Netherlands). Whole eyes were removed and fixed in 4% paraformaldehyde (PFA) for 24 hp of the eye was removed by ci nasal central retina collected. All tissues were cryoprotected in graded sucrose solutions as described in detail (20)

Immunohistochemical analysis

Trans-epithelial Electrical Resistance (TEER)

Resistance values were determined for two donors of hRPE on two different occasions with a repetition of 3 (n=6). The mean and standard deviation of all measurements for TEER was 128.82 ± 16.45 Ω . Without cells, the electrode recorded an average resistance of 89.85 ± 11.65 Ω at the two sides of the nanofibrous membrane. Corrected for the surface area, hRPE seeded on the nanofibrous membranes had a resistance of 38.61- 75.11 Ω/ cm^2.

Implantation of the hRPEs

A typical fundus appearance of the transplanted hRPEs on a nanofibrous carrier is shown in **Figure 4**, together with an OCT image of the retina. The images demonstrate subretinal location of the implants. The adherence of the implants to the surrounding structures as well as their similar hyperreflectivity appearance to the same level layers in the retina is visible on OCT.

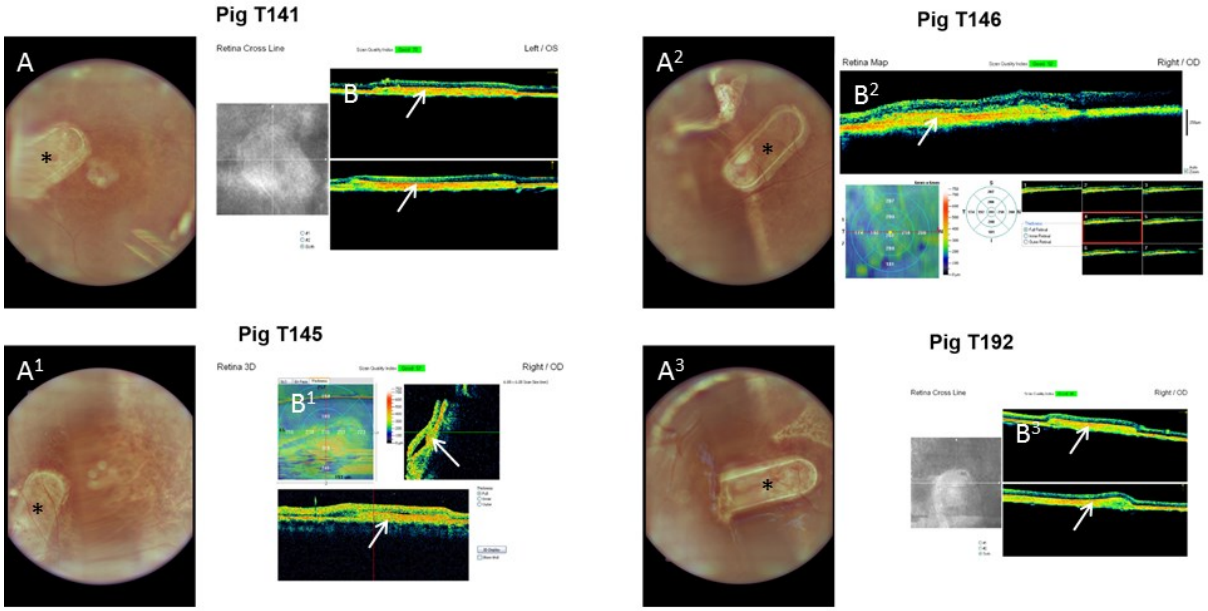

Figure 4. Fundus (A) and Optical Coherence Tomography (B) imaging of the implanted hRPEs on a nanofibrous carrier into minipigs. *(A) The star indicates the position of the implant in the superior nasal area of the retina. (B) White arrow highlights the location of the implant underneath the retina in two cross-sectional images of the retina. The strong red line indicates the reflection from the RPE, which seems to be thicker in the area of the transplant.*

Immunohistochemical analysis of the implanted hRPEs

The implanted hRPEs were positive for the human nuclear antigen (HNAA) and were located between the neuroretina and the RPE minipig layer at week 2 post-implantation, to then gradually lose this positivity at week 6 and regain it at week 8. The pigmented appearance of the implanted hRPEs could be observed throughout the whole observation period on the H&E stained images (**Figure 5**). In addition, the neuroretina over the implants showed rosette or hypertrophic reaction appearance at Week 6.

The morphology of the implanted cells appearing not in a monolayer after implantation and followed with the HNAA as well as the STEM121 human cell marker is shown in **Figure 6**. By week 8, the implanted hRPEs appear to be in a more diffuse state, yet still within the defined subretinal space. Interestingly, the initially uniform nuclear staining of both HNAA (**Figure 6A,E**) and STEM121 (**Figure 6B,F**) in the post-transplantation weeks showed over time changes into a more punctate staining (**Figure 6D,H**), indicating changes to the cell fate during the integration process.*tion* their epigenetic memory (23). Therefore, in recent years, beside the interest in iPSC- and ESC- based RPE derivation, hRPEs appear to frequently appear in the explored methods for clinical trials. The iPSC-derived RPEs have already been transplanted in AMD patients as a cell therapy module or in scaffold-based RPE patches. Results have been positive from these clinical trials (13). However, such studies have been carried out on a small scale, and can be used as proof-of-concept studies for RPE-based treatment of AMD in humans. iPSC-based RPE derivation in itself has many challenges, among others, long-duration employed to differentiate iPSCs into RPEs, which varies between 2 to 6 months (7).
iPSC- and ESC- derived RPEs have been used in clinical trials for AMD patients (24). Recent studies on clinical trials of stem cell derived RPEs include ESC-derived RPEs used for treatment of geographic atrophy in AMD (25), ESC-derived RPE patch in AMD patients (26), iPSC-derived RPE sheets in a patient having AMD. These studies have focused more on the differentiation aspect in order to reduce the differentiation time, which is not an issue when using hRPEs. More recently, a cocktail of small molecule inhibitors and growth factors have been used to derive RPEs and further fabricate a patch for transplantation in a rat and pig model to study the efficiency of RPE patch attachment and function of the transplanted construct. Commitment and differentiation of these cells is obviously important (27, 28).
Our hRPEs possessed full pigmentation during the *ex vivo* cultivation on the nanofibrous carrier, which formed folds after subretinal transplantation. Other studies have shown similar native infoldings (29) when human iPSC-derived RPEs were cultured on nanofibrous membranes, with similar morphological, electrical, and RPE markers' expression characteristics. In addition, the hRPEs formed rosettes, which have been shown before in a retinal transplantation study (30). The low thickness and high porosity of our nanofibrous membranes should also positively affect the long-term survival of the hRPEs (31). Our cells, unlike other previously reported cells (32), as well as stem cells-derived RPEs (14), produced no extracellular deposits on their basal side. Our nanofibrous membrane with degradation lifetime of at least 5 months and more (33-35), and no adverse effects known during the polymer degradation (36), appears to be a plausible and sufficient carrier for a typical 2-6 months-long cultivation of RPEs *ex vivo* (37), as well as mechanical manipulation during surgery. The degradable nature of the nanofibrous membrane seems to be also advantageous in supporting *de novo* synthesis of a Bruch's membrane equivalent by the donor RPE cells, and their integration into the host's Bruch's membrane (14). Our implanted patch of cells contained a peripheral frame (17) around the nanofibrous membrane, which seemed to provide sufficient mechanical strength during the surgical procedure.
The measurement of TEER is used to determine the overall health and confluence of a cell monolayer, and as such, an increased value thus represents a strong barrier against electric current (39, 40). The relatively low net resistance detected in our cultures (38.61-75.11 Ω/cm^2) may indicate an incomplete formation of tight junctions and cell polarization. Resistance of the native RPE layer is believed to be around 150 Ω/cm^2, however, the values range between 25 – 500 Ω/cm^2 with cultured RPE cells. Improvements in the hRPE barrier function are further needed in future transplantation studies.

In this study, we used RPE-specific markers to characterize the various morphological and functional properties of these cells including differentiation and maturation processes. Human cell markers - HNAA and STEM121 were used to localize the hRPEs in the minipig eyes in the follow-up period (41). Bestrophin and CRALBP are typical markers of the visual cycle and late differentiation of RPEs (42, 43), which expression remained unchanged or gradually diminished in the subretinal space, respectively, in the 8 weeks follow-up time. The end-stage retinal specific neuronal markers for the rod bipolar (PKC-alpha) and the cone photoreceptors (PNA) (44) appeared to show signs of stress, yet, throughout the 8 weeks follow-up period, the retina appeared capable of maintaining its inner and outer segments intact. The presence of reactive gliosis in the transplanted overlying retina (Iba1, Vimentin and GFAP expression) can have beneficial effects for the retinal remodeling in our minipig study model (45, 46).

RPE surgical transplantation

Performing intraocular surgeries *in vivo* in primates remains challenging due to the specific features of the animal's body and the eye in regards to general anaesthesia and surgical intervention, respectively. It requires a deep knowledge about the eye anatomy and special training on cadaver eyes of the certain species before starting with surgery on live animals. Development of the new surgical approaches for treatment of retinal diseases in humans usually necessitates an experimental big animal model. Different animal species are used for experimental studies, which are aimed to investigate and prove the concept of subretinal injection or implantation of a variety of cell-based or gene-based therapeutic approaches. Among the most used animal models are monkeys, rabbits and pigs (or minipigs). Up to date, there is no standardized surgical technique for vitreoretinal and subretinal surgery in primates, as every therapeutic strategy and the study protocol have been different.

In 2015, our collaborative group first reported design fabrication of a frame-supported nanofibrous membrane for the transplantation of porcine RPEs (17). All surgeries and implantations were performed on enucleated porcine eyes. The study results revealed the viability of the majority of the implanted RPE cells in the subretinal space. Since 2016, our group has developed and improved the surgical protocol for subretinal implantation of a cell carrier in the eyes of minipigs *in vivo*. The surgical intervention applied in this study is a strictly defined and documented protocol, which was followed by every surgeon of the study group with a high success rate. Minipigs belong to a large animal model, which eye size is similar to the size of the human eye. In this context, the use of minipigs for this kind of study could be considered optimal.

In 2016, Al-Nawaiseh et al. reported a step by step protocol for subretinal surgery in rabbits (47). The study described a surgical protocol based on six years' experience with subretinal implantation of cultured RPE monolayer on a scaffold into the subretinal space, with detailed description of instrumentation needed, anaesthesia, surgical technique and postoperative care. They used an implant with size of 2.4×1.1 mm on the uncoated 10-µm-thick polyester membrane with cultured human fetal RPE cells. The required sclerotomy was 1.4 mm in size (37, 47). In our study series we used minipigs as a large animal model using a similar technique of subretinal implantation of the cell carrier. However, the characteristics of the injector, cell carrier and hence certain surgical steps were different. For example, the size of the cellular scaffold was 2.1×5.2 mm and the size of sclerotomy was 3.0 mm.

In 2019, Gandhi et al. reported the results of subretinal implantation of a human fibrin hydrogel implant in pig eye in order to evaluate its degradability *in vivo* (48). Previously the

authors investigated the efficacy of fibrin hydrogel scaffold with degradation kinetics in regard to supporting the growth and differentiation of iPSC-RPE cells in vivo (49). The study was performed on the female domestic (Yorkshire) pigs cultivated on Manthei Hog Farm (Elk River, MN) with mean weight 22-35 kg. All surgeries were performed under general anaesthesia. The size of the scaffold presented in this study was 1.5×5 mm. The average thickness of fibrin gels was 202.5 µm. The sclerotomy required for insertion of the injector was 3.5 mm. The authors reported that the fibrin hydrogel membrane degraded within 8 weeks after the implantation. In our study, we used a nanofibrous carrier with an embedded supporting PET frame with the size of 2.1×5.2 mm. The thickness of the membrane was 3.7 µm with porosity of 72%. The diameter of the bead-free fibres was 380 nm with the average pore size of 0.4 µm. Semi-crystalline polymer such as PDLLA with high molecular weight could provide overall mechanical strength for delicate nanofibrous membrane during long term cell cultivation with degradation timeframe at least 5 months and more (33). The size of required sclerotomy was 3.0 mm.

In 2021, Liu et al. reported the results of surgical transplantation of human RPE stem cell-derived RPE monolayers into non-human primates following immunosuppression (50). As an animal model, they used 4 to 6 years old cynomolgus monkeys (Macaca fascicularis) with a weight of 3.0 – 5.0 kg. For immunosuppression, they used oral administration of sirolimus starting with the loading dose of 2 mg, and continuing with 1 mg everyday 7 days before and 3 months after the surgery. The size of the cell carrier and the required size of sclerotomy was the same described in the previous study (37, 47). In our study, we used subcutaneous injection of tacrolimus for immunosuppression in a low dose of 0.05 mg/kg/day.

Injection of RPE cell monolayer

Successful implantation of the scaffold with cultivated cells is directly dependent on the surgical technique as well as on instrumentation used for this purpose. To date, a small number of injector devices for subretinal implantation of cell carriers have been described. In 2017, Fernandes et al. described the preliminary results of a new tissue injector for subretinal implantation of an ultrathin non-absorbable substrate with cultivated cells (51). The study results showed the new prototype of the injector was able to efficiently deliver the tissue implant with size 3.5 mm to 6.0 mm in the subretinal space on the eyes of minipigs. Additionally, the results suggested that the use of the new injector allowed for significant prevention of cell loss, reduction of the risk of tissue trauma, surgical complications and postoperative inflammation. In our study, we used a custom-designed injector, which allowed us to implant the cell carrier with the size 5.2 mm×2.1 mm with an adherent sheet of hRPEs. The shape of the injector possessed a double bending in order to be able to place the implantation injector more parallel to the retina and reduce the risk of RPE damage during the implantation process.

Conclusions

All past and current protocols of choosing the right source of RPEs for transplantation studies in large animal models have several disadvantages which need improvement. The hRPEs can be cultivated on nanofibrous PDLLA carrier and implanted subretinally into minipigs using standard 23-gauge vitrectomy and an implantation injector. The hRPE-laden

AcknowledgmentsThe study was supported by funding allocated to an international project of The Czech Science Foundation (Project Number 18-04393S), the Norway Grants and Technology Agency of the Czech Republic (KAPPA project TO01000107).

39. Fronk AH, Vargis E. Methods for culturing retinal pigment epithelial cells: a review of current protocols and future recommendations. Journal of tissue engineering. 2016;7:2041731416650838.40. Rizzolo LJ. Barrier properties of cultured retinal pigment epithelium. Experimental eye research. 2014;126:16-26.41. Chao JR, Lamba DA, Klesert TR, Torre A, Hoshino A, Taylor RJ, et al. Transplantation of Human Embryonic Stem Cell-Derived Retinal Cells into the Subretinal Space of a Non-Human Primate. Translational vision science & technology. 2017;6(3):4.42. Limnios IJ, Chau YQ, Skabo SJ, Surrao DC, O'Neill HC. Efficient differentiation of human embryonic stem cells to retinal pigment epithelium under defined conditions. Stem cell research & therapy. 2021;12(1):248.43. Plaza Reyes A, Petrus-Reurer S, Padrell Sanchez S, Kumar P, Douagi I, Bartuma H, et al. Identification of cell surface markers and establishment of monolayer differentiation to retinal pigment epithelial cells. Nature communications. 2020;11(1):1609.44. Qiu G, Seiler MJ, Thomas BB, Wu K, Radosevich M, Sadda SR. Revisiting nestin expression in retinal progenitor cells in vitro and after transplantation in vivo. Experimental eye research. 2007;84(6):1047-59.45. Liu Z, Li Y, Cui Y, Roberts C, Lu M, Wilhelmsson U, et al. Beneficial effects of gfap/vimentin reactive astrocytes for axonal remodeling and motor behavioral recovery in mice after stroke. Glia. 2014;62(12):2022-33.46. Qu L, Gao L, Xu H, Duan P, Zeng Y, Liu Y, et al. Combined transplantation of human mesenchymal stem cells and human retinal progenitor cells into the subretinal space of RCS rats. Scientific reports. 2017;7(1):199.47. Al-Nawaiseh S, Thieltges F, Liu Z, Strack C, Brinken R, Braun N, et al. A Step by Step Protocol for Subretinal Surgery in Rabbits. Journal of visualized experiments : JoVE. 2016(115).48. Gandhi JK, Mano F, Iezzi R, Jr., LoBue SA, Holman BH, Fautsch MP, et al. Fibrin hydrogels are safe, degradable scaffolds for sub-retinal implantation. PloS one. 2020;15(1):e0227641.49. Gandhi JK, Manzar Z, Bachman LA, Andrews-Pfannkoch C, Knudsen T, Hill M, et al. Fibrin hydrogels as a xenofree and rapidly degradable support for transplantation of retinal pigment epithelium monolayers. Acta biomaterialia. 2018;67:134-46.50. Liu Z, Parikh BH, Tan QSW, Wong DSL, Ong KH, Yu W, et al. Surgical Transplantation of Human RPE Stem Cell-Derived RPE Monolayers into Non-Human Primates with Immunosuppression. Stem cell reports. 2021;16(2):237-51.51. Fernandes RAB, Stefanini FR, Falabella P, Koss MJ, Wells T, Diniz B, et al. Development of a new tissue injector for subretinal transplantation of human embryonic stem cell derived retinal pigmented epithelium. International journal of retina and vitreous. 2017;3:41.

Supplementary Figure 1. Position of the 23-gauge (G) trocars, which were inserted 2.5-3 mm from the limbus.

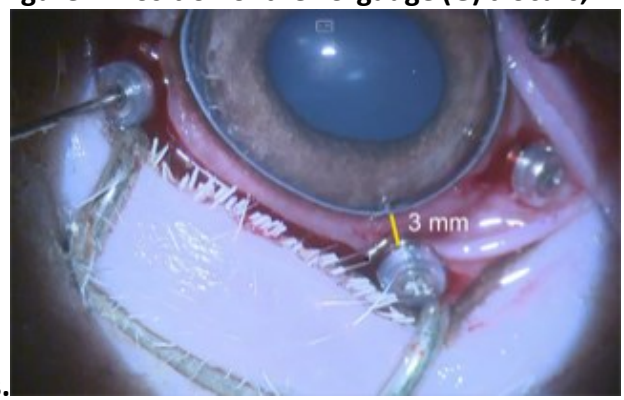

Journal of Visualized Experiments

Subretinal implantation of RPE on a carrier in minipigs: Guidelines for preoperative preparations, surgical technique and postoperative care

--Manuscript Draft--

Article Type:	Invited Methods Article - Author Produced Video
Manuscript Number:	
Full Title:	Subretinal implantation of RPE on a carrier in minipigs: Guidelines for preoperative preparations, surgical technique and postoperative care
Corresponding Author:	Lyubomyr M. Lytvynchuk, PhD, MD Justus Liebig Universität Giessen Fachbereich Medizin: Justus Liebig Universitat Giessen Fachbereich Medizin Gießen , Hessen GERMANY
Corresponding Author's Institution:	Justus Liebig Universität Giessen Fachbereich Medizin: Justus Liebig Universitat Giessen Fachbereich Medizin
Corresponding Author E-Mail:	Lyubomyr.Lytvynchuk@augen.med.uni-giessen.de
Order of Authors:	Lyubomyr M. Lytvynchuk, PhD, MD
	Zbynek Stranak
	Hana Studenovska
	David Rais
	Štěpán Popelka
	Lucie Tichotová
	Yaroslav Nemesh
	Anna Brymová
	Zdeňka Ellederová
	Jana Čížková
	Jana Juhásová
	Štefan Juhás
	Pavla Jendelová
	Richárd Nagymihály
	Igor Kozak
	Slaven Erceg
	Susanne Binder
	Brigitte Müller
	Knut Stieger
	Jan Motlik
	Goran Petrovski
	Taras Ardan
Additional Information:	
Question	Response
Please specify the section of the submitted manuscript.	Bioengineering

Subretinal implantation of RPE on a carrier in minipigs: Guidelines for preoperative preparations, surgical technique and postoperative care

Lyubomyr M. Lytvynchuk[1,2]*, Zbyněk Straňák[3]*, Hana Studenovska[4], David Rais[4], Štěpán Popelka[4], Lucie Tichotová[5], Yaroslav Nemesh[5], Anna Brymová[5], Zdeňka Ellederová[5], Jana Čížková[5], Jana Juhásová[5], Štefan Juhás[5], Pavla Jendelová[6], Richárd Nagymihály[7], Igor Kozak[8], Slaven Erceg[9], Susanne Binder[10], Brigitte Müller[1], Knut Stieger[1], Jan Motlik[5], Goran Petrovski[7]**, Taras Ardan[5]**

[1]Department of Ophthalmology, Justus-Liebig-University Giessen, Eye Clinic, University Hospital Giessen and Marburg GmbH, Friedrichstrasse 18, 35392 Giessen, Germany

[2]Karl Landsteiner Institute for Retinal Research and Imaging, Juchgasse 25, 1030 Vienna, Austria

[3]Department of Ophthalmology, University Hospital Kralovske Vinohrady and Third Faculty of Medicine, Charles University in Prague, Czech Republic.

[4]Institute of Macromolecular Chemistry, Czech Academy of Sciences, Prague, Czech Republic.

[5]Institute of Animal Physiology and Genetics, Czech Academy of Sciences, Liběchov, Czech Republic. [6]Institute of Experimental Medicine, Academy of Sciences of the Czech Republic, Prague, Czech Republic.

[7]Center for Eye Research, Department of Ophthalmology, Oslo University Hospital and Institute of Clinical Medicine, Faculty of Medicine, University of Oslo, Oslo, Norway

[8]Moorfields Eye Hospitals UAE, Abu Dhabi, United Arab Emirates

[9]Stem Cell Therapies in Neurodegenerative Diseases Lab, Research Center “Principe Felipe”, Valencia, Spain

[10]Department of Ophthalmology, Sigmund Freud University, Eye Center Donaustadt, Vienna, Austria

Lyubomyr Lytvynchuk MD, PhD: Lyubomyr.Lytvynchuk@augen.med.uni-giessen.de

Zbynek Stranak MD: zbynek.stranak@fnkv.cz

Hana Studenovska PhD: studenovska@imc.cas.cz

David Rais: rais@imc.cas.cz

Štěpán Popelka: popelkast@centrum.cz>

Lucie Tichotová: tichotova@iapg.cas.cz

Yaroslav Nemesh: nemesh@iapg.cas.cz

Anna Brymová: brymova@iapg.cas.cz

Zdeňka Ellederová: ellederova@iapg.cas.cz

Jana Čížková: cizkova@iapg.cas.cz

Jana Juhásová: juhasova@iapg.cas.cz

Štefan Juhás: juhas@iapg.cas.cz

Pavla Jendelová: pavla.jendelova@iem.cas.cz

Richárd Nagymihály: enmihaly@gmail.com

Igor Kozak: igor.kozak@moorfields.ae

Slaven Erceg: serceg@cipf.es

Susanne Binder Prof: susanne@susannebinder.com

Brigitte Müller PhD: Brigitte.Mueller@augen.med.uni-giessen.de

Knut Stieger DVM, PhD, Prof.: Knut.Stieger@uniklinikum-giessen.de

Jan Motlik Prof.: Motlik@iapg.cas.cz

Goran Petrovski MD, PhD, Prof.: goran.petrovski@medisin.uio.no

Taras Ardan MD, PhD: Ardan@iapg.cas.cz

Corresponding author:

Lyubomyr M. Lytvynchuk MD, PhD. E-mail: Lyubomyr.Lytvynchuk@augen.med.uni-giessen.de

Department of Ophthalmology, Justus Liebig University, University Hospital Giessen and Marburg GmbH, Friedrichstr. 18, 35392 Gießen, Germany. Telefon: +49 641 985-43801. Telefax: +49 641 985-43809

E-mail: Lyubomyr.Lytvynchuk@augen.med.uni-giessen.de

*, ** - These authors contributed equally to this work.

SUMMARY:

Subretinal implantation of retinal pigmented epithelium (RPE) belongs to the most promising approaches in the treatment of degenerative retinal diseases. However, performance of preclinical studies on large eye animal models remains challenging. This report presents the guidelines for subretinal transplantation of RPE on a cell carrier in minipigs.

Abstract

Degenerative disorders of the retina (including age-related macular degeneration), which originate primarily at or within the retinal pigmented epithelial (RPE) layer, lead to a progressive disorganization of the retinal anatomy and deterioration of the visual function. Substitution of damaged RPE cells with *ex vivo* cultured RPE cells using a subretinal cell carrier has shown potential to re-establish the anatomical structure of the outer retinal layers, and is therefore being further studied. We hereby present the principles of the surgical technique, which allows for effective subretinal transplantation of a cell carrier with cultivated RPEs into minipigs. The study protocol adhered to the statement of the Association for Research in Vision and Ophthalmology (ARVO) for use of animals in ophthalmic and vision research. The surgeries were performed under general anaesthesia and included standard lens-sparing three-port pars plana vitrectomy (PPV), subretinal application of balanced salt solution (BSS), 2.7 mm retinotomy, implantation of nanofibrous cell carrier into the subretinal space through additional 3.0 mm sclerotomy, fluid-air exchange (FAX), silicone oil tamponade and closure of all sclerotomies. This surgical approach was used in 29 surgeries (18 animals) over the past 8 years with a success rate of 93,1%. Anatomic verification of the surgical placement was carried out by in *vivo* fundus imaging (fundus photography and optical coherence tomography). The recommended surgical steps for subretinal implantation of RPEs on a carrier in minipig eyes could be applied in future preclinical studies using large eye animal models.

Keywords: age-related macular degeneration, retinal pigmented epithelium (RPE), large eye animal model, minipigs, pars plana vitrectomy (PPV), cell carrier, *in vivo* surgery, preoperative and postoperative care.

Introduction

Age-related macular degeneration (AMD) is considered to be the main cause of central visual loss in developed countries and belongs to the many conditions related to retinal pigmented epithelium (RPE) dysfunction [1,2]. RPE is located on the basal membrane called Bruch's membrane (BM) and provides necessary maintenance for the photoreceptors. The progressive degeneration of the RPE layer is a hallmark of the atrophic, early form of AMD. However, it accompanies the development of an exudative, late form of AMD as well. Despite many advances in therapy for retinal diseases, the development of an effective treatment modality remains challenging [3]. One of the promising methods is RPE replacement by an *ex vivo* cultured RPE layer, particularly due to the progress in stem cells research using human embryonic stem cells (hESC-RPE) and induced pluripotent stem cells (iPSC-RPE) [3,4,5,6,7]. In recent years, many research groups have focused on developing different approaches for RPE replacement with initially accepted proof-of-concept [8-15]. The RPEs have usually been delivered into the subretinal space in the form of a cell suspension, a self-supporting cell sheet, or a cell monolayer supported by an artificial carrier [3]. Injection of a cell suspension is the easiest way, but the compromised condition of the BM can often lead to inability of the transplanted cells to attach to it. This can result in the incorrect apicobasal orientation of the RPEs and failure to form a monolayer [16]. The main advantage of the other two methods - a self-supporting cell sheet and a cell monolayer supported by an artificial substrate, is that the cells are found in a differentiated monolayer state when implanted directly into the subretinal space.

Many surgical techniques aiming at delivery of a cell carrier into the subretinal space have been published in recent years [8-15]. In these studies, different approaches have been used including a type of large eye animal model, a type of cellular carrier, transplanted cellular culture, implantation instruments, as well as a surgical technique. The authors focused their reports mainly on the results of subretinal implantation. In 2015, Popelka et al. reported the use of frame-supported ultrathin electrospun polymer membrane for transplantation of RPEs into a large eye animal model - porcine cadaver eyes [8,9]. The surgical technique with subretinal

implantation of the cell carrier allowed for relatively precise handling of the carrier and easy positioning of the scaffold into the subretinal space. In this report, the feasibility of the delivery technique of a carrier with an approximate size of 2x5 mm was assessed in porcine eyes. The unique design of the cell carrier permitted its correct placement, preventing the cellular monolayer from folding and wrinkling[6]. Al-Nawaiseh et al. first presented detailed step-by-step guidelines for subretinal scaffold implantation in rabbits [17]. As published previously, transplantation of a differentiated and polarized RPE monolayer on a solid carrier resulted in improved survival and better integration of the graft in comparison to other delivery techniques [4,18,19].

The purpose of any preclinical animal studies which are performed *in vivo*, is to reveal the different aspects of transvitreal subretinal implantation of a cell carrier accomplished by a surgical procedure with focus on the safety of this procedure, the survival of the transplanted cells, the tissue response to the subretinal manoeuvres, and the short- and long-postoperative outcomes. The use of the porcine eyes as a large eye animal model has been reported to be relevant in the scope of obtained data, which could be useful and potentially applicable to humans [10,11,14]. Our study aims at reporting the principles of the surgical technique used for *in vivo* subretinal implantation of a cell carrier in a large animal model. We present a detailed description of preoperative preparation, the surgical technique of subretinal cell carrier implantation and postoperative care of the eye of minipigs, which is based on our experience over the last eight years. We aimed to describe the basic principles of the surgical approach that could be used for *in vivo* experimental studies with implantation of different types of cells and cell carriers.

Protocol: Principles of surgical approach during subretinal transplantation of cells on a carrier into minipigs

Ethical statement

All experiments were carried out according to the guidelines for the care and use of experimental animals and according to the statement of the Association for Research in Vision and Ophthalmology (ARVO) for use of animals in ophthalmic and visual research. The study protocol was approved by the Resort Professional Commission of the CAS for Approval of Projects of Experiments on Animals at the Institute of Animal Physiology and Genetics of the

Academy of Sciences of the Czech Republic (Liběchov, Czech Republic) (Approved protocol No. 60/2016 and 64/2019).

1. Large eye animal model

1.1. Animals

The Liběchov minipigs 12–36 months old of both sexes, 40-80 kg of body weight (BW) (Institute of Animal Physiology and Genetics, Czech Academy of Sciences, Liběchov, Czech Republic) were used for this study. The experimental herd of Liběchov minipigs was founded by the importing of 5 animals of the Hormel strain from the USA in 1967. These animals were crossbred for porcine blood group studies with several other breeds or strains: Landrace, Large White, Cornwall, Vietnamese pigs, and miniature pigs of the Gottingen origin [20,21]. At 5 months of age and approximately 20 kg of BW, these minipigs reach sexual maturity. Survival of parental minipig breeds (Hormel and Göttingen) has been reported to be 12-20 years. Minipigs were held indoors in a specialized facility in an air-conditioned animal house with temperatures between 18 - 22 °C, exposure to artificial 13/11 light/dark regime, in standardized individual pens with free access to water and feeding twice daily.

The retina of the minipigs lacks the macula and fovea. However, it has an area of highly concentrated zones of cone photoreceptors, which are called *area centralis* and *visual streaks* [22, 23]. These regions are responsible for the highest visual acuity. For this reason, during subretinal implantation of the cell carrier, we aimed to target the central portion of the retina.

For surgical orientation and drawing of the fundus schemes, the retina of the minipigs was schematically divided by a vertical line into temporal (from the optic disc toward the ear), nasal (from the optic disc toward the pig's snout), and central (between major retinal vessels on the nasal side) region (Fig. 1A, B). For implantation surgery, only healthy animals without any signs of injuries or diseases were selected.

All medications, which were used in minipigs, are listed in Supplemental file 1.

[Place **Figure 1** here].

1.2. Preoperative immunosuppression

Survival of the donor cells - human RPEs, during xenogeneic transplantation into the minipig eye was facilitated by a tacrolimus immunosuppressive therapy of the recipient animals. The immunosuppressive therapy was administered by subcutaneous injection of tacrolimus-eluting polymer microspheres (Prograf®, Astellas Pharma, Deerfield, Illinois, USA), which were successfully used in rats modified by Dr. Ardan for the purposes of this study [24]. We used immunosuppression six days prior to eye surgery and only once at a time. Tacrolimus was injected subcutaneously as a depot in a dose of 0.25mg/kg BW to hamper cell grafts rejection.

1.3. Anaesthesia and mydriasis

General anaesthesia of minipigs was induced by intramuscular injection of the mixture consisting of Tiletamine (2 mg/kg), Zolazepam (2 mg/kg), Ketamine (2 mg/kg) and Xylazine (0.4 mg/kg) - TKX. After induction of the sedation, the animals were moved to the operating room. We introduced ear vein cannulas, and the animals were intubated for inhalation maintenance of anaesthesia (Isoflurane 1.5%) by Wato EX-65 anaesthesia machine equipped with Mindray iMEC10 patient monitor (Mindray, Shenzen, China) (Fig. 2A, B). During eye surgery, intramuscular injections of Eficur 1ml/16kg BW and Depo-Medrol 120mg were applied, and the physiological body temperature of the minipig was maintained by an isothermal foil. When the surgery was finished, isoflurane was turned off, and after starting spontaneous breathing and awakening, the animals were extubated and transferred into the pens.

For local anaesthesia a proparacaine hydrochloride ophthalmic solution of 0.5% was administered into the conjunctival sac.

For induction of peri- and intra-operative mydriasis, eyedrops of 1% tropicamide solution and solution of 10% phenylephrine hydrochloride were applied, respectively, three times within 15 minutes into the conjunctival sac of the minipigs.

[Place **Figure 2** here].

1.4. Intraoperative animal posture and setting of the operating room

Sedated animals were transported into the operating room on a lift trolley (Fig. 2A). Then the animal was placed onto the operating table on the left side to enable surgery on the

right eye (Fig. 2B). Adjustment of the animal head's posture was performed to achieve the most suitable position of the central retina for implantation at (horizontal and parallel to the floor) (Fig. 2C). For this purpose, styrofoam pads were used. They were placed under the minipig's snout facilitating a stable position of the head.

The operating room setting was arranged according to the needs of the surgery on the eyes of the large eye animal model (Fig. 3A, B). Additionally, the height of the sitting chairs of the surgeons, as well as the height of the microscope was adjusted to achieve a comfortable position for the surgeons and in regards to the position of the pig's snout.

[Place **Figure 3** here].

1.5. Postoperative care

For the postoperative eye care, topical Ophtalmo-Framycoin ointment (Bacitracinzinc/hydrocortisoneacetate/neomycin sulfate) or Floxal ophthalmic ointment (0.3% Ofloxacin) was applied into the conjunctival sac of animals 5 times per day. For systemic postoperative care, the following antibiotics were used: 1) Eficur (Ceftiofur) was repeatedly injected 24 and 48 hours after surgery; 2) after 72 hours the animals were injected with Draxxin (Tulathromycin) 1ml/40 kg BW for prevention of secondary bacterial infection. Postoperatively, the following parameters of the eye were checked: turgor of the soft tissues of the eye, inflammatory reaction on the eye surface, squinting as a protective reaction of the eyelids. The minipigs were held indoors in a specialized facility in an air-conditioned facility with a temperature range of +18 - +22 °C, and an artificial 13/11 hours light/dark regime. The animals had free access to water and standard feeding (twice a day).

1.6. Euthanasia

Animals were sacrificed by exsanguination in deep general anaesthesia 7, 14, 28, and 42 days after cell graft implantation. Briefly, minipigs were firstly sedated by intramuscular injection of TKX mixture followed by intravenous bolus application of 1% Propofol (20 ml/animal) finished by exsanguination. The eyes were enucleated *post mortem* by experienced personnel using surgical scissors and surgical forceps.

All pharmaceuticals, which were used for local and systemic anaesthesia, mydriasis, postoperative anti-inflammatory care and euthanasia are listed in Supplemental file 1.

2. Cell carrier, cultivated cells cultures and implantation injector

2.1. Cell carrier

Ultrathin nanofibrous carriers were prepared by electrospinning of a poly (L-lactide-co-DL-lactide) (LLA/DLLA 90/10, Mw 868 270 g/mol, PDI 2.3). The thin nanofibrous membrane was reinforced with a peripheral frame that was embedded in the membrane during electrospinning following the procedure published before (Fig. 4A, B) [8]. The diameter of the bead-free fibers was 380 nm (standard deviation (SD) 10 nm) and the average pore size of the membrane was 0.4 µm (SD 0.2 µm). The membrane was 3.7 µm in thickness and its porosity was estimated to be 72% [25].

The supporting frames were cut from a bi-axially oriented poly-ethylene-terephthalate (PET) foil 36 µm in thickness using a laboratory assembled femtosecond microfabrication station. The sheets of the membrane were fixed to the body of commercial cell culture insert Falcon (Corning Inc., Kenneburg, ME, USA) to facilitate the seeding and growth of the cells. Samples were air-plasma treated for 30 seconds at the power of 7 Watt before RPE cultivation. The carriers 5.2 mm x 2.1 mm with an adherent sheet of RPE cells were cut using a shaped biopsy punch.

[Place **Figure 4** here].

2.2. Cell cultures used for cultivation on the cell carrier

For this case series, the following cell carriers were used: 1) nanofibrous cell carriers without any cells (2 cases); 2) nanofibrous cell carriers with primary human RPEs (hRPEs) (13 cases); 3) nanofibrous cell carriers with human iPSC-derived RPE cells (14 cases).

Primary hRPEs were isolated from human donor eyes according to previously reported technique [26]. The cells were obtained by enzymatic treatment of the retina for 30 minutes (TrypLE, Gibco®, Thermo Fisher Scientific, MA, USA). Then the primary hRPE cells (passage 0) were cultured for up to two weeks in DMEM/F12 (Gibco) supplemented with 10% fetal bovine serum (FBS). Once the cell cultures reached confluency, the medium was changed to 1% FBS and cultured for additional 30 days. The primary hRPEs were then seeded into trans-well plates and onto the nanofibrous cell carrier. Following further 30 days of incubation

in 1% FBS, the cell carriers with primary hRPEs were used for subretinal implantation into minipigs.

Human iPSC-derived RPEs used in the present study included previously generated hiPSCs derived from MERTK associated retinitis pigmentosa patient-derived fibroblasts [27] that were gene-corrected in two alleles using the CRISPR/Cas9 system (RP1-FiPS4F1-GC2) [28], and hiPSCs derived from a healthy subject fibroblast (Ctrl2-FiPS5F2) [29] that were used as a control. Both hiPSCs cell lines were generated and subsequently differentiated towards RPE cells (hiPSC-RPE) as reported previously [30]. The hiPSC-RPE were plated at 200,000 cells/cm^2 on laminin (BioLamina #LN521)-coated transwell inserts with nanofibrous membranes of poly(L-lactide-co-DL-lactide) with oval implantation frame in RPE medium containing knockout DMEM, 20% knockout serum, Glutamax 2 mM (Invitrogen, Carlsbad, CA, USA), 0.1 mM non-essential amino acids, 0.23 mM β-mercaptoethanol (TermoFisher, MA, USA), 100 U/mL penicillin, 0.1 mg/mL streptomycin, and 10mM nicotinamide (Sigma-Aldrich, San Luis, Mi, USA). The medium was changed every other day, and the hiPSC-RPE were cultured for two months prior to the implantation to encourage polarized growth.

2.3. Implantation injector

The implantation injector consisted of a rectangular plastic capillary and a stainless-steel blade plunger (Fig.5A, B). The plastic capillary was fabricated by the blow molding process from a tube. The length of the plastic capillary was 6 cm. The outer dimensions of the distal part of the injector were 0.8x2.8 mm. The carrier was loaded into the injector through a loading window located 6 mm from the distal end of the capillary and later ejected into the subretinal space by a push of the plunger (Fig. 5B).

Protocol for the preparation of the nanofibrous carrier and loading of the injector

Step-by-step protocol for the preparation of the nanofibrous carrier and loading the injector is presented in Video 1.

1) The nanofibrous membrane is fixed to the insert and equipped with an oval frame for better manipulation. Side orientation marks at the frame should be checked first to detect the top side of the carrier where the cells are found.
2) A small Petri dish is filled up with 2ml of phosphate buffered saline (PBS). An insert is taken out and placed in the centre under the light microscope. A custom modified punch is used to cut the carrier around the oval frame using a microscope. A carrier has a dimension of 2 x 5 mm.

3) For loading the carrier, a custom-made injector with flat transparent tubing is used; 6 mm from the distal end of the capillary, there is a window for loading the carrier. The window is filled up with PBS.
4) After cutting the carrier from the insert against a semi-soft polystyrene dish, the sample is being stuck at the bottom of the dish. An oval frame facilitates manipulation of the carrier. Using forceps, the sample is then released from the bottom, lifted up from the liquid, and transported to the window of the injector.
5) Using a dental probe, the carrier is positioned in the window of the injector, and the plunger is used to push the carrier into the closed, safe upper part of the injector. The carrier is then prepared for surgery.
6) The nanofibrous carrier can be easily unloaded from the injector by pushing a metal plunger. At each step, the side orientation of the carrier should be checked.

[Place **Figure 5** here].

3. Surgical procedure

3.1. Surgical equipment

During all surgeries the following surgical equipment was used:

1) Ophthalmic surgery microscope Hi-R NEO 900A (Haag-Streit Surgical, Wedel, Germany);
2) An operating system for surgeries on anterior and posterior eye segment R-Evolution CR (Optikon, Rome, Italy);
3) Non-contact vitreoretinal surgical system MERLIN BIOM (Volk, Mentor, OH, USA);
4) Frequency-doubled solid-state laser photocoagulator: green laser for photocoagulation with slit lamp adapter, ophthalmoscope, and endo probe Merilas 532α (Meridian, Thun, Switzerland);
5) Full HD medical 2-piece camera Sony PMW-10MD (Sony, Tokyo, Japan).

Standard parameters used during vitrectomy, exo- and endo-cautery, and laser photocoagulation are depicted in Table 1.

3.2. Surgical instruments

The reusable surgical instruments were sterilized with a mobile autoclave steam sterilizer 3870 HSG (Tuttnauer Europe B.V., Breda, NL) according to a standard protocol. Single-use

surgical instruments and materials, which were used during the surgery are listed in the Table of Materials.

3.3. Description of the surgical steps

The surgeries were performed by four experienced vitreoretinal surgeons (LL, GP, ZS, IK) with the assistance of an experienced surgical facility assistant (TA). Before the *in vivo* experiments, the surgeons were educated and obtained special knowledge on the minipig's eye anatomy. In all cases, the surgery was performed in general anaesthesia in a specially organized operating room with the implementation of standard aseptic and antiseptic measurements. The standard surgical procedure is shown in Video 2.

Step by step protocol of the surgical procedure:

Preparation

1) Approach the operating table with an upper position of the surgeon and the side position of the assistant (Fig. 3).
2) Disinfect the conjunctival sac with 5% Povidone-Iodine solution for 5 min.
3) Disinfect the periorbital area of the skin with 10% Povidone-Iodine solution and wait until it dries.
4) Cover the operating field with the eye in the middle using a standard sterile ophthalmic drape with sticky transparent foil trying to remove the eye lashes away from the eye globe (avoid cutting the eye lashes to reduce the risk of postoperative endophthalmitis).
5) Insert the eye speculum (Liberman-type or Cook eye speculum).
6) Fixate the nictitating membrane to the skin with 8-0 Vicryl (optional).
7) Open the conjunctiva on the temporary side 2 to 3 mm from the limbus (Video 2).
8) Insert three valved trocars 2.5-3 mm from the limbus. Use rotating movements during the insertion in a slightly oblique manner (100º-110º) toward the posterior retina and hold the trocar with the forceps (Fig. 6).
9) Cover the cornea with methylcellulose.

Pars plana vitrectomy (PPV)

10) Perform core PPV centrally and toward the periphery at the site of the upcoming large sclerotomy.
11) Carry out triamcinolone acetonide (TA)-assisted posterior vitreous detachment and removal.
12) Perform subretinal injection of BSS with 25/41G cannula more centrally avoiding the formation of the bleb toward the periphery.
13) Perform linear endodiathermy of the retina with 27G endodiathermy probe 3 mm large near the temporal bleb base.
14) Consequently, perform retinotomy 3 mm large with a 25G MVR blade under elevated intraocular pressure (IOP) setting of the irrigation system up to 60 mmHg. Wait 3-4 minutes to ensure that there is no bleeding from the retinotomy, then reduce the IOP to 25 mmHg.

15) Carry out bipolar exodiathermy of episcleral vessels between the two nasal trocars 2.5-3 mm from the limbus.
16) Perform 3.0 mm sclerotomy 2.5 mm from limbus with 2.75mm phaco knife.
17) Exodiathermy of the possible bleeding of the scleral vessels and ciliary body inside the sclerotomy. Enlarge the sclerotomy to 3.0 mm with the satin knife, which will accommodate the tip of the injector sized 0.8x2.8 mm.
18) Perform vitrectomy in case of the prolapsed vitreous body on the site of large sclerotomy.

Implantation of the cell carrier

19) Insert gently the injector with the dominating hand through the large sclerotomy. In case of resistance, enlarge the size of the sclerotomy.
20) Implant the cell carrier through the retinotomy into the subretinal space. During this step, the use of a bimanual technique with additional sclerotomy and chandelier light can assist the implantation during the learning phase of the surgeon.
21) Withdraw the injector and close the large sclerotomy with an 8-0 Vicryl suture.
22) Perform fluid-air exchange (FAX) and drainage of the subretinal fluid with silicone tipped cannula.
23) Direct injection of silicone oil (1000 cSt) shall be carried out until the IOP raises to normal.

Ending of the surgery

24) Close the three sclerotomies and the conjunctiva with 8-0 Vicryl suture.
25) Rinse the conjunctival sac with 3% Povidone-Iodine solution.
26) Subconjunctival injection of gentamicin 20 mg, dexamethasone 2 mg and xylocaine 2% 0.3 ml.
27) Check the condition of the fundus and lens.
28) Remove suture from the nictitating membrane (optional).
29) Apply Ophtalmo-Framycoin ointment or Floxal ophthalmic ointment into the conjunctival sac.

Intraoperative imaging and documentation

30) Perform video recording during the entire surgery with photo documentation of the key steps of implantation.
31) Complete the fundus drawing by documenting the place of sclerotomies, retinotomy, subretinal implant and any complications that occurred.

[Place **Figure 6** here].

4. Postoperative ophthalmic examinations

4.1. General ophthalmic examination

In the postoperative period, the eyes were inspected with an indirect ophthalmoscope for the presence of inflammation such as redness, tissue swelling, mucus congestion in the conjunctival sac. Intraocular pressure in the operated eye was measured using palpation.

Postoperative imaging. In the postoperative period, colour fundus images were taken with colour non-mydriatic fundus camera iCam (Optovue, Fremont, CA, USA). It allowed documenting the anterior segment, retina, and the optic disc. Additionally, iCam enabled red-free imaging of the retina. Optical coherence tomography (OCT) examination was performed using the OCT system iVue (Optovue, Fremont, CA, USA).

During the examination by OCT and fundus photography, the sedation of the minipigs was induced by intramuscular injection of TKX mixture.

For postoperative imaging, the eyedrops Unitropic (1% Tropicamide) and Neosynephrin (10% Phenylephrine Hydrochloride) were instilled into the conjunctival sac of the minipigs in order to induce mydriasis. A lid speculum was employed in order to maintain the eye opened (Chirana, Prague, Czech Republic). For moisturizing the eye surface and for obtaining a clear OCT image, the cornea of the animals was washed with saline solution (NaCl 0.9%) every 30-60 seconds.

The minipig was positioned onto the operating table in the same manner as during the operation (Fig. 2B, C, 3A). The main requirement was to place the head on the side and perpendicular to the scanning piece of the OCT device. Styrofoam pads were used and placed under the animal's snout in order to stabilize the head, bringing the eye surface in a horizontal position. During OCT or fundus imaging, the minipig's head was tilted manually toward the OCT lenses or fundus camera lenses aiming to optimize the view of the posterior retina and the area of implantation (Fig. 2C). For optimal capturing of the implanted carrier on fundus images an infrared reflectance light of the OCT device was used to focus on the implant (Fig. 7B). OCT scanning was performed in crossline and retina map modes. At the end of the examination, Floxal ophthalmic ointment was applied under the lid of the animal's eye. Finally, the minipig was moved to the indoor facility and observed for its general condition until the end of the sedation.

5. Representative results of subretinal implantation in minipigs

The results of the subretinal implantation of the cell carrier in Liběchov minipigs are presented in Table 2. Successful implantation was defined in cases in which we could obtain sufficient data for histologic and immunohistochemical study. Failed cases were defined in

eyes with severe intraoperative complications, which made further observation of the eye tissues impossible.

Fundus imaging and SD-OCT. The minipigs were examined in the postoperative period applying fundus imaging, red-free imaging and SD-OCT (Fig. 7). The high quality of the fundus images was enabled by the clear optic media including clear lens and use of silicone oil tamponade (Fig. 7A). The site of the retinotomy showed no signs of proliferative reaction, and the PTE frame of the cell carrier was clearly visible through the semi-transparent layers of the porcine retina. On the red-free imaging, the reflectivity of the cultivated hRPEs cell on the carrier did not differ from the reflectivity of the endogenous porcine RPE layer (Fig. 7B). On SD-OCT, the PTE frame caused only minor shadowing of the underlying anatomical structures and slight thickening of the retina (Fig. 7C, red arrows). No atypical hypo- or hyper-reflective zones could be noticed on SD-OCT, and the Bruch's membrane appeared to remain undamaged as well. The cell carrier itself caused no significant increase in the entire retinal thickness. These findings suggested that the intraoperative iatrogenic impact of the implant was minimal, and the implantation of the cell carrier underwent sufficient adaptation of the implanted cells to the overlying photoreceptor cells and neuroretinal tissue.

[Place **Figure 7** here].

Histological and immunohistochemical analysis

After euthanasia of the animals, the whole minipig eyes were removed and fixed in 4% paraformaldehyde (PFA) for 24 h. The anterior part of the eye was removed and the implanted nanofibrous carrier was identified in the nasal central retina and isolated with the sclera attached. All tissues were cryoprotected in graded sucrose solutions and vertical frozen sections were cut as described in detail [31].

Figure 8 shows the haematoxylin-eosin (H&E) staining of the retinal area containing the implanted primary hRPE cells on a nanofibrous carrier (yellow arrow) in the minipig eye. The pigmented appearance of the implanted primary hRPEs formed a continuous, yet irregular pigmented layer (Fig. 8, red arrows). After longer observation periods (6 weeks), the neuroretina underneath the implants showed a rosette-like- or hypertrophic reaction-like-appearance around the retinotomy site likely as a result of the iatrogenic manipulation. These

morphologic results are comparable to the SD-OCT findings and support the evidence of the minimal impact of the carrier delivery onto the retinal tissue.

[Place **Figure 8** here].

Immunostaining was performed employing the two-step indirect method. Sections were incubated at room temperature overnight in monoclonal primary antibody CRALBP (Novus Biologicals UK, Abingdon, (B2) cat. no. NB100-74392) at a dilution of 1:100. Immunofluorescence was performed using Alexa Fluor 488-conjugated secondary antibody (#21202, Thermo Fisher Scientific, Germany).

The implanted primary hRPEs were present in the area of implantation and expressed the typical RPE marker CRALBP similar to the endogenous minipig RPE cells (Fig. 9A). In contrast, the morphology of the implanted cells appeared not to assume a monolayer shape after implantation, yet still localized within the defined subretinal space (Fig.9A, B white arrows).

[Place **Figure 9** here].

Ocular complications

In total, the rate of successfully performed operation was 93.1% (27/29 cases). Reduced transparency of the optical media impacted the postoperative imaging in 13.7% (4 cases), yet these eyes were processed with further histologic and immunohistochemical analysis.

Intraoperative peripheral retinal detachment occurred in four cases (13.8%). In two cases it was managed by aspiration of subretinal fluid during fluid-gas exchange and application of endolaser photocoagulation of the retina in the area of detachment. In other two cases (6.9%), the retinal detachment was associated with massive retinal and subretinal bleeding, which made implantation of the cell carrier impossible and led to the termination of the surgery and immediate euthanasia of the minipig on the operating table.

Discussion

Subretinal implantation of RPE cells of different origin belongs to the most promising modern and developing trends in eye research, which aims to treat retinal degenerative disorders, such as AMD [3,4,8-15,17]. The main idea of this approach is to substitute the damaged RPEs with new healthy RPEs cultured *ex vivo* [32-36]. Subretinal implantation of cell carriers with cultivated RPE cells of different origin remains the most reasonable approach, as the porous membranes maintain the polarized RPE cell layer in the correct orientation with regard to the photosensory layer.

Currently, a number of animal models have been used to develop the surgical technique and to prove the concept of substitutional therapy of retinal diseases associated with RPE degeneration [8-15,17]. Rabbits, pigs, dogs and non-human primates belong to the most frequently used big eye animal models [37].

Large eye animal model on miniature pigs. The choice of a large eye animal model of minipigs for experimental studies with subretinal implantation of a cell carrier to develop an effective treatment approach for retinal degenerative disorders in humans has some potential advantages. In 2005, Vodička et al. reported the advantages of the use of the miniature pig as an animal model for biomedical research based on their experience with the animal model of Liběchov minipig [21]. Among numerous indications the authors described the importance of the miniature pig model for current biomedical research in the field of neurodegenerative diseases, such as Parkinson's or Huntington's disease [38,39]. It appeared that miniature pigs possess a relatively large brain with a blood supply and immunologic response, which are similar to those in humans. The pig model could be also a valuable animal model for allogenic transplantation experiments [40,41]. The authors summarized that due to human-like physiology the miniature pigs should be considered as a first-choice animal model, which can ensure a highly relevant experimental data for human-related therapeutic research. Additionally, this kind of species appeared to be non-expensive and simpler to keep in controlled condition compared to other non-human primates.

In 2018, Shrader and Greentree published a detailed description of Göttingen minipigs used for ocular research, which have been used since the 1960s in biomedical research including ocular studies due to their handling simplicity, reasonable size, well-monitored genetic processes and similar to human anatomy of the eye [42]. The authors pointed out that pig as a model in many research projects is replacing dogs and non-human primates for preclinical studies. Göttingen minipigs have been used for different kinds of studies, including

efficacy and safety of pharmaceuticals, development of surgical techniques, natural development and treatment of glaucoma, implantation techniques with new materials and intraocular devices. The animal model of minipigs enables to perform *in vivo* ophthalmologic examinations similar to humans (applanation tonometry, fundus imaging, OCT, fluorescein angiography, electroretinography, etc.). The human eye and the eye of the minipig have many anatomical and functional similarities, such as the size of the eye globe, magnifying properties of the eye (approximately 78 dioptres), volume and quality of the vitreous body, open visual field, binocular vision, colour vision. Even though the retina of the minipigs to the contrary to humans does not possess a macula and fovea, it contains so-called "area centralis" and "visual streaks" – the regions of the retina with a high concentration of cone photoreceptors [22]. All this is applicable to the Liběchov minipigs, as they were crossbred with several other breeds, including Gottingen minipigs [21]. For this reason, we consider a minipig model to be one of the most efficient and appropriate experimental big eye animal models for the development of new surgical techniques for subretinal implantation of the cell carrier to address the retinal degenerative diseases.

To the best of our knowledge, there is no standardized and widely accepted surgical technique developed for vitreoretinal intervention on big eye animal models as these studies are relatively new and their performance is associated with a wide range of ethical, logistic and financial issues. Nevertheless, there are a number of studies focusing on the progress in the field of subretinal delivery of a cell carrier in different animal models [8-15,17]. Popelka et al. in 2015 were the first to report the results of subretinal implantation of a novel frame-supported nanofibrous membrane as a scaffold for the porcine RPE cells in cadaver eyes of Liběchov minipigs [8]. These experiments and the surgical technique with custom made implantation injector were then improved and transferred to *in vivo* studies on minipigs. In the current study, the accurate acquisition of the well-defined and established preoperative-, surgical- and postoperative- care enabled to obtain reproducible data, which could be efficiently analyzed and demonstrated to certain extent the proof-of-concept of subretinal substitutional implantation of RPE cells.

Recently, Duarri et al. reported the results of subretinal injection of suspension of hiPSC-RPE cells in a swine model of geographic atrophy [43]. In our opinion, for RPE replacement and the right physiological function of implanted RPE cells of different origin, the correct polarization, namely right orientation of apical and basal parts of transplanted RPE is very

important. It might be difficult to reach a correct polarization of the RPE cells in the case of subretinal implantation of cellular suspension. However, the fact that the authors performed the experiments with the porcine model emphasizes the importance of the large eye animal model of the pigs in this field.

Nevertheless, one of the key points of cell replacement therapy is a challenging surgical technique with the risk of intraoperative and postoperative complications, which determine the success or failure of the whole transplantation process. The size and the site of the large sclerotomy and retinotomy shall be considered perioperatively. It can be linked to the risk of retinal detachment, hypotony, episcleral, choroidal and/or retinal bleeding, and high intraocular turbulence, which can lead to scaffold damage. Postoperatively, there is a risk of proliferative vitreoretinopathy, endophthalmitis, hypotony, retinal detachment, and cataract formation [10,13,14,15].

Surgical procedure. In 2012, Stanzel et al. reported a newly developed surgical technique, which was aimed to implant a cell carrier into the subretinal space as a model of therapeutic approach to treat degenerative retinal disorders. For their experiment, they used chinchilla bastard rabbits (BW 2-2.5 kg). The authors demonstrated the overall success rate of 74.2% in 23 cases (range between 70.6% and 78.6% in two subgroups) [13]. In our study, the success rate is reported to 93.1% in 29 operated cases.

In previous reports, the authors proposed a custom-made 23G infusion cannula with two side ports in order to redirect the jet stream, which helped to resolve collapse of the bleb and consequent retinal detachment [13]. During our surgeries, we did not notice any such collapse of the bleb. The possible reason for that could be the bigger size of the eyeball and performance of the core vitrectomy with spared vitreous on the periphery on the site of infusion cannula, which could reduce the force of the directed jet stream.

Difficulties during the ejection of the cell carrier from the instrument was one of the intraoperative obstacles noticed in the surgical series of Stanzel et al., which were categorized as “trapped with the instrument”. Additionally, the authors suggested that residual vitreous on the retinal surface could cause a backwards “jump” of the carrier out from the retinotomy orifice after implantation. This problem could be solved with enzyme-assisted vitrectomy, which enabled a smooth continuous ejection of the cell carrier into the subretinal space. In the majority of the cases, the authors repositioned the carrier to obtain a more distant location of the implant away from retinotomy [13]. In our case series, we also experienced a

situation when the cell carrier remained attached to the tip of the injector. However, that was managed by slow and gentle manipulation of the light pipe and the injector's tip. We observed no residual vitreous at the site of retinotomy in all of our cases. The use of TA-assisted PPV applied in our surgeries could be suggested as a factor to reduce the risk of residually attached vitreous. Multiple staining with TA may be necessary to remove the overlying vitreous completely. In this case scenario, the role of enzyme-assisted vitrectomy is debatable. We also did not reposition the implants away from the retinotomy site and tried to perform the implantation from the first attempt. It could be suggested that any additional manipulation of the retina or underneath the retina or extending of the area of retinal detachment could cause further iatrogenic complications, which will impact the timing and outcome of the surgical procedure on the very valuable and expensive large eye animal model of minipigs.

Stanzel et al. closed the sclerotomies with Vicryl 7-0 suture stating that the large suture-on floor plate appeared to be more efficient for the rabbit's thin sclera [13]. In our surgeries, we always used Vicryl 8-0 suture to close both sclerotomies and conjunctival wounds. The standard 3-2-2 single knot sutures were used. We did not observe any postoperative opening of the sclera.

In 2014, Stanzel et al. published the results of the subretinal implantation of human RPE stem cells, which were grown as polarized cellular monolayer on a polyester membrane in rabbits. During their experiments on sixty female chinchilla bastard rabbits, they used the same surgical technique described by Stanzel et al. in 2012 [13,16]. In their experiments, they applied a two-port PPV approach. Finally in 2016, Al-Nawaiseh et al. published a step-by-step protocol for subretinal implantation of cell carrier surgery in rabbits [17]. The study presents a very detailed and well repeatable description of the surgical procedure including preoperative- and postoperative- care, which is based on the previous experience as well.

In 2021, Liu et al. published the results of successful subretinal implantation of human stem cell-derived RPE monolayers in non-human primates. In this study, nine cynomolgus monkeys (Macaca fascicularis) were used as a big eye animal model [15]. During the experimental study, all animals underwent a systemic immunosuppression, which consisted of sirolimus (loading dose 2mg, daily dose 1mg) and tetracycline (7.5 mg/kg^{-} BW) starting seven days prior to the surgery and lasting three months after the surgery. In general, the surgical procedure was performed according to protocols described by Stanzel et al. in 2012 and Al-Nawaiseh et al. in 2016. In non-primates, the authors used a 25G three-port PPV

approach with chandelier endoillumination. Importantly, a TA-assisted PVD was applied to exclude residual vitreoretinal adhesion on the posterior retina. As an addition to the primary described procedure, the authors performed removal of the host RPE layer in the area of future implantation using a 20G custom made extendable loop instrument. The characteristics of the injector and the cell carrier remained the same as they were described earlier [16,17]. In our study, we have also performed a systemic immunosuppression of minipigs. However, the type of immunosuppression differed from the one described above. We administered subcutaneous injection of tacrolimus-eluting polymer microspheres as a depot in dose 0.25mg/kg BW to hamper cell grafts rejection and inflammatory reaction. We did not remove the host RPE cell layer during the surgery, as our primary aim was to analyze the safety of the procedure and the viability of implanted cells, but not their integration into the host retina.

Koss et al. reported in 2016 the safety and feasibility results of subretinal implantation of a monolayer of hESC-derived RPE on a foldable non-degradable mesh-supported submicron parylene-C membrane (6.25x3.5 mm, 0.4 µm thick) in 14 female Yucatán minipigs [10]. After the cultivation, passage three cells were seeded onto a mesh-supported membrane. Immunosuppression was performed using systemic administration of tacrolimus (no regime and dose indicated) and intravitreal injection of 0.7 mg dexamethasone implant (Ozurdex) at the end of the surgery. For anaesthesia, an intramuscular injection of Telazol (100 mg/ml) followed by inhalation of sevoflurane gas was used. PPV was performed with a 20G approach. The authors used intravitreal injection of TA (Triesence) for better visualization of the vitreous body. Intraocular pressure was elevated to 60 mmHg during retinomy to prevent bleeding. The large sclerotomy was 2 to 3 mm in size. After subretinal injection, the retina was flattened with temporary injection of perfluorocarbon liquid. After fluid-air exchange, a silicone oil tamponade (1000/5000 cSt) was performed. The sclerotomies were sutured with 6-0 Vicryl suture. Postoperative care included ocular application of dexamethasone/neomycin/polymyxin B ointment (Maxitrol) one week after the surgery. The authors reported a success rate of 91% in the operated cases, in which they could perform efficient subretinal implantation and obtain sufficient postoperative imaging data. In our study, intravitreal injection of TA crystals was used intraoperatively and mainly to visualize the vitreous body. However, the local immunosuppressive action of this drug remains unclear. Nanofibrous cell carriers used in our study were 5.2x2.1mm large, 3.7 µm thick with size of

pores of 0.4 µm. In eight cases, we used primary hRPEs from passage zero, which were cultivated onto the nanofibrous cell carrier. During the surgery, we performed direct FAX instead of injecting perfluorocarbon liquid as previously reported by others. To close the sclerotomies, we used 8-0 Vicryl, which appeared to be satisfactory. Our surgical success rate (93.1%) correlated and was slightly better than that obtained by Koss et al. [10]

In 2019, Gandhi et al. published a report in which they presented for the first time an *in situ* presentation of fully degradable cell carrier (scaffold) for subretinal implantation of different cell types as possible treatment modality for retinal degenerative diseases [14]. The study was mainly focused on the biodegradable characteristics of the fibrin hydrogel implant. Experiments included surgeries on the female domestic pigs (Yorkshire pigs). The authors discussed that aggressive immunosuppression used on the domestic pigs could inhibit a local inflammatory reaction potentially caused during the biodegradation of the fibrin hydrogel implant. However, they did not specify the immunosuppressive therapy used in the pigs. During PPV, Gandhi et al. performed a 3.6mm long sclerotomy for insertion of a subretinal implantation device parallel to and approximately 3.5 mm posterior to the limbus. Additionally, they used a pneumatic-driven injection system aiming to reduce hand-placement instability caused by finger manipulation [14]. In our case series, we performed all sclerotomies 2.5mm to 3.0mm from the limbus. The location of the pars plicata of the ciliary body and accordingly, the required distance from the limbus for sclerotomies was established on the section of cadaver pig eyes of the same BW minipigs, which was performed before every surgical session. The large sclerotomy for insertion of the injector was 3mm long. The implantation injector used in our study was operated by the hands of the surgeons. The removal of the vitreous body from inside in projection of the site of large sclerotomy shall be done thoroughly, as well as the removal of the prolapsed vitreous inside the large sclerotomy. Thorough cautery of the pars plana of the ciliary body and its sufficient cut inside the large sclerotomy appears to be crucial in avoiding intraoperative complications such as iatrogenic peripheral retinal detachment, bleeding and loss of the implant.

The implantation of a larger size cell carrier brings several drawbacks as well. One of the major considerations remains the range of immune response to the implanted cells due to immune-privilege of retinal tissues of the minipigs. To address this issue, we applied immunosuppressive therapy using one-time subcutaneous injection of depot tacrolimus. Another limitation of the surgical approach remains the size of the large sclerotomy. Gandhi

et al. performed 3.6 mm sclerotomy to implant the fibrin hydrogel implant [14]. Stanzel et al. applied custom made 20G implantation injector, which requires 20G sclerotomy [13]. In our study, we performed a large sclerotomy with the size of 3.0 mm. Ongoing improvements of the instrumentation for implantation could facilitate the reduction of required sclerotomy size for cell carrier implantation in future studies. The risk of intra- and post-operative complications, such as intraocular retinal/choroidal detachment, retinal bleeding, inflammation, lens opacification, proliferative vitreoretinopathy, could influence the study results. However, the strict adherence to study protocol established by the expert team (preparation, surgical technique and postoperative care), allowed us to minimize the rate of complications with a high success rate of 93.1 % in our cohort of operated animals.

In summary, we propose the big eye animal model of minipigs to be one of the most appropriate models for future application of novel concepts for treatment of retinal diseases due to their similarity to the human eye anatomy and physiology. These similarities allow to develop and improve the surgical techniques and instrumentation for subretinal implantation of cells, which could be transferred easily to the treatment of human eye disorders. It is important to assure that the surgeries on minipigs are performed with the same instrumentation (including implantation delivery tools), which would also be utilized in human surgeries, thus making the application of gained experience and know-how to humans without difficulties. Alternative big eye animal models (rabbits, non-human primates) with presence of macular area, such as non-human primates, could be useful to follow-up and analyze the anatomical and functional changes after subretinal implantation of a cell carrier to treat degenerative disorders in the central retinal area. The detailed description of the preoperative-, surgical- and postoperative- care procedures could be useful for future studies by increasing efficient and standardized data generation.

ACKNOWLEDGMENTS:

The project was supported by The Czech Science Foundation (Project Number 18-04393S), Norway Grants and Technology Agency of the Czech Republic (KAPPA Programme, Project Number TO01000107).

DISCLOSURES:

All authors have disclosed no conflicts of interest regarding the presented material.

References:

1. Pascolini, D., Mariotti, S.P. Global estimates of visual impairment: 2010. British Journal of Ophthalmology. 96 (5), 614–618, doi: 10.1136/bjophthalmol-2011-300539 (2011).
2. Bressler, N.M., Bressler, S.B., Fine, S.L. Age-related macular degeneration. Survey of ophthalmology. 32 (6), 375–413 (1988).
3. Binder, S., Stanzel, B.V., Krebs, I., Glittenberg, C. Transplantation of the RPE in AMD. Progress in retinal and eye research. 26 (5), 516–554, doi: 10.1016/j.preteyeres.2007.02.002 (2007).
4. Falkner-Radler, C.I. et al. Human retinal pigment epithelium (RPE) transplantation: outcome after autologous RPE-choroid sheet and RPE cell-suspension in a randomised clinical study. The British journal of ophthalmology. 95 (3), 370–375, doi: 10.1136/bjo.2009.176305 (2011).
5. Ramsden, C.M., Powner, M.B., Carr, A.-J.F., Smart, M.J.K., da Cruz, L., Coffey, P.J. Stem cells in retinal regeneration: past, present and future. Development (Cambridge, England). 140 (12), 2576–2585, doi: 10.1242/dev.092270 (2013).
6. Carr, A.-J.F., Smart, M.J.K., Ramsden, C.M., Powner, M.B., da Cruz, L., Coffey, P.J. Development of human embryonic stem cell therapies for age-related macular degeneration. Trends in neurosciences. 36 (7), 385–395, doi: 10.1016/j.tins.2013.03.006 (2013).
7. Tezel, T.H., Kaplan, H.J., Del Priore, L.V. Fate of human retinal pigment epithelial cells seeded onto layers of human Bruch's membrane. Investigative ophthalmology & visual science. 40 (2), 467–476 (1999).
8. Popelka, S. et al. A frame-supported ultrathin electrospun polymer membrane for transplantation of retinal pigment epithelial cells. Biomedical materials (Bristol, England). 10 (4), 045022, doi: 10.1088/1748-6041/10/4/045022 (2015).
9. Kozak, I. et al. Safety and feasibility of new nanofiber subretinal delivery system with injector for RPE cell transplantation. Investigative Ophthalmology & Visual Science. 59 (9), 5670–5670 (2018).
10. Koss, M.J. et al. Subretinal implantation of a monolayer of human embryonic stem cell-derived retinal pigment epithelium: a feasibility and safety study in Yucatan minipigs. Graefe's archive for clinical and experimental ophthalmology = Albrecht von Graefes Archiv fur klinische und experimentelle Ophthalmologie. 254 (8), 1553–1565, doi: 10.1007/s00417-016-3386-y (2016).
11. Ghosh, F., Wong, F., Johansson, K., Bruun, A., Petters, R.M. Transplantation of full-thickness retina in the rhodopsin transgenic pig. Retina (Philadelphia, Pa.). 24 (1), 98–109, doi: 10.1097/00006982-200402000-00014 (2004).
12. Christiansen, A.T. et al. Subretinal implantation of electrospun, short nanowire, and smooth poly(epsilon-caprolactone) scaffolds to the subretinal space of porcine eyes. Stem cells international. 2012, 454295, doi: 10.1155/2012/454295 (2012).
13. Stanzel, B.V., Liu, Z., Brinken, R., Braun, N., Holz, F.G., Eter, N. Subretinal delivery of ultrathin rigid-elastic cell carriers using a metallic shooter instrument and biodegradable hydrogel encapsulation. Investigative ophthalmology & visual science. 53 (1), 490–500, doi: 10.1167/iovs.11-8260 (2012).

14. Gandhi, J.K. et al. Fibrin hydrogels are safe, degradable scaffolds for sub-retinal implantation. PloS one. 15 (1), e0227641, doi: 10.1371/journal.pone.0227641 (2020).
15. Liu, Z. et al. Surgical Transplantation of Human RPE Stem Cell-Derived RPE Monolayers into Non-Human Primates with Immunosuppression. Stem cell reports. 16 (2), 237–251, doi: 10.1016/j.stemcr.2020.12.007 (2021).
16. Stanzel, B.V. et al. Human RPE Stem Cells Grown into Polarized RPE Monolayers on a Polyester Matrix Are Maintained after Grafting into Rabbit Subretinal Space. Stem Cell Reports. 2 (1), 64–77, doi: 10.1016/j.stemcr.2013.11.005 (2014).
17. Al-Nawaiseh, S. et al. A Step by Step Protocol for Subretinal Surgery in Rabbits. (115), doi: 10.3791/53927. (2016).
18. Yaji, N., Yamato, M., Yang, J., Okano, T., Hori, S. Transplantation of tissue-engineered retinal pigment epithelial cell sheets in a rabbit model. Biomaterials. 30 (5), 797–803, doi: 10.1016/j.biomaterials.2008.10.045 (2009).
19. Sheridan, C.M., Mason, S., Pattwell, D.M., Kent, D., Grierson, I., Williams, R. Replacement of the RPE monolayer. Eye (London, England). 23 (10), 1910–1915, doi: 10.1038/eye.2008.420 (2009).
20. Hruban, V. et al. Inheritance of malignant melanoma in the MeLiM strain of miniature pigs. VETERINARNI MEDICINA. 49 (12), 453–459, doi: 10.17221/5739-VETMED (2004).
21. Vodicka, P. et al. The miniature pig as an animal model in biomedical research. Annals of the New York Academy of Sciences. 1049, 161–171, doi: 10.1196/annals.1334.015 (2005).
22. Vízina, M. Comparative ocular anatomy in commonly used laboratory animals. Ocular Toxicology in Laboratory Animals (A. B. Weir and M. Collins, eds.) pp. 9-12. Humana Press, Totowa, NJ (2013).
23. Chandler, M.J., Smith, P.J., Samuelson, D.A., MacKay, E.O. Photoreceptor density of the domestic pig retina. Vet. Ophthalmol. 1999;2(3):179-184, doi:10.1046/j.1463-5224.1999.00077.x
24. Sevc, J. et al. Effective long-term immunosuppression in rats by subcutaneously implanted sustained-release tacrolimus pellet: effect on spinally grafted human neural precursor survival. Experimental neurology. 248, 85–99, doi: 10.1016/j.expneurol.2013.05.017 (2013).
25. Eichhorn, S.J., Sampson, W.W. Statistical geometry of pores and statistics of porous nanofibrous assemblies. Journal of the Royal Society, Interface. 2 (4), 309–318, doi: 10.1098/rsif.2005.0039 (2005).
26. Szatmári-Tóth, M. et al. Clearance of autophagy-associated dying retinal pigment epithelial cells - a possible source for inflammation in age-related macular degeneration. Cell death & disease. 7 (9), e2367, doi: 10.1038/cddis.2016.133 (2016).
27. Lukovic, D. et al. Human iPSC derived disease model of MERTK-associated retinitis pigmentosa. Scientific reports. 5, 12910, doi: 10.1038/srep12910 (2015).
28. Artero Castro, A. et al. Generation of gene-corrected human induced pluripotent stem cell lines derived from retinitis pigmentosa patient with Ser331Cysfs*5 mutation in MERTK. Stem cell research. 34, 101341, doi: 10.1016/j.scr.2018.11.003 (2019).

29. Artero Castro, A., León, M., Del Buey Furió, V., Erceg, S., Lukovic, D. Generation of a human iPSC line by mRNA reprogramming. Stem cell research. 28, 157–160, doi: 10.1016/j.scr.2018.02.011 (2018).
30. Artero-Castro, A. et al. Gene Correction Recovers Phagocytosis in Retinal Pigment Epithelium Derived from Retinitis Pigmentosa-Human-Induced Pluripotent Stem Cells. International journal of molecular sciences. 22 (4), doi: 10.3390/ijms22042092 (2021).
31. Müller, B., Wagner, F., Lorenz, B., Stieger, K. Organotypic Cultures of Adult Mouse Retina: Morphologic Changes and Gene Expression. Investigative ophthalmology & visual science. 58 (4), 1930–1940, doi: 10.1167/iovs.16-20718 (2017).
32. Radtke, N.D., Aramant, R.B., Petry, H.M., Green, P.T., Pidwell, D.J., Seiler, M.J. Vision improvement in retinal degeneration patients by implantation of retina together with retinal pigment epithelium. American journal of ophthalmology. 146 (2), 172–182, doi: 10.1016/j.ajo.2008.04.009 (2008).
33. Maaijwee, K.J.M. et al. Histological evidence for revascularisation of an autologous retinal pigment epithelium--choroid graft in the pig. The British journal of ophthalmology. 91 (4), 546–550, doi: 10.1136/bjo.2006.103259 (2007).
34. Schwartz, S.D. et al. Human embryonic stem cell-derived retinal pigment epithelium in patients with age-related macular degeneration and Stargardt's macular dystrophy: follow-up of two open-label phase 1/2 studies. Lancet (London, England). 385 (9967), 509–516, doi: 10.1016/S0140-6736(14)61376-3 (2015).
35. Ghosh, F., Engelsberg, K., English, R.V., Petters, R.M. Long-term neuroretinal full-thickness transplants in a large animal model of severe retinitis pigmentosa. Graefe's archive for clinical and experimental ophthalmology = Albrecht von Graefes Archiv fur klinische und experimentelle Ophthalmologie. 245 (6), 835–846, doi: 10.1007/s00417-006-0437-9 (2007).
36. Radtke, N.D., Seiler, M.J., Aramant, R.B., Petry, H.M., Pidwell, D.J. Transplantation of intact sheets of fetal neural retina with its retinal pigment epithelium in retinitis pigmentosa patients. American journal of ophthalmology. 133 (4), 544–550, doi: 10.1016/s0002-9394(02)01322-3 (2002).
37. Slijkerman RW., et al. The pros and cons of vertebrate animal models for functional and therapeutic research on inherited retinal dystrophies. Prog Retin Eye Res. 2015 Sep;48:137-59. doi: 10.1016/j.preteyeres.2015.04.004.
38. Schramke S. et al. The Libechov Minipig as a Large Animal Model for Preclinical Research in Huntington´s disease - Thoughts and Perspectives. Cesk. Slov. Neurol N. 78/111 (Supplementum 2): 55-60, doi: 10.14735/amcsnn20152S55 (2015)
39. Hruban, V. et al. Inheritance of malignant melanoma in the MeLiM strain of miniature pigs. VETERINARNI MEDICINA. 49 (12), 453–459, doi: 10.17221/5739-VETMED (2004).
40. Tohyama, S., Kobayashi, E. Age-Appropriateness of Porcine Models Used for Cell Transplantation. Cell transplantation. 28 (2), 224–228, doi: 10.1177/0963689718817477 (2019).
41. Dall, A.M. et al. Quantitative [18F] fluorodopa/PET and histology of fetal mesencephalic dopaminergic grafts to the striatum of MPTP-poisoned minipigs. Cell transplantation. 11 (8), 733–746 (2002).

42. Shrader, S.M., Greentree, W.F. Göttingen Minipigs in Ocular Research. Toxicologic pathology. 46 (4), 403–407, doi: 10.1177/0192623318770379 (2018).
43. Duarri A., et al. Transplantation of Human Induced Pluripotent Stem Cell-Derived Retinal Pigment Epithelium in a Swine Model of Geographic Atrophy. Int J Mol Sci. 2021 Sep 28;22(19):10497. doi: 10.3390/ijms221910497

Legends to figures, tables and videos:

Figure 1. A - Schematic drawing of the retinal zones in relation to the minipig's head: yellow ellipse depicts the desired area of subretinal implantation, T – refers to the temporal retinal area, N – refers to the nasal retinal area. B – Example of the fundus scheme after subretinal implantation of the cell carrier (yellow) through retinotomy (red).

Figure 2. Transportation of the sedated animal into the operating room (A). Placement of the animal during intubation (B). Adjustment of the head of the animal for optimal access of the central retina during the surgery (red arrow) (C).

Figure 3. The standard setting of the operating room. A - schematic depiction of the surgeons' position (S – surgeon, A – assistant) in relation to the position of the operating table with a minipig, operating microscope (OM), vitrectomy machine (VM), instrumental table (IT), and anaesthesiology machine (AM). There are two possible positions of the vitrectomy machine (yellow and grey). B – real-life setting in the operating room.

Figure 4. Nanofibrous carrier with embedded supporting PET frame. A - three visible marks on the frame allow to control a side orientation of the carrier (white arrows). B – enlargement view of the PET frame fragment embedded in the nanofibrous membrane (white arrows) of the cell carrier.

Figure 5. Implantation injector. Presentation of parts of the injector (A). Nanofibrous cell carrier with embedded supporting PET ring loaded to the plastic rectangular capillary of the implantation injector (B).

Figure 6. Insertion of the trocars in the eye of a minipig. A - Schematic depiction of the trocars, which are inserted perpendicularly to the sclera toward the centre of the vitreous cavity in human eye (grey colour) and in oblique manner toward the posterior retina in minipig eye (blue colour) to avoid the damage of the lens. The lens of the minipig (blue coloured) is larger than that in humans and relative to the vitreous cavity size. B - Intraoperative view of the inserted trocars in a three-port PPV. The cornea is covered with methylcellulose to prevent it from drying and swelling.

Figure 7. Fundus photography (A), red-free image (B) and optical coherence tomography imaging (C) of the nanofibrous carrier with primary human RPE cells in a 4-weeks follow-up after subretinal transplantation in a minipig's eye. A - yellow arrows indicate the site of retinotomy. B – red arrows demonstrate the margins of the nanofibrous cell carrier. C – red arrows show the slight shadowing of the OCT signal caused by the supporting PET frame of the nanofibrous carrier, which was implanted into the subretinal space.

Figure 8. Haematoxylin-eosin staining of the retinal area containing the implanted nanofibrous carrier (yellow arrow) with the primary hRPEs in the minipig eye. The animal was euthanized and analyzed 6 weeks after the implantation. The primary hRPEs were clearly distinguishable by their size, round shape and pigmentation (red arrows) in the subretinal space opposite the photoreceptors. The photoreceptor nuclei in the ONL build rosette-like structures. The subretinal space appears hypertrophic. Legends: hRPE - primary human retinal pigmented epithelium, ONL - outer nuclear layer, INL - inner nuclear layer.

Figure 9. Immunolabeling with the RPE cell marker CRALBP (cellular retinaldehyde binding protein) in a minipig 6 months after implantation of primary hRPEs. A - vertical frozen sections of the treated pig eye were immunolabeled with CRALBP monoclonal antibody (green) and counterstained with DAPI (blue). B - single depiction of cell nuclei labelling with DAPI in black and white, as high contrast reveals the round shape of the individual hRPE cells (some shown with white arrows) (hRPE = human retinal pigment epithelium, ONL = outer nuclear layer).

Table 1. Standard parameters used during vitrectomy and laser photocoagulation.

Table 2. Results of the standardized surgical technique with subretinal implantation of the cell carrier in Liběchov minipigs over in the period between 2016 and 2020.

Video 1. Protocol for the preparation of the nanofibrous carrier and loading of the injector.

Video 2. Step by step protocol of the surgical procedure of subretinal cell carrier implantation in minipigs.

Supplemental file 1. List of medications, which were used in minipigs during experimental study.